TRANSACTIONS

30 May to 2 June 2010, Palau de Congressos de Catalunya, Barcelona, Spain

ENC 2010

EUROPEAN NUCLEAR CONFERENCE

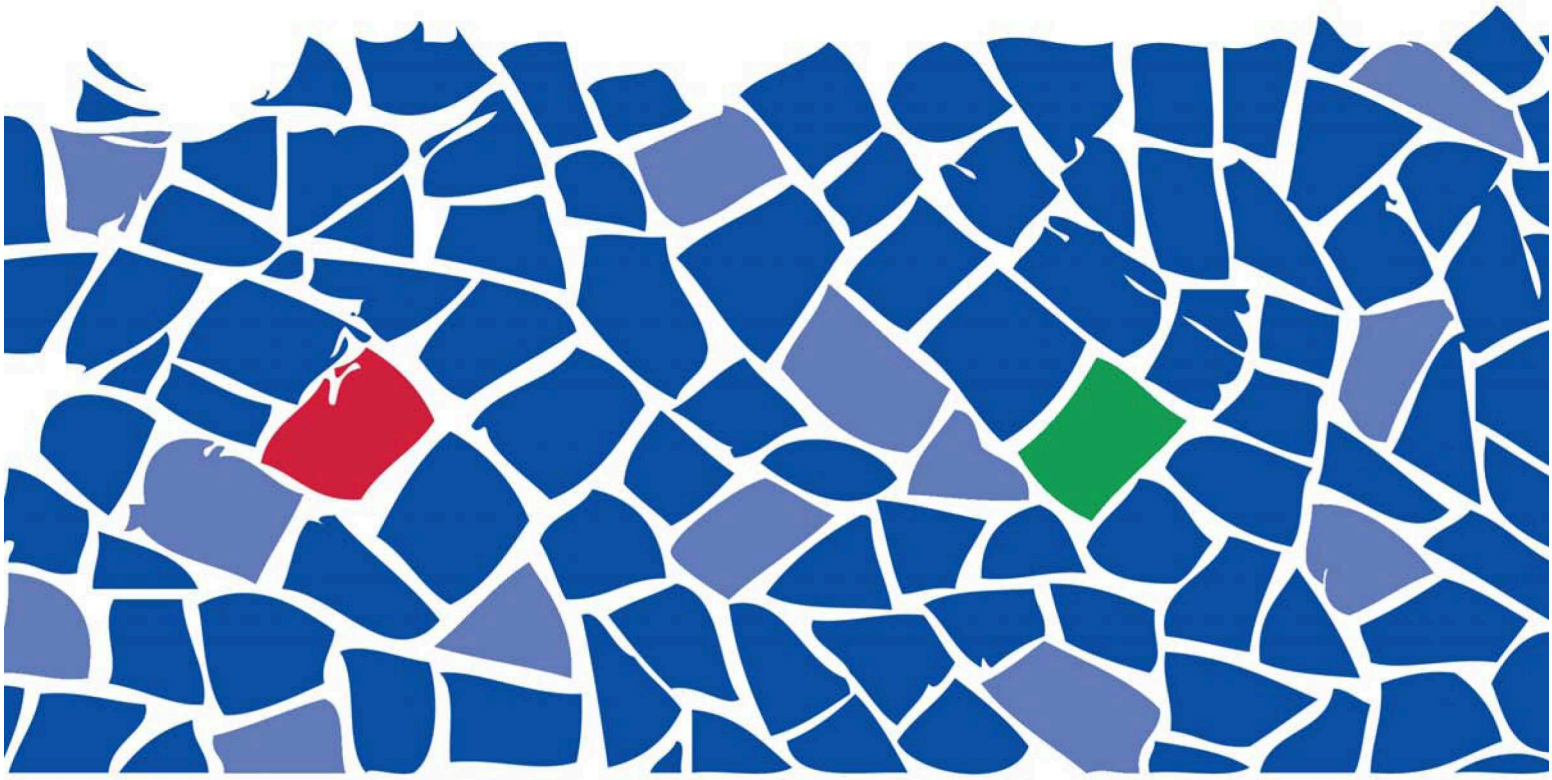

EUROPEAN NUCLEAR SOCIETY

AEN NEA

SNE SOCIEDAD NUCLEAR ESPAÑOLA

AMERICAN NUCLEAR SOCIETY

IAEA International Atomic Energy Agency
Atoms For Peace

Rue Belliard 65
1040 Brussels, Belgium
Phone + 32 2 505 30 54
Fax +32 2 502 39 02
E-mail ens@euronuclear.org
Internet www.euronuclear.org

ISBN 978-92-95064-09-6

These transactions contain all contributions submitted by 28 May 2010.

Poster

Plant operations

REQUIREMENTS REGARDING THE LAYOUT AND HANDLING OF RADWASTE CONTAINERS FROM THE RADIOLOGICAL VIEWPOINT

M. SOKCIC-KOSTIC, R. SCHULTHEIS
Nukem Technologies GmbH
Industriestrasse13, 63755 Alzenau - Germany

ABSTRACT

The most significant package for RadWaste handling, transport and storage is the RadWaste Container. When developing the layout of such a container, one of the most important aspects is the fulfilment of several radiological conditions, ranging from retrieval, over treatment to storage. To guarantee and observe these requirements, NUKEM Technologies has developed special measurement (monitoring) and tracking systems.

1. Introduction

The most significant package for RadWaste handling, transport and storage is the RadWaste container. RadWaste means waste containing radioactive isotopes with short and long lifetime, emitting alpha, beta, gamma or neutron particles. The container, as discussed in this paper is a stainless steel box, where the waste with or without additional material for shielding is filled in. The lifetime of enclosure of RadWaste is in-between a few tens of years up to several hundreds of years.

2. Filling, transport and storage of container

The container is used for a safe transportation of the waste and for a safe storage. Corresponding different requirements can be defined from the radiological viewpoint: The requirement for a safe transport of radwaste is different from the requirements for a safe storage of radwaste.

For transportation it is required, that the container is a sealed box withstanding different kinds of mechanical impacts. From the radiological viewpoint the requirements are different: the container must separate the environment from the waste to avoid a spread of the radioactive isotopes. In addition the radiation emitted from the waste must be limited to an acceptable value. The limitation of radiation outside of the container is relatively easy to perform. Inserting appropriate shields inside the container, made of concrete or other material with high density can limit the radiation as long as the distribution of radioactivity inside the container is stable during the transport. To avoid surface contamination the clean filling procedure has priority against a cleaning of the container after filling, because the cleaning process produces new waste. Best results are obtained if the container outside surface is covered during the filling. Nevertheless the container has to be measured to prove the conditions before leaving the filling station.

3. Measurements and calculation methods for container characterisation

NUKEM Technologies (NT) has developed full automated monitoring stations for measurement of container (Fig 1.), where all surfaces are scanned by dose rate meters and

the surface contamination is checked by wipe tests. These results are part of the container passport which has to accompaign the container during transportation.

Fig 1. NT Container Monitoring System

Different requirements are given for the storage of waste inside of containers. If the container is placed inside storage, the emitted radiation is of secondary importance. But the risk potential for the environment has to be considered. The first point is that the activity content of the container must be known. This requires that the activity of all radioactive isotopes must be measured. This can be done by measuring of the emitted gamma radiation with high sensitive HPGe detectors. The isotopes are identified by the gamma energy and the activity by the gamma intensity. Nevertheless the results give an uncompleted image of the activity potential because the radiation is partly shielded by the waste matrix. To overcome this effect, Monte Carlo simulations can be performed to estimate the shielding effect. If the matrix as well as the isotope distribution is homogenous, this method gives acceptable results for isotopes with gamma energies above (roughly) 100kev. For lower energies, the statistical errors dominate the measured values and therefore the extrapolation using absorption factors are also not very reliable. In addition this type of measurement is only applicable for isotopes emitting gammas. But there is a group of isotopes which do not emit measurable gammas like the beta emitters (Sr-90 for example) or alpha emitters (Am-241 for example). To overcome the problems, the key nuclide method was introduced. The method is based on the measurement of isotope vectors by radio-chemical analysis of the waste and scaling the not measurable isotopes from the measurable isotopes. This is not a perfect method but allows a rough estimate. In some cases there is another way to establish a usable isotope vector: if the origin of the waste is well known and if it can be estimated, that the isotope vector is not changed during the waste treatment and filling procedure, than the isotope vector can be calculated by the simulation of the process which have produced the isotopes. This can be applied for waste originating from nuclear fuel. A comparison of isotope vectors from radio-chemical analysis and burn-up calculations using codes like ORIGIN (1) or KORIGIN (2) has shown that the isotope vectors are the same within the experimental errors (mainly form the radio-chemical analysis). The influence of different reactor types and different burn up histories is small, if the cooling time of the waste is in the order of 10 years or longer, i.e. the short living isotopes have decayed during the cooling time. In cases where the waste is not homogenous in respect to the isotope distribution the burn up calculation give a higher quality because of the problems of sample taking strategy for the radio-chemical analysis.

Another method to overcome the problems is the measurement of neutron emission (only in respect to the alpha emitters). The neutrons are generated by spontaneous or induced fission but also by (alpha) processes, where the alphas are absorbed by light elements like Oxygen. The high penetration of neutrons reduces the influence of the waste matrix. The disadvantage of the neutron measurement is the physical fact, that the neutrons must be

moderated before they can be registered by He filled counter tubes. For an efficient moderation the complete container must be surrounded by a moderator (usually using a plastic moderation material – Fig 2.). This also implicates thta for large containers a large number of counter tubes is necessary. All this implications make the apparatus for measurement expensive.

Fig 2. NT Neutron Monitoring System FEMOS

4. Tracking method for container characterisation

As a consequence, while large containers make measurements (of gammas or neutrons) difficult; NUKEM Technologies has developed an improved method to establish the activity of waste by constructing waste treatment facilities which are equipped with a tracking system (fig 3.). The tracking system collects information about the waste as early as possible. This starts with the delivery of loose waste and collecting the history of the delivered waste. During the treatment process different monitors are measuring parameters like gamma emission, dose rates etc. at small batches, where all effects as described above like absorption etc. are reduced. Because the complete waste flow in the treatment facility is tracked, the activity of the waste container can be calculated by the activities of the batches filled into the container.

The filled and closed container are also measured by simple dose rate meters or by HPGe gamma spectrometers, but now the results are compared only for consistency with the accumulated activities from the different batches filled in.

At the same time the waste flows can be separated according the live time of the isotopes or the gamma radiation intensities to optimise the storage time of the waste, which is important for economical reason.

Fig.3 Clipped survvey of the Tracking System

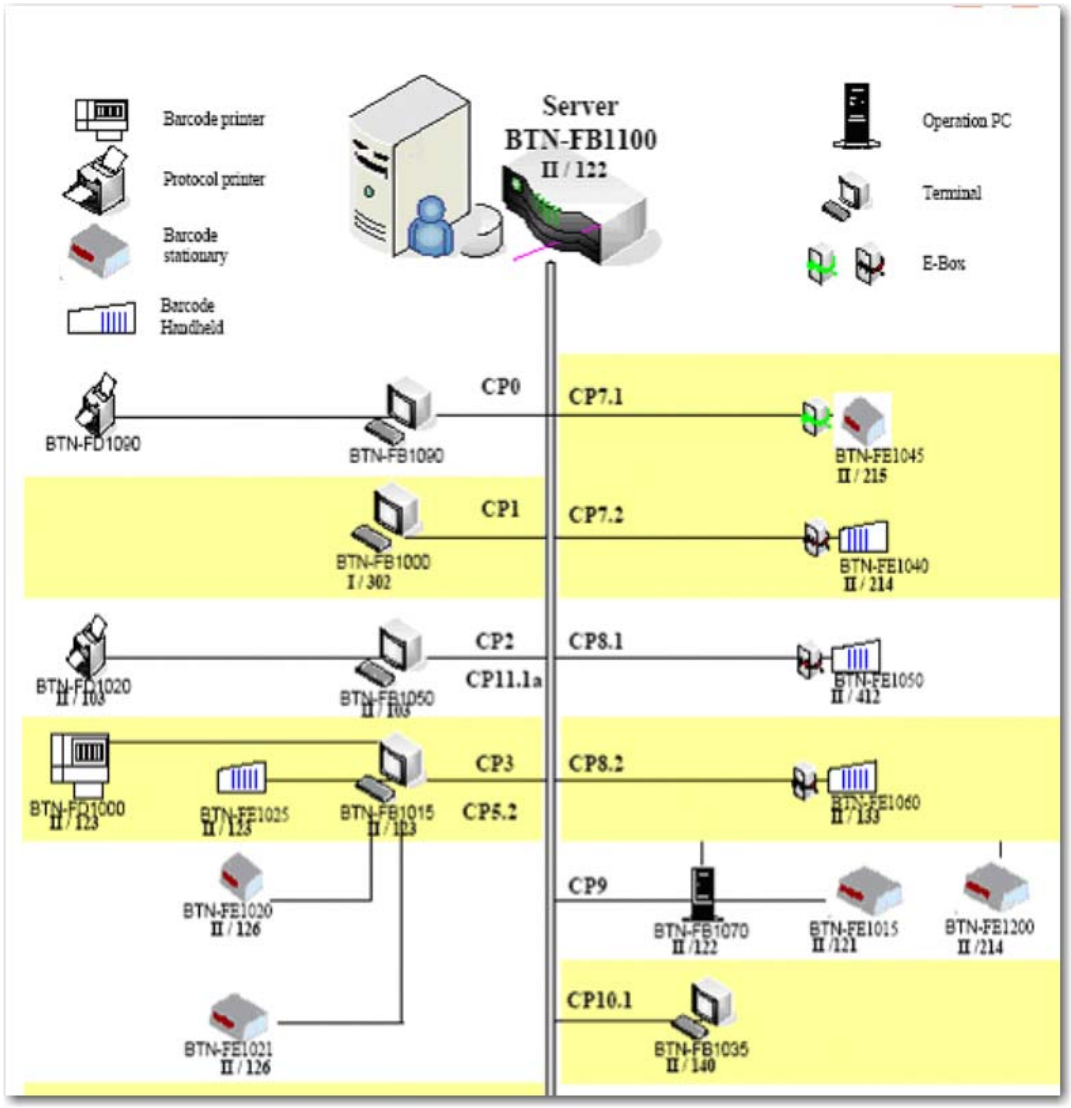

5. New developments

In the storage the container material is an important barrier between the radio-active waste and the environment, which can be influenced by the waste matrix in different ways. For high active waste the hydrolysis can release gases which build up an overpressure inside the container. Another danger is the corrosion of the container walls. Having a storage time of some hundreds of years in mind, it is very important that the barrier contains its functionality. If it is not possible to guarantee the correct function like the container walls as barrier against the environment, the integrity of the container should be controllded. A possible solution is the implication of measuring simple parameters like temperature and pressure inside the container to control the integrity. A promising idea is to put the simple sensors in containers that are communicating with a control room via RFID chips. It seems to be possible to operate these chips with long time batteries for a period of 10 years. A supply of the RFID and the sensors via the radio-frequency radiation seems to be possible; in this case no batteries are needed. The development is just beginning, and the search for methods and radiation hardened sensors has started. The RFID chip can alos be used to store information about the containers content and allows a quick location of the containers. In case that the sensors give alarm, the container must be opened and the waste treated and repacked.

6 Conclusion

For RADWASTE container with destination storage it is no longer sufficient to make a single radiological measurement just before the container is exported. Refined procedure are starting at the origin of the waste, collecting all available data during the waste processing and combining these data with the final container measurement to a data set which gives a consistent survey about the waste and its dangerous potential. In the near future the measurements will be continued during the storage time with automated information if important parameters like pressure, humidity or temperature.

7. References:

1. A.G.Croff: ORIGEN2 – A revised and updated version of the Oak Ridge isotope generation and depletion code ORNL – 5621, July 1980

2.. Improved and consistent determination of the nuclear inventory of spent PWR fuel on the basis of cell-burnup methods using KORIGEN, U. Fischer and H.W. Wiese, INR, Forschungszentrum Karlsruhe, Kfk 3014

ON BASIC PRINCIPLES FOR MODIFYING WATER AS A COOLANT OF PWR

P.N. ALEKSEEV, YU.M. SEMCHENKOV, A.L. SHIMKEVICH
RRC "Kurchatov Institute"
Kurchatov Sq., 123182 Moscow – Russia

ABSTRACT

Enhancing heat transfer of water as a coolant for PWR can play a major role in increasing the efficiency of this reactor system. However in spite of considerable research efforts, major improvements in water heat transfer capabilities have been lacking due to its effective operation characteristics without additives. Therefore, it is necessary to develop a new strategy in improving the effective heat transfer behaviour of water coolant. Recent developments in nanotechnology have resulted in nanofluids which have a great potential for cooling applications. They are a mixture of liquid and dispersed phase of extremely fine solid particles usually less than 50 nm in size. A material of these particles can be a metal, any oxide or carbide. Many tests have shown that the thermal conductivity of such the mixture can be increased by almost 20% compared to that of the base fluid for a relatively low particle loading (of 1 up to 5% in volume). It is confirmed by experimental data and simulation results. In given studying, the authors consider an effect of additive clustering on stabilizing structure of colloidal water solution for cooling the fuel elements of the PWR core. The task consists of providing the stability of a water nanofluid embedded with such the nanoparticles that flowing inside a loop without changing their microstructure. The results of theoretical investigation maybe useful for motivated choosing the composition of heat-transfer suspension and developing technology for making the appropriate nanofluid operated in the PWR system.

1. Introduction

Nanofluids, as a new class of coolants, are suspensions of nanoparticles with sizes less than 100 nm in non-metal base liquids with solid volume fractions typically less than 4% [1]. These coolants have shown the ability of enhancement (up to 40%) in thermal conductivity compared with the base liquid [2] and significant increases of critical heat flux [3]. Oxides (Al_2O_3, CuO, TiO_2), nitrides (AlN, SiN), carbides (SiC, TiC), and metals (Ag, Au, Cu, Fe) are used in nanofluids as nanoparticle materials [4].

Presently, nanofluids are produced by two techniques [4]. A two-step technique starts with nanoparticles produced by one of physical or chemical synthesis techniques as a dry powder and then dispersed into the base liquid. This method may result in a large degree of nanoparticle agglomeration. The single-step (evaporation) one simultaneously makes and disperses the nanoparticles directly into the base liquid. Nanofluids containing oxide nanoparticles are produced by the two-step process and the ones containing metal nanoparticles are produced by the single-step process. The last is unlikely to become the mainstay of commercial nanofluid production due to it requires low vapour pressure, typically less than 1 torr, that limits the rate of nanofluid production. Furthermore, producing nanofluids by this process is expensive.

Although nanoparticle agglomeration in this case is minimized as a result of the liquid flowing continuously, the effect of temperature and operation conditions on nanoparticle allocation

maybe significant due to changing the electric potential on the surface of colloidal particles as a main factor to provide the stability of nanofluid [5].
From this point of view, systematic studies of water nanofluid composition are needed [6], since a key factor in understanding thermal properties of nanofluids is clustering effects that provide paths for rapid heat transport [7]. Therefore, it is very important to consider the large collective displacements of water molecules that occasionally occur in between many sequential small displacements due to significant coupling among a subset of the normal modes in the low energy dynamics and the most stable atomic configurations, where the system spends most of its time, consist of five-member rings [8].

2. Additive residence in water

The effect of solid-liquid phase transition on ion-water-cluster properties is investigated both through the multi-state empirical valence bond potential and a polarization model [9]. Equilibrium properties of the ion-water clusters $H^+(H_2O)_{100}$, $Na^+(H_2O)_{100}$, $Na^+(H_2O)_{20}$, and $Cl^-(H_2O)_{17}$ in the temperature region 100–450 K are explored using a hybrid parallel basin-hopping and tempering algorithm. It is found that sodium and chloride ions largely reside on the surface of water clusters below the cluster melting temperature but are solvated into the interior of the cluster above the melting temperature, while the solvated proton was found to have significant propensity to reside on or near the surface in both the liquid- and solid-state clusters. It should be noted that the exclusion of the Cl^- ion from the cluster surface was far less dramatic than that for the Na^+ clusters studied. With increasing temperature the Cl^- maxima transitions occur gradually from near surface to interior, displaying a significant interior bias only at the highest temperatures considered [10].

On the other hand, a position of any impurity in the liquid matrix has dual character due to density fluctuations of liquid consist of almost regular tetrahedrons connected in pairs by faces in ramified n-chains [11, 12]. At a low concentration, Impurity atoms place on the external faces of these chains not changing the microstructure of the dense liquid part i.e. form an “introduction solution”. Then in increasing the concentration, the impurity can add its tetrahedral clusters to the dense part of the basic component, so that the solution becomes nano-heterogeneous as a diphase for the impurity component and single-phase for the basic liquid, i.e. it forms an “addition solution” [13].

In two-structured water, the low-density tetrahedral-ordered ice-regions are divided by higher density clusters with an asymmetrical structure [14]. These tetrahedral clusters of water density fluctuations (see Fig 1) are more complicated due to hydrogen bonds but the frame of them as a broken red line connecting the centres of tetrahedrons is also ramified.

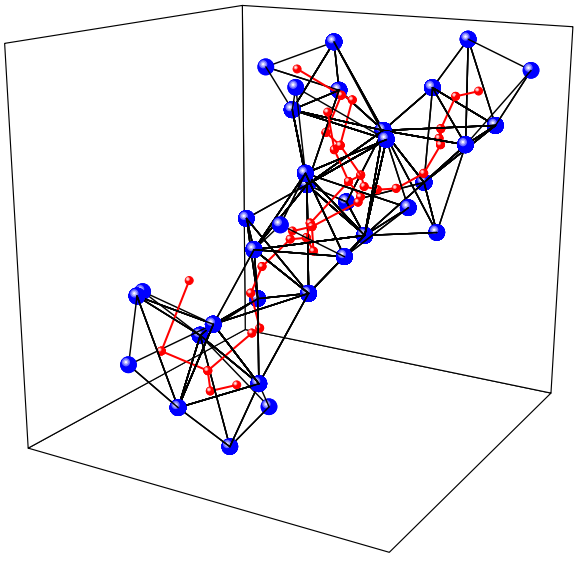

Fig 1. Dense-part cluster in MD model of water at 300 K and its frame (broken red line); blue points are the molecules and red points – centres of the cluster tetrahedrons

Thus, additive residence in water is practised in the interface of low and high density regions. In increasing its concentration, impurity atoms can form additive tetrahedral clusters of the dense part of water solution [13]. Just such the nanometre clusters may be stable in water at different conditions of its operation as a coolant.

3. Principles for nucleating nanoparticles in water

The topological structure of density fluctuations of the condensed matter in different aggregative states (liquid, crystal, and amorphous body) is represented as instant densely packed fours of atoms as tetrahedrons connected in pairs by faces in Bernal's n-chains [12].

At the same time, a parameterization of the energy functional cannot be arbitrary since the condensate structure at the fixed density weakly depends on a temperature for a wide class of the matter: metals and ionic melts, liquid semiconductors and non-conductors [13].

Such the model can explain many properties of the liquid state, in particular, fractal properties of additive clusters in any liquid which can be formed at changing the composition of binary mixture.

The last is very important for synthesis of inherent nanoparticles from additives in water as the "addition solution", but not the "foreign" nanoparticles from the outside. In Fig 2, one can see such the microstructure behaviour of any solution as changing the correlation radii of fluctuations of liquid density, R_1, and its composition, R_2 [13].

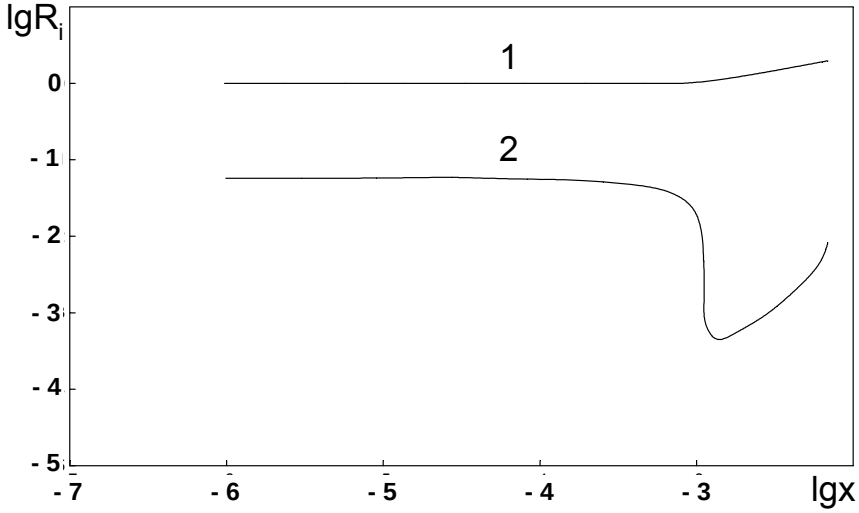

Fig 2. Logarithm of correlation radii, R_i, for fluctuations of the solution density (1) and the ones of its composition (2) as a function of additive concentration x

One can see a sharp falling R_2 at the some value of additive concentration that specifies a disintegration of the composition fluctuations in molecular clusters against a background of long-wave fluctuations of the solution density. Monotonous increasing the correlation radius of the composition fluctuations in some interval of the additive concentration should be interpreted as a region of cluster existence and then, the allocation of nanoparticles from the solution when the correlation radius, R_2, increases sharply [13].

The observed additive clustering into the solution differs from the first-order phase transition. It may be considered as an analogue of such the transition only in micro regions of liquid which has continuous character without a singularity and concerns only to change an additive form in the solution. For example, as an illustration of additive clustering, Fig 3

shows typical кластер $(K_2O)_n$ received by molecular-dynamic simulation [13] in oxygen-non-saturated melt of potassium.

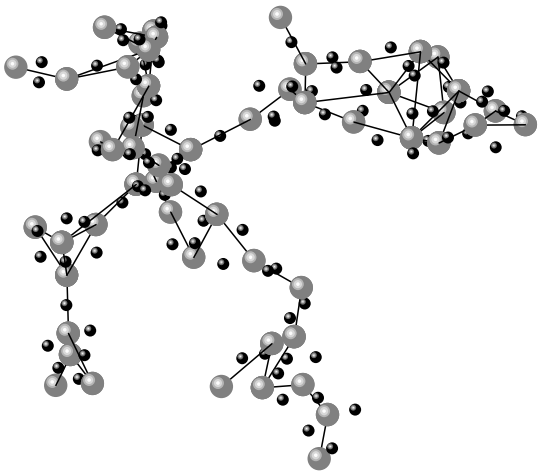

Fig 3. The oxide cluster in oxygen-non-saturated melt of potassium, big circles are oxygen anions and small circles are potassium cations

4. Discussion of results

As one can see in Fig 2, the lower limit of the additive concentration for clustering additives in liquid is $\sim 0.1C_s$, where C_s is the saturation additive concentration. It is clear that this range for additive clustering in water as a solid-like state of the impurity is an effective way to stabilize the nanofluid structure in water for different conditions (high temperature, flow rate, radiation etc) of its operation in any nuclear system.

The theoretical studies show [12] that fluctuation-induced additive clustering considered here will be possible if the solid phase allocated from such the water solution is a hydroxide. Therefore, the degree of control required over the effective nanostructure component in water suspension and their nature depending on the correct selection of additives for water solution.

To prepare stable nanofluids with nanoparticles of specific size and shape, it is important to understand the fundamentals of particle formation in water directly from additives which we can dissolve there. For this, ramified fractal clusters as natural solid-state part of addition solution is considered within the framework of the fluctuation theory when density fluctuations in water stimulate forming additive clusters as fractal nanoparticles [12]. The example of such the cluster as possible solid-like filaments is shown in Fig 4.

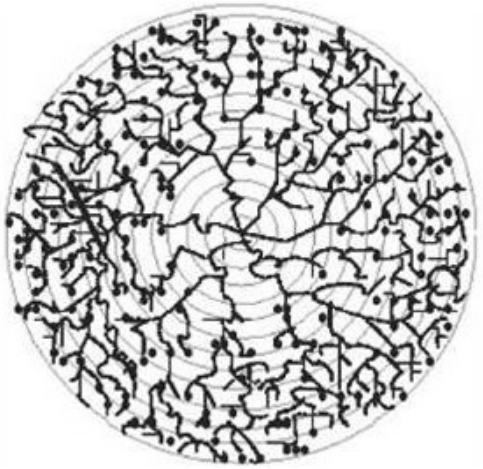

Fig 4. The scheme of percolation fractal cluster of solid-like filaments

5. Conclusions

The theoretical studies show how one can provide the stable formation of nanoparticles in water solution. It is important to form clusters in water directly from additives which are dissolved there. Then, ramified fractal clusters as natural solid-state part of addition solution can be stable constituents of nanofluid on water base.

It will provide the stability of a water nanofluid embedded with such the nanoparticles that flowing inside a loop without changing their microstructure.

The results of microscopic investigation maybe useful for motivated choosing a composition of a heat-transfer suspension, developing technology for making the appropriate nanofluid, operated in the first circuit of PWR.

6. Acknowledgements

Authors are pleased to acknowledge Dr. A.S. Kolokol for giving some data on molecular-dynamic simulation of water structure and discussing this work which is supported by the Russian Foundation of Basic Researches (Grant # 10-08-00217).

7. References

[1] S. Choi, Enhancing thermal conductivity of fluids with nanoparticles, In Development and Applications of Non-Newtonian Flows, Ed. D A Siginer, H P Wang, P. 99, New York: ASME, 1995.
[2] M. Bahrami et al, Assessment of relevant physical phenomena controlling thermal performance of nanofluids / In Proceedings of IMECE 2006 ASME International Mechanical Engineering Congress and Expo November 5-10, 2006, Chicago, Illinois, USA, IMECE2006-13417.
[3] S. M. You et al, “Effect of nano-particles on critical heat flux of water in pool boiling heat transfer,” Applied Physics Letter, 2003, **83**, 3374.
[4] W. Yu et al, Review and assessment of nanofluid technology for transportation and other applications / Report of Argonne National Laboratory, ANL/ESD/07-9, 2007.
[5] Nanofluid datasheet / Meliorum Technologies, Inc., 2008.
[6] C.-H. Lo and T.-T. Tsung, Low-than-room temperature effect on the stability of CuO nanofluid // Rev. Adv. Mater. Sci., 2005, **10**, 64.
[7] Keblinski et al., Mechanisms of heat flow in suspensions containing nano-sized particles (nanofluids) // Int. J. Heat Mass Trans., 2002, **45**, 855.
[8] A.L. Shimkevich, On enhancing water heat transfer by nanofluids / In Proceedings of the 17th International Conference on Nuclear Engineering (ICONE17), ICONE17-75054, 2009.
[9] A. Baba et al, Fluctuation, relaxation and rearrangement dynamics of a model $(H_2O)_{20}$ cluster: Non-statistical dynamical behaviour // J. Chem. Phys., 1997, **106**, 3329.
[10] C.J. Burnham et al, The properties of ion-water clusters. II. Solvation structures of Na^+, Cl^-, and H^+ clusters as a function of temperature // J. Chem. Phys., 2006, **124**, 024327.
[11] J.D. Bernal, The Structure of Liquids // Proc. R. Soc., 1964, **280A**, 299.
[12] A.S. Kolokol, A.L. Shimkevich, Topological structure of density .fluctuations in condensed matter // J. Non-Crystal. Solids, 2010, **356**, 220.
[13] A.L. Shimkevich, The composition principles for designing nuclear-reactor materials / ed. N.N. Ponomarev-Stepnoi, Moscow: IzdAt, 2008 (Rus.)
[14] C. Huang et al, The inhomogeneous structure of water at ambient conditions // Proc. Natl. Acad. Sci. USA, 2009, **106**, 15241.

OVERVIEW OF MANAGEMENT OF LOW AND INTERMEDIATE LEVEL RADIOACTIVE WASTES AT THE INSTITUTE FOR NUCLEAR RESEARCH FOR TO SAVE MANAGEMENT OF THE WASTE FROM DECOMMISSIONING OF NUCLEAR FACILITIES

D. BUJOREANU, L.BUJOREANU
Waste Management Department, Institute for Nuclear Research
Str. Campului no 1, POB 78, Pitesti, Romania

ABSTRACT

The national policy of radioactive waste management fully complies with the international requirements established by "Joint Convention on the Safety of Spent Fuel Management and on the Safety of Radioactive Waste Management and with the EURATOM treaty, directives, recommendations and policy of radioactive waste management promoted at the level of the European Union.
The Institute for Nuclear Research Pitesti (INR) has its own Radwaste Treatment Plant. The object of activity is to treat and condition radioactive waste resulted from the nuclear facility.
According to the National Nuclear Program, the institute is the main support for implementation of the methods and technologies for conditioning and disposal of radioactive waste generated by Cernavoda NPP.
For all these, in accordance with the Governmental order no. 11/2003, INR shall must prepare and manage the decommissioning projects of its own facilities and to upgrade the facilities for the management of the radioactive waste resulting from decommissioning activities.

1. Introduction

The Institute for Nuclear Research Pitesti (INR), of the Autonomous Company for Nuclear Activities has its own Radioactive Waste Treatment Plant (STDR).
Among the most important practices that generate radioactive waste it shall be mentioned the operation of the TRIGA reactor, the operation of the Post Irradiation Examination Laboratory, the secondary radioactive waste from operation of STDR and the waste resulted from different research laboratories of INR.
Also, the institute is responsible for the management of the waste arising from decommissioning activities of TRIGA research reactor and all other nuclear and radiological installation.

2. Waste management technologies

A strategy for management of radioactive waste that is in concordance with the national policy involves the selection of technologies available to manage the waste into a form so that it may be easily treated, conditioned, and packaged for storage and/or disposal.
At INR Pitesti radioactive wastes are categorized in:
• Solid low-active radioactive waste;
• Spent ion exchangers;
• Solid combustible radioactive waste containing natural uranium (produced in the FCN Pitesti);
• Liquid low - active radioactive waste;

• Liquid radioactive waste containing natural uranium (produced in FCN Pitesti);
• Organic liquid radioactive wastes from CNE Cernavoda.
The Radioactive Waste Treatment Station has the following facilities:
• Installation for treatment of low - active β-γ liquid wastes;
• Installation for conditioning in concrete of the radioactive concentrate obtained during the evaporation treatment of liquid radioactive waste. The installation is used also for conditioning in concrete the solid radioactive waste;
• Installation for conditioning into bitumen of spent ion exchangers from the TRIGA reactor;
• Installation for treatment, with uranium recovery, of liquid radioactive waste resulting from the fabrication of CANDU-type nuclear fuel;
• Installation for the incineration of solid radioactive waste contaminated with natural uranium from FCN Pitesti;
• Installation for treatment/conditioning of organic liquid radioactive waste with tritium content from CNE Cernavoda;
• Installation for decontamination of sub-assemblies and spare parts;
• An Industrial-type laundry washing machine for decontamination of individual protective clothes.
The basic steps of the radioactive waste management system are given in Fig. 1.

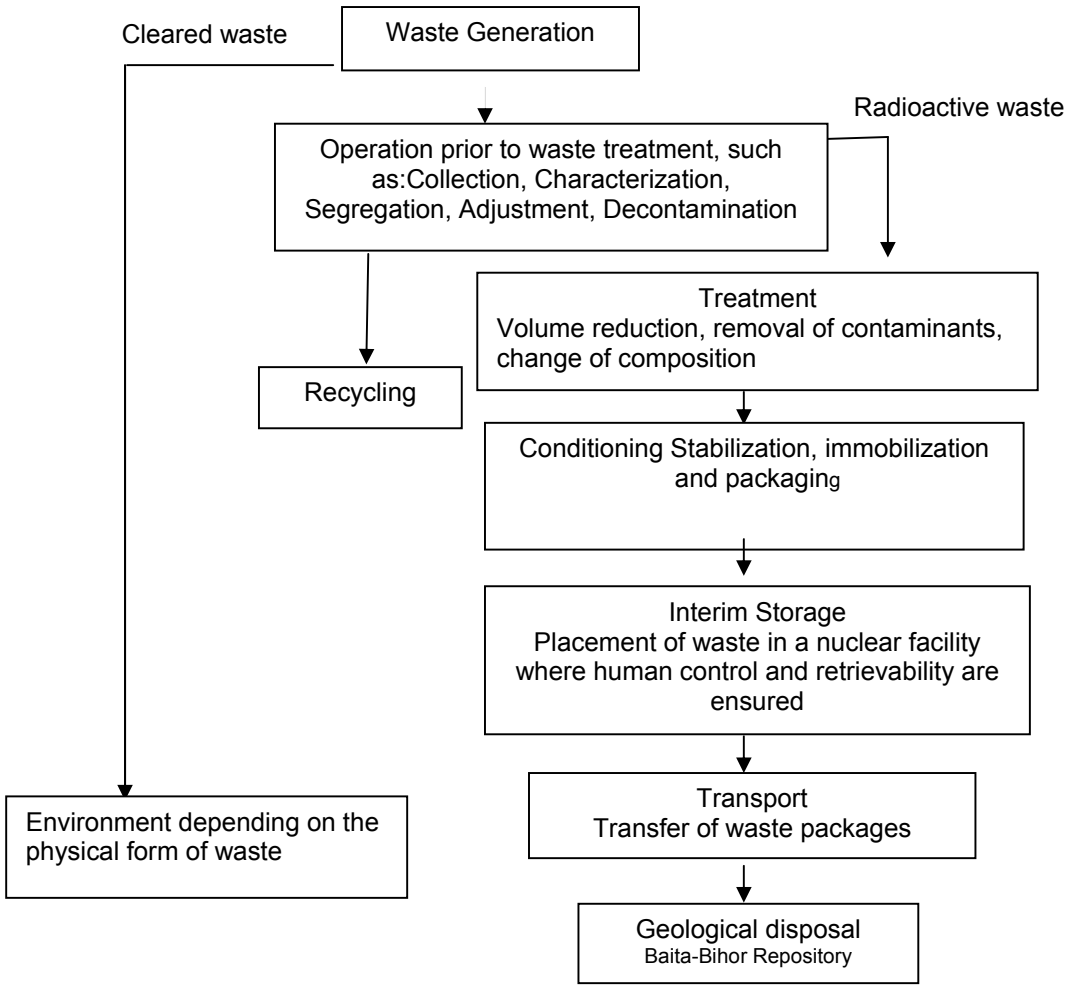

Fig. 1 Schematic diagram of waste management steps

3. Quality Assurance

Quality assurance (QA) is an essential aspect for the good management of radioactive waste at INR.
The QA programme defines the organization, responsabilities and steps involved in a waste management process.
Considering the development of the market economy and the competition in the business area, INR fostered and implemented an Integrated Management System – Quality-Environment-Safety and Health [2], in compliance with the provisions of national and international standards and regulations.
The system has been developed and implemented within the institute in order to ensure an efficient operation, to guarantee the optimum quality of a product and the intrinsic quality of the process.
The system is certified by Lloyd's Register Quality Assurance and authorized by the National Commission for Nuclear Activities Control (CNCAN).

4. Knowledge Management related to nuclear facilities decommissioning

This kind of knowledge should lead to the draw-up of programs for the assessment and implementation of decommissioning activities, consisting of formal documents, technical reports, procedures, etc., which are assumed to comply with knowledge and applicable legislation.
At the same time, one should keep in view that, between the groups of basic decommissioning processes and management processes, a close correlation and interaction must exist with regard to internal communication. This one should allow identification and coordination of knowledge required for the progress of decommissioning and ensures they are correct.
The structural knowledge regarding decommissioning processes has in view three major objectives:

(a) Strategic framework;
(b) Planning Process;
(c) Dismantling Process.

5. Acceptance criteria for waste package

The waste form and package are determined by the acceptance criteria which include security tests and physical protection that are established by the competent authority, in our case the Romanian National Commission for Nuclear Activities Control for the final disposal in the National Repository Baita, Bihor.
Waste acceptance criteria are used to identify, control and document the type and quantity of the radioactivity, as well as the physical handling and long term stability of the waste.
Waste packages are designed to provide primary containment during handling, interim storage, transport, operational phase of the disposal facility and, in some cases, to retard release and migration of radionuclides and hazardous constituents on long term.
The process parameters which affect the quality of the final product are standardized and comply with the following acceptance criteria for waste packages:

- each waste package will contain only one type of waste;
- the maximum content of radionuclide contained (maximum admitted activity) will be in accordance with the criteria for final disposal at the repository Baita-Bihor (Table no.1);
- the contamination at the 200 l drum outer surface should not exceed 4 Bq/cm^2 ;
- the surface exposure rate of steel drum must be less than 2mSv/h;
- the determined lixiviation rate must be of maximum 10^{-3} cm/day.

Radionuclide	Maximum admitted activity (Bq/m^3)
C-14	$1\ 10^9$ (10^{11} Bq for all the repository)
Ni-59	$2\cdot 10^9$
Nb-94	$2\cdot 10^7$
Tc-99	$1.5\cdot 10^8$
I-129	$3\cdot 10^5$
Cl-36	$1.5\cdot 10^7$
H-3	$1{,}5\cdot 10^{10}$
Co-60	$1\cdot 10^{11}$
Ni-63	$1\cdot 10^{11}$
Sr-90	$5\cdot 10^9$
Cs-137	$1\cdot 10^9$
β and γ -emitting radionuclide with a lifetime over 5 years	$1\cdot 10^7$
Radionuclide with a lifetime below 5 years.	$5\cdot 10^8$

Table 1: Maximum content admitted for packages disposal at Baita-Bihor repository

6. Disposal of conditioned wastes

The method of disposal of conditioned wastes that are resulted is emplacement in repositories within deep geological formations.
In Romania, is in operation the National Repository for Low and Intermediate Radioactive Waste Baita, Bihor. The repository is an underground construction in an old exhausted uranium mine that was dimensioned to dispose about 21,000 standard drums.
The product obtained is kept in interim storage at the STDR storage facility, until it will be transported to the National Repository Baita-Bihor for disposal (Fig. no.2).

Fig 2 Final product for disposal at National Repository Baita-Bihor

7. Conclusions

Using the existing concepts at `80 year's level, concerning the final disposal of low and intermediate level radioactive waste, in 1984 was built and given in operation the Radioactive Waste Treatment Plant from the Institute for Nuclear Research Pitesti.
The object of activity of requires STDR within the INR Pitesti is to treat and condition radioactive waste resulted from the Nuclear Fuel Factory, the TRIGA reactor, Post Irradiation Examination Laboratories and other research laboratories of the INR.
The objective of Romanian radioactive waste management policy is to assure safe management of radioactive waste, according to the principles states in IAEA and the requirements presented in IAEA Requirements No. GS-R-1 [3].
At INR Pitesti, the volume of radioactive waste resulting from various activities may be reduced using a minimization processes such as compaction, incineration, filtration and evaporation.
The using of any waste minimization process takes into consideration factors such as: worker dozes, costs of recovering materials generated, duration and cost of interim storage of waste compared with the estimated ultimate disposal costs.
Radiation exposure of the operating staff and members of public during processing and storage of radioactive waste is maintained as low as reasonably achievable – ALARA (social and economic factors taken into account).

8. References

[1] Joint Convention on the Safety of Spent Fuel Management and on the Safety of Radioactive Waste Management, Romanian National Report, Third National Report, 2008.
[2] Manually of Integrate Management System, Ed.2, MSMI-CMSSM-ICN, Pitesti, 2009.
[3] Safety Standards Series No. GS-R-1, Legal and Governmental Infrastructure for Nuclear, Radiation, Radioactive Waste and Transport Safety-REQUIREMENTS, IAEA, Vienna, 2000.

ECOLOGICAL CONDITION AROUND THE URANIUM TAILING PITS IN TAJIKISTAN.

I.Mirsaidov, U.Mirsaidov, N.Khakimov, Kh.Nazarov,

Nuclear and Radiation Safety Agency under the
Academy of Sciences of the Republic of Tajikistan
33 Rudaki avenue, Dushanbe 734025
Tel: +992 372 27 77 91; Fax: +992 372 21 55 48;
E-mail: ulmas2005@mail.ru

One of the basic sectors of the economy in Tajikistan is the mining industry. Its development in the past led to an accumulation of large amounts of waste mainly associated with the uranium milling facilities. These wastes contain radionuclides in high concentrations (basically uranium-thorium series) and other hazardous substances. These facilities are often located in residential areas and in the upper side of the main watersheds of the region, such as Amu-Daria and Syr-Daria (see Fig.1.1)

1. Evaluation of the status of former Uranium facilities and current remedial activities

Tajikistan has a number of uranium ore deposits and mining and milling facilities, which operated in the past. This country's own ores and imported raw materials were processed mainly at the former Leninabad Geochemical Combine facility (currently State Enterprise (SE) "Vostokredmet") and also at other hydro-metallurgical plants located in the vicinity of uranium ore extraction sites (Adrasman , Taboshar, Isphara etc.). Presently the only operating enterprise in the Republic of Tajikistan, which still has the potential to process Uranium ores, using an acid leach extraction process, is the SE "Vostokredmet".

It is interesting is to note that the mine wastes at the Adrasman site were recently successfully reprocessed to produce a lead concentrate. Otherwise, all underground and open pit mines and old radium and uranium facilities have been decommissioned, but most of them are still not remediated. Due to the recent significant increase in the price of uranium, the uranium mining residues have become a focus of interest for various different investors and commercial companies who are considering reprocessing the waste rock piles and mill tailings of Northern Tajikistan.

Based on estimates from SE "Vostokredmet", the total amount of residual uranium in the tailings and waste rock piles in the Republic of Tajikistan is about 55 million tons. The total activity of these wastes is estimated to be approximately 240-285 10^{12} Bq (Table 1). The total volume of waste rock piles and tailings in the vicinity of former hydrometallurgical plants and chemical-leaching sites is more than 170 million tons.

The waste rock piles and tailings at Taboshar, Adrasman and Degmay (which is near the outskirts of Chkalovsk) are not well contained. In particular the surfaces of the tailings usually have no protective cover; and the surface is eroded or damaged by burrowing animals. There is exposure of

significant amounts of contaminants, which are subject to dusting and wind blow. Any cover of these tailings and waste rock piles has usually been washed away by water, mudslides and wind, thus becoming a source of highly contaminated drainage water which is migrating into surface and ground water bodies. The same sources of water are commonly used by local population.

In many areas where water is in short supply it is common to have livestock grazing and watering using such contaminated waters; also local horticulture uses these drainage waters for irrigation and even for rice paddies and orchards located near the sites of uranium waste piles.

Illegal excavation and collection of non-ferrous metals from areas of tailings and waste rock piles and mines has become more frequent. This creates serious concerns over transfer of contamination as well as the exposure of the individual diggers. There is concern that these metals are sold on at local, illegal, markets in Tajikistan or even transported abroad.

Some estimates of status of the former uranium facilities in Tajikistan are presented below in this paper.

Table. 1. Tailings of the former Uranium facilities according to data of SE “Vostokredmet”

Name of disposal site	**Locations and distance to the closest settlement**	**Period, when tailings were created**	**Sanitary protection zone, (м) Square, (ha)**	**Efficient disposal volume ($м^2$)**	**Cover characterization**	**Gamma dose exposure rate at the surface , μR h^{-1}**	**Amount of disposed waste in million of tons, ---------- Curies**
1. Tailing	Degmai, Gusion 1.5 km	1963	400 90.0	$194*10^5$	No cover	650-2000	20.8 4218
2. Tailing	Ghafourov 0.5 km	1945-1950	- 4.0	$2.4*10^5$	Soil, 2.5 m	20-60	0.4 159
3. Tailing	Cells 1-9. Chkalovsk , 2 km	1949-1967	50.0 18.0	$26*10^5$	Soil, 0.5 m	20-60	3.034 779
4. Tailing I-II	Taboshar, 2 km	1945-1959	50.0 24.7	$9.88*10^5$	Soil, 0.7-1 m	40-60	1.69 218
5. Tailing III	Taboshar, 0.5 km	1947-1963	50.0 11.06	$10.6*10^5$	Soil, 0.7-1 m	40-60	1.8 232
6. Tailing IV	Taboshar, 1.0 km	1949-1965	50.0 18.76	$24.3*10^5$	Soil, 0.7-1 m	40-60	4.13 510
7. Tailing N 3	Taboshar, 3.0 km	1949-1965	50.0 2.86	$0,69*10^5$	Soil, 0.7-1 м	40-60	1.17 15.2
8. Storage of the factory of “barren ore” (FBO)	Taboshar, 4.0 km	1950-1965	- 3.35	$11.9*10^5$	No cover	40-100	2.03 253
9. Tailing N2	Adrasman, 1 km	1991г.	- 2.5	$2.4*10^5$	Soil up to 1 m	50-60	0.4 160
10. Mine-3 (4 units)	Khujand, 2 km	1976-1985	- 5.9	$2.07*10^5$	Soil, 0.5 m	60-80	3.5 11.0

1.1. Uranium tailings in vicinity of Chkalovsk town

Chkalovsk is a suburb of the city of Khujand (formerly Leninabad – the center of Sogd oblast of the Republic) this is the location for several mining industries including "Vostokredmet" (former Leninabad Mining Chemical Complex), which was previously involved in the milling and processing of the uranium ores.

During the soviet period, the uranium ores processed at the hydrometallurgical plant of Chkalovsk were obtained from Tajikistan, Kazakhstan and Uzbekistan. During the last three years of operation ores from a Kazakhstan plant were also transported to Chkalovsk in the form of acid extraction material obtained by heap leaching and underground leaching (up to 200 mg l^{-1} U). These concentrates were processed into uranium protoxide-oxide and returned to Kazakhstan.

Fig. 1.1. Tailings site at the vicinity of Chkalovsk (Sells 1-9)

Residues from the extraction process and acid residues following the neutralization were transported and deposited in the nearest tailings. Pumping was conducted through an existing coal slurry pipeline. In the outskirts of Chkalovsk there are three plots (Fig.1.1), where these tails were placed (Ghafourov, Sell 1-9, Degmay). This site was located on the outskirts of the town with some buildings nearby. The topographical form of the facility was a gently mounded site with no obvious erosion scars on the flanks. The site was reported as extending over 18 ha; containing 2.9 million tones of residues that had been covered with a soil layer 0.5 to 1 m thick.

The total amount of radioactivity in the heap was stated to be about 29000 GBq. Gamma-dose rate exposure observed at the surface of tailing was 0,2-0,6 μSv/h (20-60 μR/h). The cover over the tailings is 0.5-0.7 m. There are no warning signs or fencing around the site which is about 6 km from the mill. There were a number of pipelines from this area to the mill, which are mostly very rusty but are apparently monitored, checked and operational. The difference in elevation from the mill to the distant tailings sites is about 100 m.

According to "Vostokredmet" reports the present monitoring consists of a network of 10 monitoring wells and two distant downstream monitoring wells. The wells are cased and up to 150 m deep. However, no observations were made during the past 5 years.

The surface of the tailings was covered with grasses which are attractive to flocks of sheep as grazing. There is free access of population to the surface of the tailings. The area around this tailings site is cultivated with orchards for apples and stone fruit (plums. apricots etc.) and it was stated that a bioassay program is to commence in the future.

1.2. "Gafurov" tailings

The tailings site at "Gafurov" is located 5 km west of the city of Gafurov. It was in

operation during period 1945-1950, at the same time as the so-called "Experimental hydrometallurgical plant".

This facility is located some 10 km from Degmay and 2000 metres from the mill. The site extends over 5 ha, is approximately 13 meters high and contains some 400,000 tones of residues including tailings, waste rock, and scrap metal and decommissioned machines. The waste rock reportedly contains up to 800 tones of U_3O_8. The cover is apparently sedimentary material comprising gravel and cobble-sized stones and sand in a silt-clay matrix, and is between 1 and 2 meters thick. The heap was constructed on the natural land surface without any special site preparation. The waste was reportedly layered into the heap and it was claimed that selective extraction would be easy to perform if it was decided to try to recover the remaining uranium.

Fig. 1.2. Ghafourov tailings site: Note the proximity of dwellings, the cover appears intact with no obvious erosion features

The site is located adjacent to a main road with blocks of apartments less than 50 m away and a railway station within 150 m (Figure 1.2). There were no signs of abnormal erosion or human or animal intrusion on the surface of the heap. There are no reports of any significant problems with this facility. However, it was reported that there is only a visual monitoring program in place and thus there is no evaluation of possible contamination plumes or ground water impacts. There was some discussion about the general remediation options with the host group. The participants' opinion was divided over the issue of re-processing of the material before finally relocating it.

Currently, these abandoned tailings have the status of a dormant mine. Surveillance of the surface and periodic sequential sampling of radon releases and Gamma dose rate are conducted by "Vostokredmet".

Due to effective ground coverage the condition of the tailings is considered satisfactory, meaning that they have no apparent significant impact on human population around it. Meanwhile, these tailings are located near a residential area, and therefore it is necessary to conduct regular observations regarding the exhalation of radon in aerosols and the content of radon decay products in atmospheric air. Simple observations are needed at the surface of tailings with selected atmospheric air pump sampling to evaluate possible contamination with the radon decay products.

1.3. Degmay tailing

Degmay tailing was in operation during the period from 1963 to 1993. It is located in the Ghafourov region on the Degmay hill, 1,5 km away from the nearest settlement (Guzyen) and approximately 10 km from the city of Khujand. This facility is the largest single uranium mill tailings site in Central Asia. It extends over 90 ha and holds about 20 million tones of uranium residue wastes, about 500 thousand tones of sub-economic uranium ores and 5.7 million tones of

vanadium raw material wastes; the estimated total contained activity is about 16000 GBq. The dam was described as being 83% full and approximately 50% of the tailings are derived from imported ores. The site is located on a hill-top site that is a combination of a basin and a saddle. At one end of the facility there is a dam across the basin with a length of 1800 meters and a maximum height of 35 meters.

Artificial plantations of mat rush (*Scirpus validus*) over the surface of tailings were established in the early 90s in order to reduce dust transfer. However, the extent of the rush plantation declined after significant losses of water area down to 2/3 of its initial extent; the surface is now covered with cracks and clefts 1-2 m deep and 30 to 80 cm wide (Fig.1.3)

Figure 1.3. Scheme of Degmay tailings in the surroundings of Khujand and Chkalovsk. Arrows 1 and 2 point place where aerosol and soil samples were taken (Table 1.2)

Residues of uranium extraction were pumped to the tailings dam contained high concentrations of ionic sulfate (average 20 g l^{-1}). As a result of the significant decline in 1992-1993 of the volumes of milling the uranium ores, the transmission of material into the tailings dam declined. During the period 1991 to 2000 less concentrated solutions were pumped into the tailings dam after filtration through strata layers; this resulted in partially cleaner, filtered waters. At the same time it showed that ultimate cleaning was not attained and contaminated ground waters were transferred to Syr Daria River. Until the middle of 90s the surface of tailings was partially covered with water, but later the water gradually dried out and the tailings surface became completely dry by the year 2000. It then became covered with cracks that intensified the exhalation of radon and increased the risk of erosion of the surface and increases in dusting by the wind.

According to the data obtained during the IAEA mission of 2006 the high gamma dose rates measured on the tailing surface (4.5-20 μSv·h^{-1}) were significantly higher than the reasonable safety levels permitting public access to the area.

At the other end of the facility a small earth dam creates a small basin in the saddle area.

The maximum depth of tailings was stated to be 20 m (Fig. 1.4). Above the saddle the land is being used as a municipal landfill. Seepage waters are reportedly collected from the toe of the dam and pumped back to the main reservoir. This system was not seen during the visit and there was no evidence of any pump-back flow. The site was freely accessible there being no gates on the access track with only one warning sign remaining in place and sheep grazing across the tailings area. There was clear evidence of human intrusion into the tailings where people had been excavating to remove scrap metal for sale.

Fig. 1.4. Degmay tailings site: looking towards the overflow basin. Note municipal landfill on hill at left background. Close up of area of human intrusion and site of digging for scrap metal.

The main spectrum of natural radionuclide in technogenically increased concentrations, which are characteristic for tailings, consists of the isotopes of uranium, thorium, radium and their decay products, such as ^{210}Pb and ^{210}Po. The results of analysis of tailings material and aerosols sampled in different locations of tailings were obtained by the laboratories in Ukraine as part of analyses conducted for the IAEA (Tables 2, 3 and 4). Isotope contents were measured at the UHMI on the samples collected during the IAEA expert's mission.

In accordance with the classification used in the Russian Federation (Radiation Safety Norm 99), used as a basis for Radiation Safety Norms in Tajikistan, the tailings materials having such levels of alpha-active natural radionuclides in technogenically-increased concentrations belong to the category of low-level radioactive wastes requiring regulatory control.

Table 2. Activity (Bq kg^{-1}) of natural radionuclides in the samples of tails, collected at the territory of Degmay tailings

№	Sampling location	^{238}U	^{226}Ra	^{230}Th	^{210}Pb	^{210}Po
1	Sample 1 (Fig. 3.4)	980 ± 100	7620 ± 580	15600 ± 1700	14600 ± 1070	13200 ± 1320
2	Sample 2 (Fig. 3.4)	820 ± 80	7250 ± 560	11165 ± 1240	10140 ± 740	12350 ± 920

Guidelines of the IAEA RS-G-1.7 define that natural radionuclides having the above concentrations in a mixture significantly exceed the figures for activity concentrations of natural radionuclides, which can be exempted from regulatory control. Therefore, the region affected by the tailings via the main pathways of their migration through ambient air and ground water

should be subjected to regular monitoring observations and the site should be controlled.

The surface of tailings is not covered, thus allowing a significant constant radon exhalation from the tailings. Exhalation of radon -222 into the atmosphere is sufficiently increased after drying of the tailings surface, especially in parts of the tailings pond where cracks, some reaching to a depth of over two meters and having a width of 20 to 40 cm, occur. The outdoor radon concentration in the air over the tailings surface during the summer time, when IAEA experts visited the site (under windy condition), was observed to be in range of several hundreds up to 1000 Bq/$m^{3.}$ Exhalation of radon-222 was found by direct measurements in June 2006 at different places to vary from 10 to 60 Bq m^2 c, which is significantly higher that the recommended safety level in case of covered surface of the tailing in Tajikistan (1 Bq m^2 c).

Depending on the meteorological conditions and parameters of atmospheric stability the air masses with high concentrations of radon and daughter decay products could spread over a distance of a few kilometers from Degmay tailings.

The volume activity of ambient radon concentration over the tailings site (observed under windy conditions when the dilution in the air is rather high) also increases considerably the mean background value of Rn concentrations in this area (Table 3).

This result suggest that there might be a problem which could be more acute than previously estimated, because this flow of radon into the ambient air may create high concentrations of decay products such as ^{210}Po and ^{210}Pb in the air and atmospheric precipitation, which in turn could remain in the ambient air and/or become deposited on agricultural lands. Dispersion of the radon decay products by the airflows may contribute to the spread of soil surface contamination into the adjacent areas. Thus, observation well No.18 shows in the surface soil layer behind the tailings pond a ^{210}Pb content of 98 ±14 Bq·kg^{-1} and a ^{210}Po content of 62 ±16 Bq·kg^{-1} this is twice the mean background level of these radionuclides in local soils.

This may be evidence that contamination from the radon decay products of ^{210}Pb and ^{210}Po has occurred in the area adjacent to the Degmay tailings. Therefore, it is necessary to consider a new program of observations with focus on the contamination of ambient air (aerosols) with the above radionuclides, and to assess dusting and the effect of wind dispersal on distribution of radionuclides from the tailings through the air.

Table 3. Gamma-dose rate and Radon exhalation measured during IAEA expert mission at the Degmay uranium tailing (June 2006). Wind 7 m s^{-2}

№	**Locations (See Fig 3.3.)**	**Gamma-dose rate,** μSv·$hour^{-1}$	**Outdoor Rn-222** **Bq·m^{-3}**	**EEVA Rn-222,** **Bq·m^{-3}**	**Rn –exhalation,** Bq m^2·c^{-1}
1	1a	3,9-4,0	102±24	5,2	9,18±2,75
2	1б	18,0-20,0	321±68	8,15	65,5±19,7
3	2a	6,5-7,0	187±36	15,85	50,8±16
4	2б	4,5-5,0	207±57	12,75	31,4±9,4
Regional background		**0,2-0,3**	**15-20**		

Independent measurement carried out during spring period by P. Stegnar and NATO project partners from SE "Vostokredmet" show that at some parts of Degmay tailing the ambient concentration of Rn-222 near soil surface reached 1000 Bq·m^{-3} .

Currently the surface of tailings is not covered and the site is surrounded by a reinforced concrete fence; however, access of people and livestock to the tailings is not prevented. Dusting

from the uncovered surface of the tailings may become a serious problem. Measurements of the activity of the aerosols over the tailings surface are not available. Collections of aerosols (dust) from the ambient air in large volumes up to 300 m^3 was conducted in June 2006 at two plots on the tailings. Air filtering devices were arranged at the height of 0.5 m above the ground. Aerosols were sampled on large diameter Petri filters and the collection time averaged 3 hours. The filters were measured after combustion by a semi-conductor gamma-spectrometer.

The results are shown in Table 1.4 and compared with the data for the same period from the locations of Chkalovsk and Taboshar. Dusting from the tailings is a major concern with average wind velocity often exceeding 15m/sec. Experiments with artificial coatings of the tailings surface using latex based and similar materials were tested for prevention of dusting, however without any long-lasting effect.

Table. 4. Aerosol activity in air samples taken at the tailing sites (06-15.06.2006)

Location	Volume ($м^3$)	Aerosols activity , 10^{-5} Bq/m^3											
		^{238}U		^{226}Ra		^{210}Pb		^{228}Th		Be-7 *		K-40	
			+/-		+/-		+/-		+/-		+/-		+/-
Taboshar, U-Pit	430	**1.8**	**0.8**	**1.9**	**0.5**	**47.5**	**3.4**	**0.5**	**0.2**	**421**	**11.2**	**10.4**	**0.9**
Degmai 1 (Fig 3.3)	220	**3.4**	**1.4**	**40.9**	**1.7**	**125**	**6.3**	**5.8**	**2.3**	**447**	**20.8**	**20.2**	**1.7**
Degmai 2 (Fig 3.3)	300	**4.6**	**1.8**	**33.2**	**1.5**	**92.4**	**4.6**	**4.6**	**1.8**	**450**	**23.0**	**35.2**	**1.9**
Chkalovsk, HMP	350	**15.6**	**2.2**	**4.8**	**0.6**	**12.9**	**6.3**	**0.5**	**0.2**	**485**	**19.5**	**12.7**	**1.1**

The screening data show that, Degmay tailings is a potential source of dispersion of natural radionuclides of increased concentrations and it may have a negative impact on the human population in the nearby settlement in case of people have access to this territory, mainly because high gamma dose rate of expose and ambient Rn concentration in the air, which will create main contribution to the human dose exposure. It should be considered if an evaluation of the effective individual radiation dose to the critical groups of the local population needs to be carried out.

During the IAEA expert mission the condition of the groundwater observation network was assessed. There have been no observations of the ground water dynamics and contamination carried out around Degmay during the past 10 years. Most of the wells are unserviceable for observation of the contamination movement and will require reconstruction or replacement (Fig.3.5). Therefore, the assessment was done based on archive data of SE “Vostokredmet”.

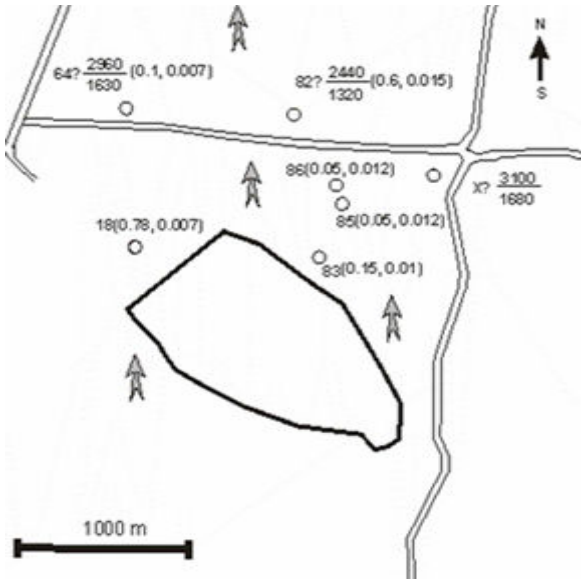

Fig. 1.5. The groundwater observation wells at Degmay tailings sites and its vicinity

The nearest settlement is a village about 1500 meters away from the tailings dam. The drinking water supply used by the villagers comes from wells. Water from the wells is also used for irrigation purposes. The wells are monitored. The agricultural activities come as close to the site as 200 m. Livestock may also be grazing vegetation on the tailings site. The river is about 3500 m away from the site and directly in the downstream flow path of any material washed out from the dam. The underground pathway for water to the river has reportedly been determined to be 8000 m.

In the previous studies carried out by SE «Vostokredmet» it was revealed that there is a significant contamination of ground waters with sulfate ions, thus implying a possible contamination with radionuclides from the accumulated tailings materials. The main macro-ions of technogenic contamination, including the radionuclides are within the sulphate plume characterized by increased mineralization. The spatial distribution within the plume is in direct relationship to the degree and range of formation of the contaminants.

This peculiar property of ground water contamination was applied by the specialists of SE “Vostokredmet” for studying the aureole of distribution of the contamination using geophysical methods of electro-sensing (Bezzubov et al, 2005). The results obtained with this method in 1994 and later in 2003 are the only observations; these can predict dispersion of the polluted groundwater front on the way toward the river. The potential propagation of the groundwater contamination was estimated using mathematical modeling. This evaluation (Koptelov et al., 2005) show that in recent times the contamination plume has gone from the tailings on the surface and is moving toward the Khoja-Bakyrgan and Syr Daria Rivers. The contamination plume consists of several lenses containing highly concentrated sulphate and soluble uranium.

The specifics of the situation need a more detailed analysis. According to model forecasts the contaminated ground water from the tailings site will discharge into Syr Darya and subsequently may be used by the local residents for irrigation of orchards and horticultural crops. Under these circumstances it would be prudent to evaluate and predict the development of the ground water quality near the Degmay tailings pond from the point of view of a potential risk to humans using the water for irrigation (Fig.1.6).

Fig. 1.6. Exploitation wells used irrigation and flooded rice paddies in the area of Degmay.

In the surroundings of the tailings it is necessary to undertake monitoring of the chemical contamination of ground waters, because the crushed ores, which were disposed of here over a long period of time, have high contents of ionic sulphate (from 0.5 to 20 g/l). In earlier studies, the status of the ground water contamination with sulphates due to infiltration through the tailing body and its migration towards the Syr Darya River was evaluated by "Vostokredmet" using mathematical models. The results of modeling show that the front of the contamination plume extends toward the river and the mineralization of the water falls significantly with distance from the tailings. The ground water near the tailings pond must be considered unfit for drinking purposes and related uses. The existing wells around the tailings pond are unsuitable for reliable monitoring of the spread of the contamination in the groundwater system beneath and around the tailings pond; most of them would require overhaul and, subsequently, proper maintenance. Any new monitoring boreholes should be designed taking into account the location and depth of the contamination plume. In case of any continued assistance of the IAEA in this matter, the Tajik partners would welcome SE "Vostokredmet" receiving advice on the proper installation and instrumentation of the monitoring wells, introduction of methods of quality control and estimation of the movement of the contamination plume from the Degmay tailings pond towards the Syr Darya River.

Rolls-Royce successful modernization of safety-critical Instrumentation and Control (I&C) equipment at the Dukovany VVER 440/213 Nuclear Power Plant, based on SPINLINE 3 platform.

Presentation:

poster

Authors:

Rebreyend, P. (1); Burel, J.-P. (1); Spoc, J. (2); Karasek, A. (3)

1 - Rolls-Royce Civil Nuclear SAS, France

2 - Skoda JS, Czech republic

3 - CEZ, Czech republic

Description:

Rolls-Royce has provided on-time delivery of a substantial safety-critical I&C overhaul for four Nuclear reactors operated by Czech Republic utility, ČEZ a.s. This nine-year project is considered to be one of the largest I&C modernization projects in the world.

The Dukovany VVER 440 I&C modernization project and its key success factors are profiled in this paper. The project is in the final stages with the last unit to be completed in 2009. Beginning in September 2000, the project is in compliance with the initial schedule.

Rolls-Royce has been designing and manufacturing I&C solutions dedicated to the implementation of safety and safety-related functions in nuclear power plants (NPPs) for more than 30 years. Though the early solutions were non-software-based, since1984 software-based solutions for safety I&C functions have been deployed in operating NPPs across France and 15 other countries. The Rolls-Royce platform is suitable for implementation of safety I&C functions in new NPPs, as well as in the modernization of safety equipment in existing plants.

ČEZ a.s. is a major electricity supplier for the national grid. At Dukovany, ČEZ a.s. operates four units of VVER-440/213-type reactors producing one quarter of ČEZ a.s. electricity production. The first of these units was connected to the grid in 1985.

Since the year 2000, the nine-year modernization program has been underway at Dukovany, at a cost of more than 200 million Euros. The equipment replacement was implemented during regular, planned outages of the original equipment and systems.

After an international bidding phase, ČEZ a.s. awarded a contract to Škoda JS for general engineering and project management. Individual subcontracts were then signed between Škoda JS and a consortium between Rolls-Royce and Areva for modernization of the safety systems, including the Reactor Protection System (RPS), the Reactor Control System (RCS), and the Post-Accident Monitoring System (PAMS).

Two digital I&C platforms were selected with Rolls-Royce providing the primary technology for use in the modernization of the safety I&C. The additional platform was provided by Sagem for implementation of the Post Accident Monitoring System (PAMS). This solution offers hardware and software diversity and it provides advantages aimed at decreasing the probability of failure during the performance of safety actions and increasing the overall plant reliability thus reducing the workload in test and maintenance activities.

About Rolls-Royce

Rolls-Royce is a global business providing integrated power systems for use on land, at sea and in the air. The Group has a balanced business portfolio with leading market positions.
Rolls-Royce has a broad range of civil nuclear expertise, including work related to licensing and safety reviews, engineering design, supply chain management, manufacturing, installation and commissioning of the nuclear island systems and equipments, as well as operational management and through life support. Rolls-Royce has a world-class reputation as a power

systems provider and has unique experience in the nuclear market.

NUCLEAR COMBINED HEAT AND POWER - ANALYSES OF HOT WATER PIPELINE BREAKS IN A SERVICE TUNNEL WITH APROS SIMULATION SOFTWARE

T. HENTTONEN, M. PAANANEN
Fortum Nuclear Services Ltd.,
P.O. Box 100, 00048 Fortum, Finland

ABSTRACT

This paper presents a computer model and simulation results for a long-distance heat transport system. The system can be used e.g. to transport heat from a nuclear power plant with combined heat and power (CHP) production. CHP production is considered for new build NPP projects in Finland.

Emphasis is on the environmental conditions during a hot water pipeline break in a service tunnel. The modelled pipeline system is designed to transport 1000 MW of heat over a distance of 77 km for district heating purposes. The hot water pipeline is assumed to be 1200 mm diameter with a water temperature of 120 °C. Cooled water returns with a temperature of 55 - 60 °C in a similar 1200 mm diameter pipe. Both pipelines are installed to a service tunnel which is excavated into bedrock and divided into 2 kilometres long compartments.

Both the 77 km long pipeline and the tunnel are modelled with Apros simulation software. A leak is modelled from the pipeline to the tunnel and the results are analyzed. This paper includes three different leak sizes (1 %, 10 % and 100 % of the pipeline's cross-sectional area). The leaks are calculated with water temperatures of 95 °C and 120 °C in the pipeline. Apros calculates dynamically the phenomena inside the pipeline with two-phase 6-equation calculation model. The tunnel conditions are calculated with a lumped parameter model.

The size of the leak has a substantial effect on the leak's consequences in the tunnel. Also the water temperature in the pipeline influences the results strongly. If the water temperature is over 100 °C, a considerable amount of the water boils as it leaks to the tunnel. The boiling of water makes the conditions in the tunnel much more severe than they would otherwise be. If there is a substantial flow out of the tunnel, the air in the tunnel can be replaced by hot steam. Obviously, this can mean hazardous conditions in the tunnel.

1. Introduction

Nuclear energy has been used for district heating in several countries both in dedicated nuclear heating plants and in combined heat and power (CHP) plants. Fortum is applying to build a new nuclear power plant (NPP) in Loviisa, Finland. It has been suggested that this new NPP could be a CHP plant. The heat produced in Loviisa NPP could be utilized for the district heating of Helsinki metropolitan area [1,2]. This would require transporting of heat over a distance of approximately 77 km. To our knowledge, the longest existing delivery distance so far for nuclear district heating is 24 km in Slovakia [3].

This kind of a long-distance heat transport system transporting heat over 77 km is studied in this paper. The transported heat power considered is 1000 MW. Modelling is an important tool in designing such a system. Modelling and simulations are especially useful when the behaviour of such a large-scale system under transients is examined. Tripping of pumps or leaks from the circuit into the surrounding tunnel can cause safety risks which can be examined with an extensive model of the system.

The diameter of the pipeline was chosen to be 1200 mm. A large enough diameter is required to restrict the flow velocity and pressure losses. It is essential to make sure that this pipeline works reliably for the designed lifetime of 60 years. Mechanical failure is one example of failure mechanisms that may result in a pipeline break. These mechanical failures can be, however, avoided with high certainty if appropriate maintenance and inspection measures are taken. This paper studies the conditions inside the service tunnel in this highly unlikely pipeline break.

In our case, the 77 km long pipeline is assumed to be located in an excavated tunnel in the solid bedrock. The tunnel guarantees a reliable physical protection for the pipeline. Operations and maintenance works can be easily done in the tunnel, as it is large enough for a service vehicle. Tunnel solution also minimizes the harms to the landscape and the environment.

The environmental conditions inside the service tunnel are important to know in order to guarantee the safety at work for the service crew working inside the tunnel. Detailed study of the environmental conditions can be used to reveal possible risks and can be used e.g. to create evacuation plans for the service crew.

This paper presents a computer model for a long-distance 1000 MW heat transport system and simulation results for different transients. Safety of the heat transport system is also discussed and ways to improve it are presented.

2. Calculation model

2.1 Apros simulation software

Heat transport system is modelled with Apros (Advanced Process Simulation Environment) simulation software. The pipeline model includes pipeline, pumps, valves, heat accumulator, tunnel and some automation. The pipeline model is presented in detail in reference [4].

The same Apros calculation model included the pipeline with six-equation calculation for the water and steam as well as the tunnel modelled with lumped parameter calculation. The principle of the modelled pipeline circuit is seen in Figure 1. One dimensional 6-equation model is used for the water and steam in the circuit.

2.2 The pipeline

The pipeline is modelled to both directions in the circuit (i.e. hot and cold leg). Pressure losses and heat losses in the pipeline are included in the solution. The pipeline is modelled as a steel pipe with a diameter of 1.2 m and a polyurethane insulation layer with a thickness of 100 mm. Pipeline is divided into calculation nodes and the length of the nodes is limited to a maximum of 200 m. An elevation profile for the pipeline is modelled. The pipeline is thought of as being in an underground tunnel and the elevation profile of the tunnel determines the profile of the pipeline. The profile follows a realistic elevation profile scenario of the tunnel. Elevation difference between the lowest-lying and highest-lying points in the pipeline is almost 90 m.

Four pump stations are modelled in the pipeline as can be seen in Figure 1. Three of these pump stations include a pump in both hot and cold leg and one pump station has only one pump in the NPP end of the cold leg. All the pumps are identical and operated at the same rotation speed. This gives a symmetric pressure head in the pipeline.

There are also sectioning valves included in the modelled pipeline at 2 km intervals. These valves can be used to separate the circuit in 2 km sections in the case of a leak. A heat accumulator is modelled in the city end of the circuit. The accumulator operates in atmospheric pressure and is connected directly to the transport pipeline. The district heating

circuit of the city is separated from the accumulator by heat exchangers. The purpose of the accumulator is to store heat and to keep a constant pressure in the circuit. The liquid volume of the accumulator was chosen to be 50 000 m^3.

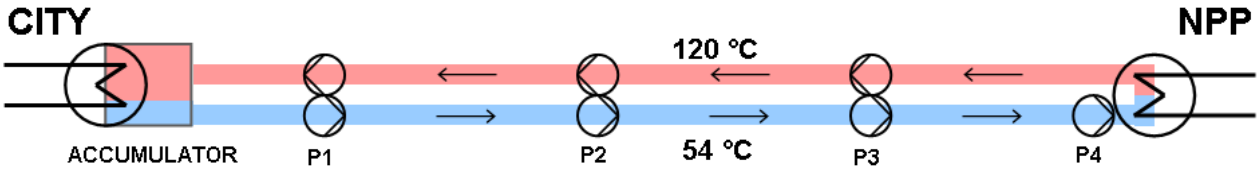

Fig 1. A greatly simplified representation of the heat transport circuit. There are two 77 km long pipelines and 7 pumps arranged in 4 pump stations in the model.

2.3 The tunnel

A 2 km section of the 77 km long underground tunnel is modelled. This section is separated from the rest of the tunnel by fire doors. The cross-sectional area of the tunnel is 30 m^2. The elevation of the tunnel floor is 42-62 metres below sea level. The tunnel has a slope of 2 %. Each end of the 2 km long tunnel section includes a 2 m^2 ventilation shaft which is connected to the environment and remains open at all times. The nodal structure of the modelled tunnel section is shown in Figure 2.

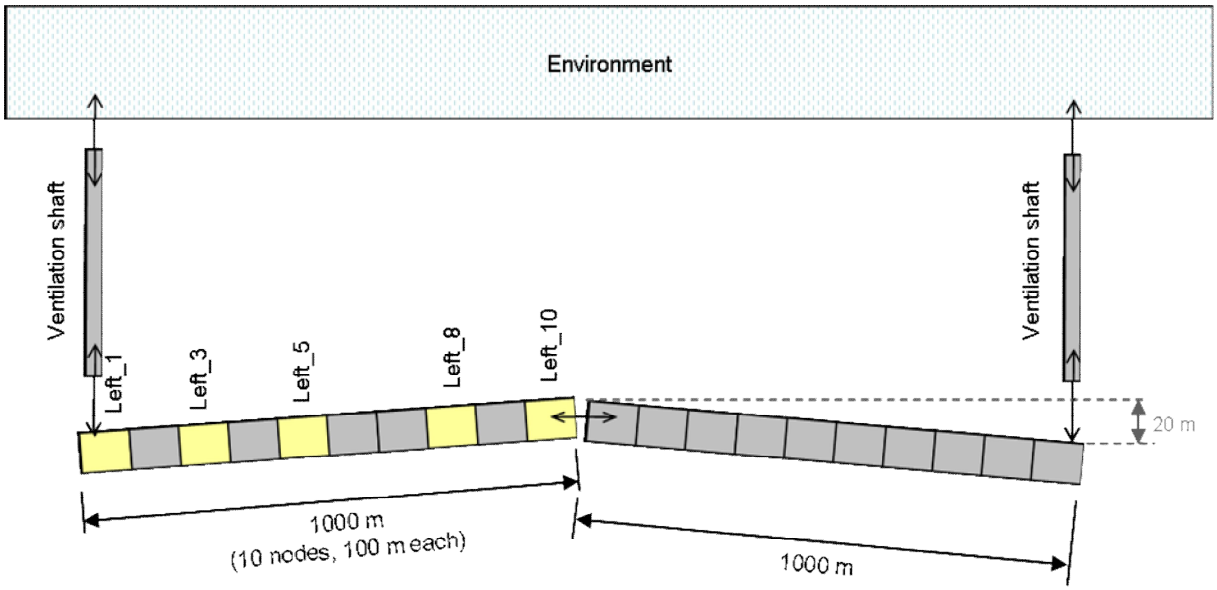

Fig 2. The principle of the tunnel section. The tunnel consists of 20 calculation nodes each 100 m long.

The tunnel is divided into 20 nodes each 100 meters long. Nodes are connected with gas and water branches and also heat structures. The principle and the geometry of a single node can be seen in Figure 3. The ventilation shafts are modelled with one calculation node each.

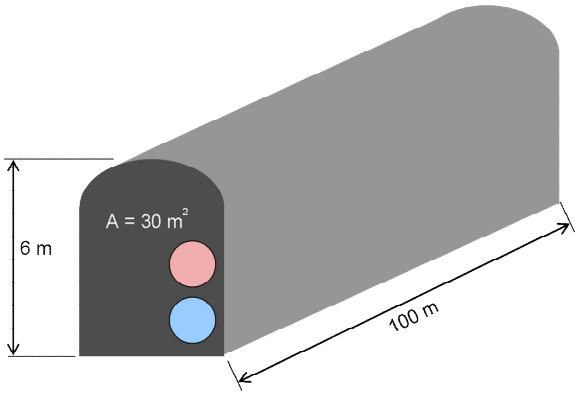

Figure 3. The principle of one node in the tunnel.

Walls, floors and roofs are modelled with 2 m thick heat structures. 90 % of the heat structures are plain rock and the rest 10 % have 0.2 m shotcreted concrete on top of a 1.8 m thick layer of rock. Initial conditions in the tunnel are: temperature of the gas region and heat structures is 15 °C and relative humidity is about 60 %.

3. Simulations

Simulated properties of the heat transport system in steady state are shown in Table 1. The pressure profile in the circuit in steady state is shown in Figure 4. The effect of hydrostatic pressure is removed from the pressure profile (i.e. the pressure is normalised to sea level). There is also a 25 bar reference pressure curve and also 120 °C and 50 °C water boiling limit pressure curves in Figure 4.

Mass flow	3580	kg/s
Volume flow:		
• cold leg	3.63	m^3/s
• hot leg	3.79	m^3/s
Flow velocity:		
• cold leg	3.21	m/s
• hot leg	3.35	m/s
Inner diameter of the pipes	1200	mm
Hot water temperature	120	°C
Cold water temperature	54	°C
Transferred heat power	1000	MW
Power of circulation pumps:		
• cold leg	5.8	MW/pump
• hot leg	5.5	MW/pump
• total power	39.7	MW
Heat losses from the pipes	11	MW

Tab 1. Basic information of the modelled circuit in steady state.

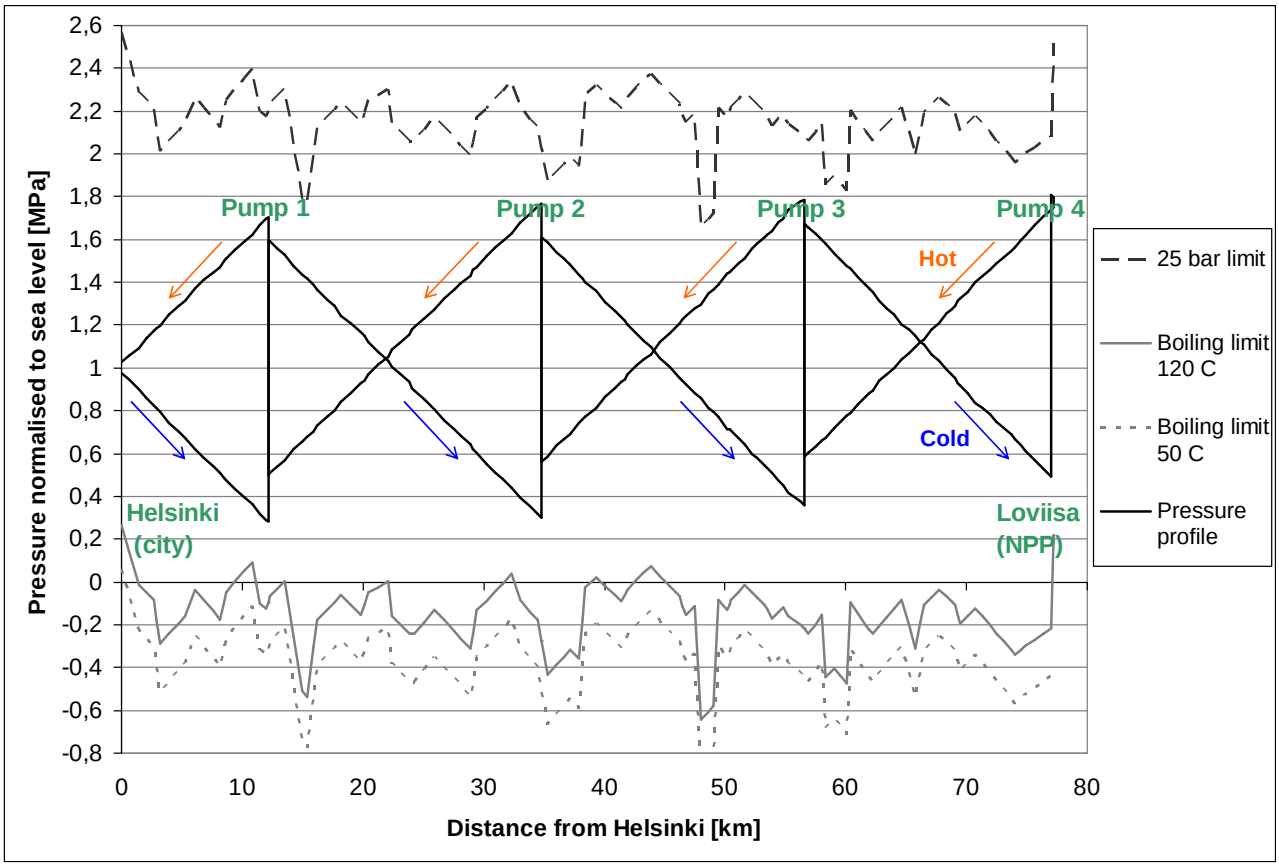

Fig 4. Simulated pressure profile in steady state. Hydrostatic pressure is removed from the profile. Pump stations' locations and pressure limits are also shown in the picture.

Three different leak sizes were simulated: 1 %, 10 % and 100 % of the pipeline's cross-sectional area. Also the temperature in the circuit was varied: 95 °C, 120 °C and 150 °C leak temperatures were studied. However, the most important aspect to consider is whether the temperature is above 100 °C or not. If the temperature is above 100 °C, much of the leaking water will boil inside the tunnel and lots of steam is formed inside the tunnel. Therefore leaks cause remarkably higher risks inside the tunnel when the temperature is above 100 °C. Detailed results in this report are shown only for 120 °C water leaks. The leak was connected to node "Left_10" as seen in Figure 2. That node is almost in the middle of the 2 km tunnel section.

The pressure inside the pipeline falls close to the leak point - the more the bigger the leak. Eventually the pressure drop extends to the whole pipeline. Since it is not feasible to operate the heat transport system after a major leak has occurred, all the pumps were stopped in the simulation 10 s after the beginning of a leak. Also all the sectioning valves in the circuit were closed gradually after the leak to limit the consequences. There were sectioning valves every 2 km in the circuit. Closing of the valves was simulated to be three-staged - slowing down towards the end of the closing - and to have a total closing time of 10 minutes. Obviously, closing of the sectioning valves does not stop the leak. In a separated 2 km section of a pipe with 1.2 m diameter there is 2260 m^3 water. Even though the leak cannot be stopped, it is important to limit it.

4. Results

The effects of a leak were strongly dependent on the leak size, as expected. The simulated leak mass flow for 1 %, 10 % and 100 % leaks is shown in Figure 5. Critical mass flow limits the flow from the pipeline into the tunnel considerably. The pressure in the tunnel increases

when steam is formed. The increased pressure can cause very fast flow out of the tunnel. The flow velocities in the ventilation shaft are shown in Figure 6.

High flow velocities - up to 100 m/s and above - obviously create a safety risk in the ventilation shaft. The pressure increase and flow out of the tunnel also means that some of the air in the tunnel is replaced by hot steam. This happens especially in the vicinity of the leak. All the consequences of a leak are worse the bigger the leak is. Some simulation results are gathered in Figure 7. Gas temperature and steam volume fraction in the tunnel are shown in 5 different nodes for 1 %, 10 % and 100 % leak.

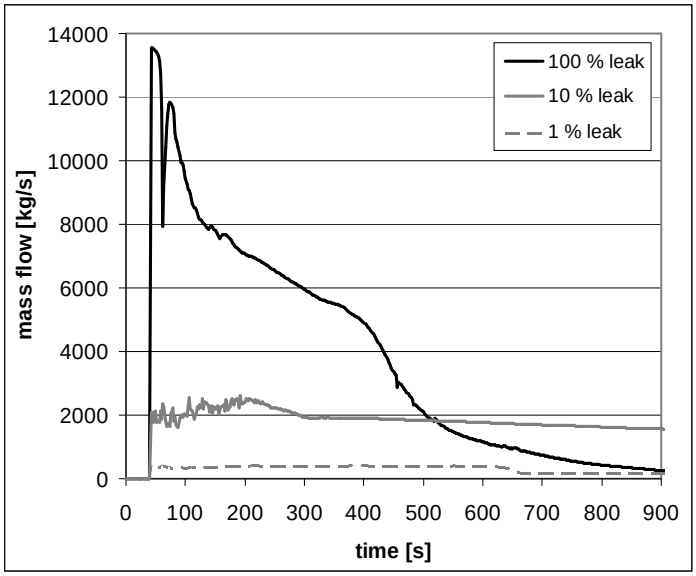

Fig 5. Simulated leak mass flow for three different leak cases (1 %, 10 % and 100 % leak).

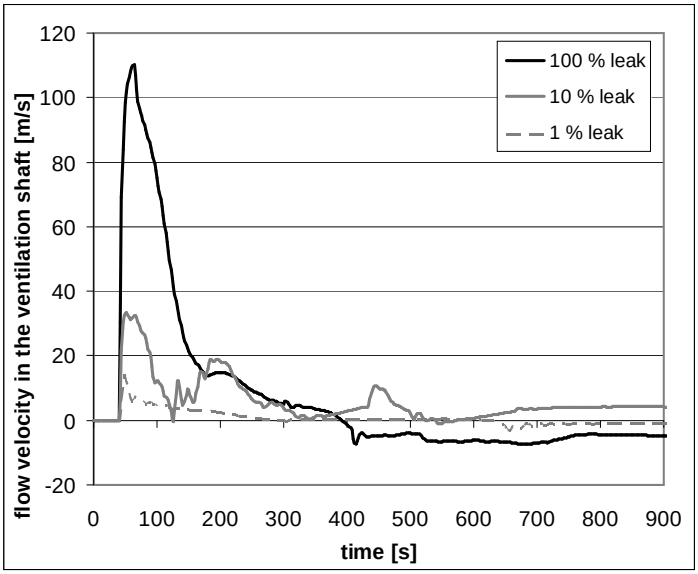

Fig 6. Simulated flow velocity in the ventilation shaft for three different leak cases (1 %, 10 % and 100 % leak). The flow area of the shaft is 2 m^2.

A leak of any size poses a risk if there are workers inside the tunnel near the leak. However, if the leak is relatively small (1 %), the severe conditions remain quite local - 200 m away from the leak the conditions remain tolerable in 10 minute time scale as can be seen in Figure 7. If the leak size is larger, the conditions in the tunnel become unbearable more rapidly and further away from the leak. If there is a full 100 % leak, the conditions can get dangerous in the entire 2 km tunnel in a few minutes. As a precaution, it would be good to minimize the time spent by the maintenance staff in the tunnel when there is over 100 °C water in the pipeline. It should be noted, though, that a major leak is a very improbable event

in a well constructed, maintained and operated pipeline. Another question concerning a leak is how well the system (e.g. fire doors and pipeline support) can handle the consequences.

Water level and water temperature on the tunnel floor is shown in 5 different nodes for 10 % leak in Figure 8. The tunnel had a slope away from the leak in the simulation. Therefore, the highest water level is eventually accumulated 1 km away from the leakage in the end of the tunnel. Water temperatures remain high in the entire tunnel for a long time.

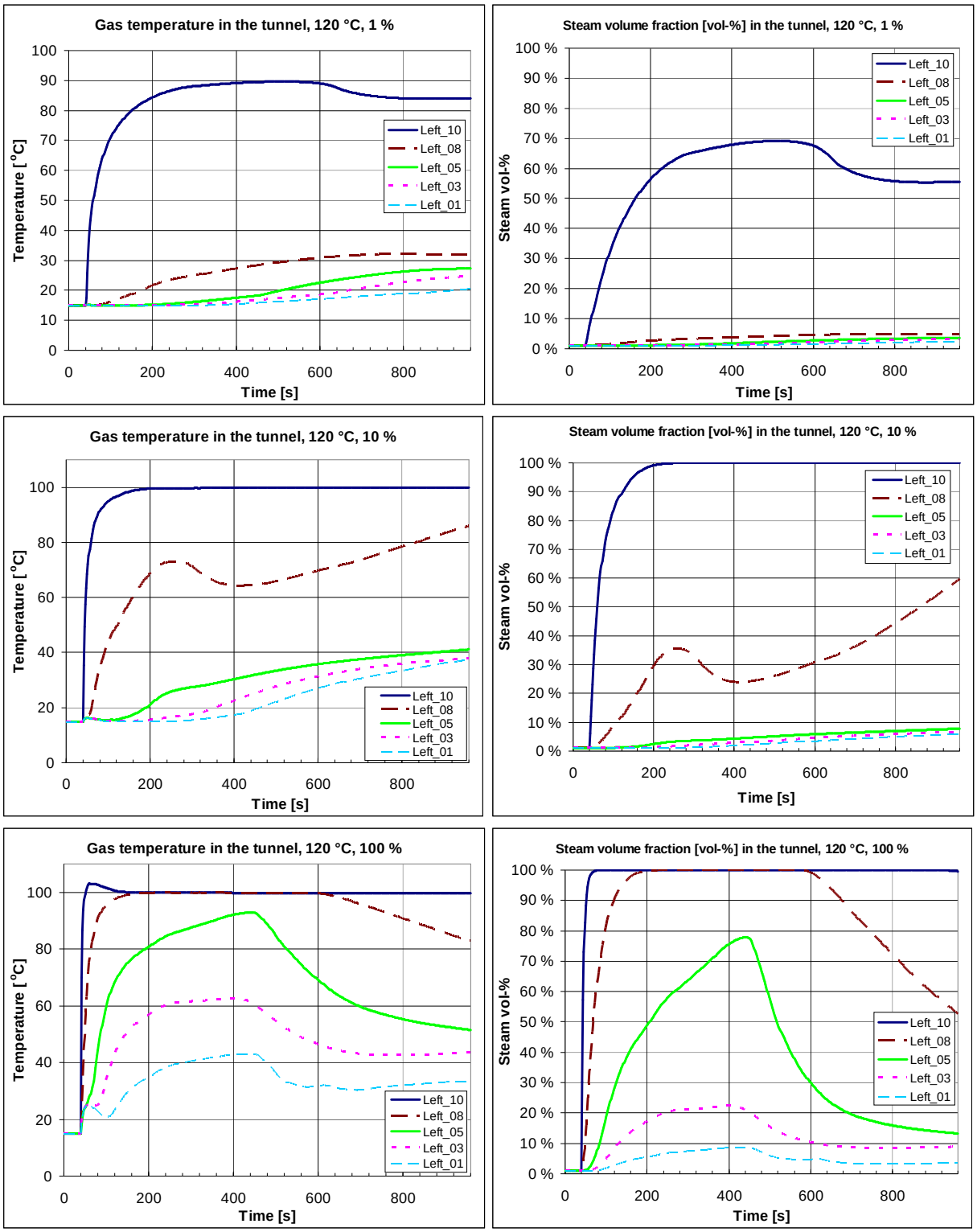

Fig 7. Gas temperature and steam volume fraction in 5 different nodes inside the tunnel for the simulation cases of 1 % (top), 10 % (middle) and 100 % (bottom) leak. The leak begins at time 60 s.

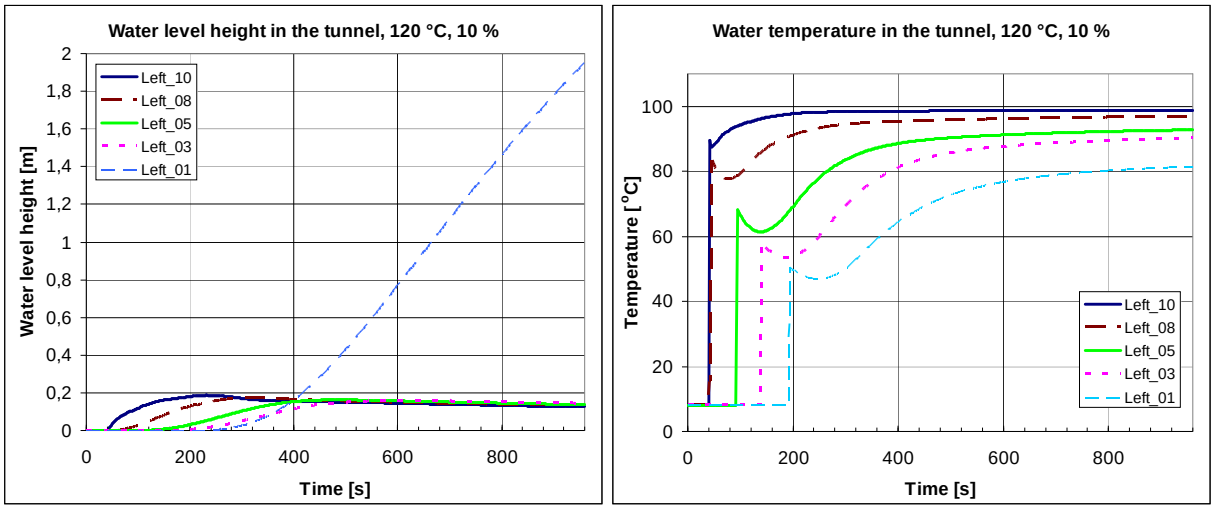

Fig 8. Water level and water temperature in 5 different nodes inside the tunnel for the simulation case of 10 % leak.

5. Conclusion

The pipeline and a 2 km section of the tunnel were successfully modelled with Apros simulation software. The whole heat transport system was modelled dynamically and various leak transients were simulated. Water having temperature over 100 °C boils when it leaks into the tunnel and can thus cause challenging transients. The bigger the leak, the faster and further away from the leak the conditions inside the tunnel become dangerous, as expected. The model can be used to study transients and improve the safety of a heat transport system. The system under investigation was a nuclear CHP heat transport system but the obtained results are also applicable to any other type of service tunnel containing hot water or steam pipeline.

6. References

[1] Fortum Power and Heat Oy. 2009. Application for a Decision-in-Principle Concerning the Construction of a Nuclear Power Plant Unit – Loviisa 3

[2] Bergroth, N. Large-Scale Combined Heat and Power (CHP) Generation at Loviisa Nuclear Power Plant Unit 3, Proceedings of the 8th International Conference on Nuclear Option in Countries with Small and Medium Electricity Grids, Dubrovnik, Croatia, 16-20 May 2010

[3] IAEA. 1998. Nuclear heat applications: Design aspects and operating experience. IAEA-TECDOC-1056

[4] Paananen, M., Henttonen, T. Investigations of a Long-Distance 1000-MW Heat Transport System with APROS Simulation Software, SMiRT 20 Proceedings, Finland, 9-14 August 2009

NEUTRON TOMOGRAPHY FOR VOID DISTRIBUTION MEASUREMENTS

P. ANDERSSON, S. JACOBSSON SVÄRD, H. SJÖSTRAND

Department of Physics and Astronomy, Uppsala University

Box 516, 751 20 Uppsala – Sweden

ABSTRACT

Neutron tomography has previously been performed using large, stationary neutron sources such as reactors and spallation sources for applications where the object under study can be transported to the source. This paper accounts for the challenges met when applying neutron tomography using a portable accelerator driven neutron generator, which is required when studying non-transportable objects. In general, portable sources offer significantly lower neutron yields than stationary sources, implying the need for either longer measurement times or highly efficient measurement and/or analysis procedures.

The particular application investigated here is the mapping of steam distributions in water (void distribution), which is of high importance for the performance of nuclear fuel assemblies in boiling water reactors (BWR). The void distribution cannot be measured directly in a reactor core, so instead various electrically-heated thermal-hydraulic test loops are used. In these loops, void correlations can be determined in full-size fuel-assembly models, such as FRIGG in Sweden and DESIRE in Holland, but measurements are also performed in smaller, less complicated geometries. Previously, gamma tomography has been used to measure the void distribution in the FRIGG loop. However, improved capabilities to map the void distribution can be expected using neutrons because of their higher sensitivity to water relative to metal structures, as compared to gamma rays. At the same time, neutrons as probe also give rise to some challenges, such as high background from scattering.

This paper investigates the possibility to use neutron tomography at axially symmetric objects such as the HWAT test loop in Sweden, where an annular two-phase flow of water/void is confined and heated by a steel cylinder. Monte Carlo simulations of the HWAT geometry and a suggested measurement setup have been carried out, using the particle transport code MCNPX. A reconstruction technique which exploits the symmetries in the test loop has been developed, making it possible to reconstruct the internal void distribution from one single projection. A reconstruction is presented, which is based on simulated data corresponding to a 13-min measurement using a DT source emitting $2 \cdot 10^9$ neutrons/s. The reconstruction offers a radial view of the local void fraction in 10 annular sections of HWAT, with uncertainties between 2 and 5 void percent units.

1. Introduction

1.1 Neutron tomography

Tomography is a diagnostic technique where a cross section of an object is depicted by means of external measurements. In neutron tomography, neutrons are transmitted through the object, whereby its internal attenuation distribution can be deduced. Previously, gamma tomography has been applied for void distribution measurements in thermal-hydraulic test loops [1]. However, as compared to gamma, neutrons have low reaction cross sections in the containing structures of metal relative to the cross sections in water. Accordingly, using neutrons as a probe may be beneficial.

Neutron tomography has been demonstrated as a method for non-destructive measurement by various installations, such as SINQ, FRM-1 and BER-II. [2] Typically, spallation sources or test reactors are used to create a collimated beam of thermal neutrons. Tomography with portable neutron generators has not been widely utilized and it has even been argued [2] that it is impossible.

One of the main drawbacks of portable neutron generators is the low neutron yield; 10^8 to 10^{10} n/s emitted quasi-isotropically, whereas at a research reactor, the neutron flux can be up to 10^8 n/s/cm^2 in a collimated beam [2]. This makes such sources a superior choice, when available. However, some objects, such as thermal hydraulic test loops, may not be taken to a stationary neutron source, and in this case a portable source is required.

1.2 Void distribution of two-phase flows

Void is defined as the volume fraction of steam in a two-phase flow of liquid water and steam. In a boiling water reactor (BWR), the void goes from 0% in the core inlet to about 70-80% in the core outlet, and detailed knowledge of the void distribution is important for two reasons (1) Liquid-phase water is needed to cool the fuel, and (2) the water molecules moderate the neutrons in the core, making the power locally in the core highly dependent on the local density of the coolant. Because of its great importance to BWR safety and performance, the void distribution in BWR fuel has been studied at several thermal-hydraulics test loops in the world, where the heat transfer of nuclear fuel is mimicked in electrically heated models. The most advanced models are full-scale models of a fuel bundle, but simplified geometries are also used.

This paper relates to the test loop HWAT [3], which has a cylindrical test section with electric heating. The present work focuses on a test section with one cylinder, enclosing the two-phase flow. This geometry is illustrated in fig. 1 a.

2. Applying neutron tomography for void distribution measurements

2.1 Suggested measurement setup

The planned measurement setup, which is under investigation, is illustrated in Figure 1 b. A typical, commercially available, portable DT source is envisaged, emitting monoenergetic neutrons of 14.1 MeV at a rate of $2 \cdot 10^9$ neutrons per second.

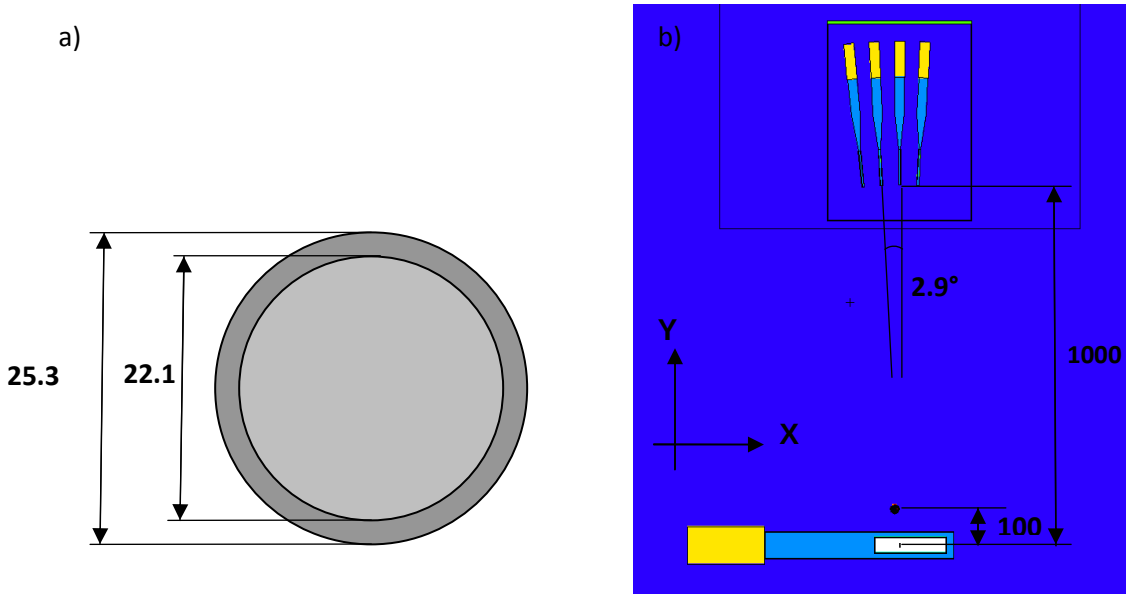

Figure 1. a) The cross section of a test section at the HWAT test loop in Stockholm using one electrically-heated cylinder. Distances are given in mm. Outer, dark-grey annulus represents the steel cylinder containing and heating the two phase flow, which is represented by the inner, light-grey area. b) The MCNPX model of the planned measurement geometry. In the lower part is the neutron source and in the upper part are four detectors with light guides and potomultiplier tubes. The HWAT object can be found just above the neutron source.

The detector array consists of four BC412 plastic scintillators. They are situated at 1 m distance from the neutron generator. All detectors have the same dimensions; 5 mm width, 100 mm height and 100 mm depth. They are placed with an angular interval of 2.9°. The rear ends of the detectors are connected to light guides and photomultiplier tubes (PMT). The HWAT object is situated at a distance of 100 mm from the neutron generator (centre to centre).

2.2 Tomographic reconstruction of the void content

The void distribution may be determined experimentally by measuring the loss of intensity from a radiation source in a number of lines-of-sight through the object, and by applying tomographic reconstruction algorithms. In this section the principles of this procedure is presented.

The local void fraction (α) is derived from the local density (ρ) of the water/void mixture, according to eq. 1.

$$\rho = (1-\alpha)\rho_{liquid} + \alpha\rho_{steam} \qquad \text{(eq. 1)}$$

In the two-phase flow, the local attenuation coefficient (μ) is proportional to the density according to eq. 2,

$$\mu = (2\sigma_H + \sigma_O)N = (2\sigma_H + \sigma_O)_{tot}\frac{\rho}{m_{H_2O}} \qquad \text{(eq. 2)}$$

where σ is the microscopic cross section, N is the number of water molecules per unit volume and m_{H2O} is the mass of one molecule.

By substituting eq. 2 into eq. 1 and rearranging, an expression for the local void fraction is given as a function of the attenuation (eq. 3).

$$\alpha = \frac{\mu_{liquid} - \mu}{\mu_{liquid} - \mu_{steam}} \qquad \text{(eq. 3)}$$

Tomographic reconstruction is normally based on a large number of radiographic projections of the object, where the object has a unique rotation in each projection. However, since HWAT is an axially symmetric object, only one projection is required. This has been demonstrated previously with portable neutron sources [4]. Accordingly, tomography of void distributions can be performed with reduced measurement time as compared to objects of the same size without such symmetry.

The methodology developed in this work uses reference intensities ($S_{m,0}$) of a void-filled HWAT object, which can be recorded separately before the actual measurement. Ideally, the neutron signal intensity (S_m) in the detector in a certain line of sight (m) then relates to the reference intensity with a relatively simple exponential dependence on the integral of the local attenuation coefficient along the line of sight. By introducing pixels (indexed with n) with constant attenuation, the integral is discretized to a sum of the attenuation coefficients of the pixels (μ_n) weighted by the path lengths ($w_{m,n}$) of the lines of sight, through the pixels. This is shown in eq. 4.

$$S_m = S_{m,0}e^{-\sum_{i=1}^{n}\mu_n w_{m,n}} \qquad \text{(eq. 4)}$$

For HWAT, the pixels are annular to exploit the symmetric properties of the test loop, which is mentioned above. Such pixels are here referred to as rixels.

However, in a real measurement setup, the total neutron intensity (I_m) also has a background component (B_m) due to gammas and scattered neutrons, as shown in eq. 5.

$$I_m = S_m + B_m = S_{m,0} e^{-\sum_{i=1}^{n} \mu_n w_{m,n}} + B_m \qquad \text{(eq. 5)}$$

In the equation above, only the total intensities, I_m, can be measured. The path length coefficients, $w_{m,n}$, can be calculated since the measurement setup is known. $S_{m,0}$ and B_m need to be estimated in order to use eq. 5 to determine the internal attenuation coefficients, μ_n. However, since neutrons as a probe are highly scattering, it is not straight forward to estimate the background, B_m. Much of the background will be scattered from metal structures in the object, the detector array and auxiliary equipment, giving rise to a fairly constant background component from these structures, $B_{m,SC}$, for each line of sight. On the other hand, the water in the object also has a high scattering cross section, giving rise to a fluid background component, B_{FC}, which is a function of the amount of water in the two phase flow.

It can be noted that B_{FC} reflects the total change of the total background due to introduction of liquid water in the object: (1) Neutrons scatter more in the liquid water, which increases the background, and (2) at the same time it decreases the neutron signal intensity behind the object, which will decrease the scattering from structures in the detector array. For simplicity, B_{FC} is in this work assumed to be the same in all lines-of-sight and proportional (with the proportionality constant k) to the sum of the attenuation in all the lines-of-sight used in the projection as illustrated in eq. 6.

$$B_m = B_{m,SC} + B_{FC} = B_{m,SC} + k \sum_m \left(S_{m,0} \left(1 - e^{-\sum_{i=1}^{n} \mu_n w_{m,n}} \right) \right) \qquad \text{(eq. 6)}$$

Inserting eq. 6 into eq. 5 gives an expression for the predicted detector intensity as a function of the internal attenuation of the object, see eq. 7. The unknown variables $S_{m,0}$, k and $B_{m,SC}$ are here deduced from separate background calibration procedure, involving measurements of a void filled and water filled object. In this procedure, $B_{m,SC}$ is assumed to be constant and unique for each detector used and a least-squares method is used to fit the variables to resemble the two measured data sets.

$$I_m = S_{m,0} e^{-\sum_{i=1}^{n} \mu_n w_{m,n}} + B_{m,SC} + k \sum_m \left(S_{m,0} \left(1 - e^{-\sum_{i=1}^{n} \mu_n w_{m,n}} \right) \right) \qquad \text{(eq. 7)}$$

Accordingly, for a certain measurement, all I_m are measured, the variables $S_{m,0}$, k and $B_{m,SC}$ are given from the background calibration procedure and the path lengths ($w_{m,n}$) are calculated. Thus, the local attenuation coefficients may be reconstructed according to eq. 7. In the reconstruction procedure, the MATLAB function *fminsearch* is used to iteratively change the numerical values of the attenuation in a model of the local attenuation to find the minimum of the χ^2-sum, which is here the squared sum of the deviations between the measured and predicted intensities, weighted by the inverted variances of the measured intensities.

3. Simulations

The particle tracking code MCNPX 2.5.0 has been used to model and test the instrumental setup described in section 2.1. In the model (shown in figure 1 b), the neutron generator is placed with the ion beam hitting the target in an axis perpendicular to the direction of the detector array to minimize the geometrical blurring due to the neutron-source spot size. A monoenergetic, isotropic neutron source (14.1 MeV) is modelled with an extension of 5 mm (FWHM) in the y- direction (see figure 1) and 0 mm in the x direction. So far, gammas have been excluded from tracking to save simulation time. Each measurement consists of 50 lateral positions, i.e. in total of 200 lines of sights. The data points are separated by 0.533 mm.

For the simulations of the background calibration procedure, leading to the fitting of variables $S_{m,0}$, k and $B_{m,SC}$, the HWAT is filled with water of density 0.74 gcm^{-3} respectively with void of density

0.037gcm^{-3}, corresponding to a pressure of 70 bar. For the void measurement simulation the HWAT model has discrete bins of 0.5 mm width. These bins have a density which is mimicking a local void fraction ranging from 0.05 to 0.3, see Figure 2. The MCNPX F4:N tally is used to extract the energy-resolved neutron flux at each detector and object translation. The data is post-processed to give the recoil proton spectrum and the count rate, where the latter is estimated assuming an energy threshold of 6.4 MeV.

4. Reconstructed void distributions

The result of the MCNPX simulations has uncertainties corresponding to a real measurement time of 13 min (40 min in total, including the two reference measurements), assuming a typical DT source with a yield of $2 \cdot 10^9$ neutrons per second.

The attenuation profile has been discretized in rixels in two different ways for comparison. First the rixel width is constant in the object at 0.5 mm to allow a spatial resolution of 1 mm in the entire object. In the second reconstruction, the rixels have a radial increment that is decreasing with the radius, to keep the area of each rixel constant. In addition, the total number of rixels is fewer to provide an overall better precision. The reconstructed attenuation distributions can be seen in Figure 2.

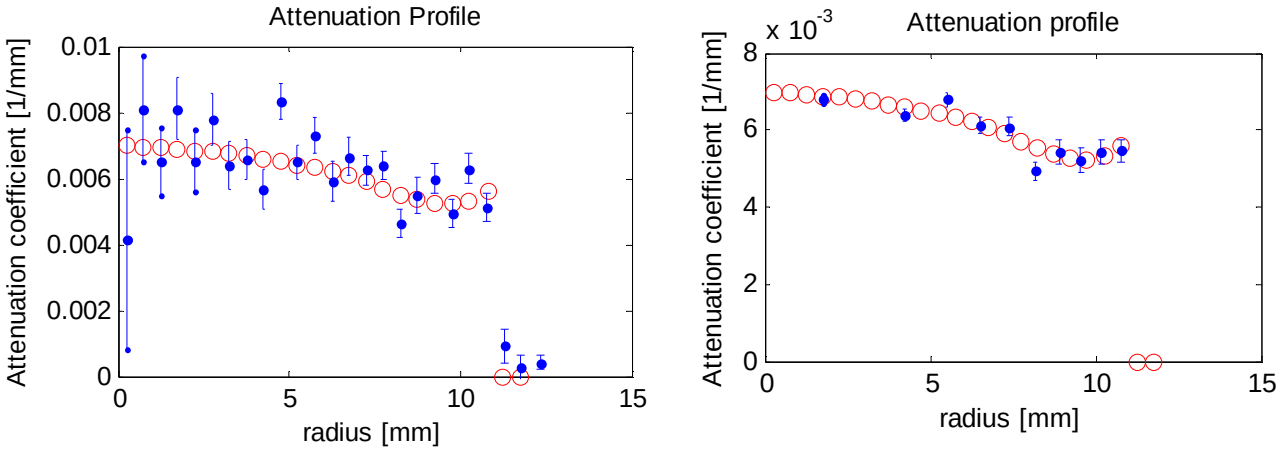

Figure 2. Reconstructions of the radial profile of the attenuation of the simulated void distribution. The red circular data points denote the modeled attenuation profile and the blue points show the reconstructed attenuation distribution, with error bars corresponding to 1-sigma uncertainty. (Left) Rixel width 0.5 mm. (Right) Rixel width corresponding to constant rixel area of 1/10 of the total area.

The reconstruction using constant rixel width shows relatively high levels of noise in the centre of the object, where the rixel areas are small. This characteristic of the noise has been reported previously in x-ray tomography of axially symmetric objects. [5] In the second reconstruction, where the rixel area is constant, this characteristic is not seen. This reconstruction also shows a generally lower level of noise, which can be expected since fewer rixels are being fitted to the simulated data. The latter attenuation profile has been used to calculate the local void fraction according to eq. 3, giving the results presented in Figure 3. Uncertainties in the reconstruction are between 2 and 5 void percent units.

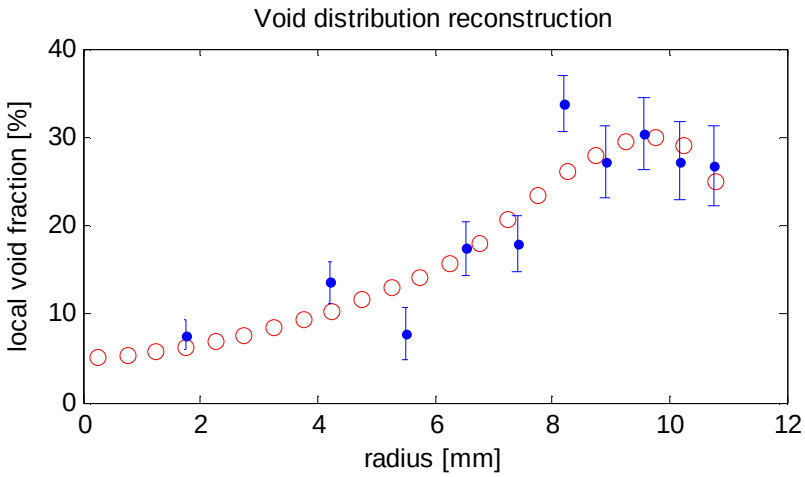

Figure 3. Void distribution reconstructed from simulated data. Rixel widths correspond to constant rixel areas. The uncertainty of the reconstructed void fractions are between 2 and 5 void percent units.

5. Discussion, conclusions and outlook

The reconstruction using annular rixels with constant area shows the main features of the modelled void distribution with only small deviations. With this positive result laboratory tests can now be started. Currently a neutron generator with $3 \cdot 10^7$ neutrons/second is available for this work, indicating that measurement times in the order of 13 hours are required to achieve the quality of the results presented in this work. However, using a typical neutron source commercially available today and/or longer measurement times, further improvements of the precision of the measurements may be expected.

Further work will also include the modelling of the gamma-ray background to take that into account in the reconstruction procedure. Also, additional sources of systematic uncertainties will be investigated by modelling various measurement geometries and strategies.

6. Acknowledgements

This work has been economically supported by the Swedish Centre for Nuclear Technology (SKC).

7. References

[1] Windecker, G., Anglart, H. (1999). Phase distribution in BWR fuel assembly and evaluation of multidimensional multi-fuel model. Ninth International Topical meeting on Nuclear Reactor Thermal Hydraulics (NURETH-9)

[2] E. H. Lehmann *, P. V. (n.d.). Status and Prospects of Neutron Tomography in Europe. Retrieved 02 23, 2010, from http://neutra.web.psi.ch/publication/Status_tomo_vers_end.pdf

[3] Persson, H. A., Anglart, H. (2007). Experimental investigation of post-dryout heat transfer in annulus with spacers. International Journal of Multiphase Flow , 809-821.

[4] P.A. Hausladen, P. B. (2007). Portable fast-neutron radiography with the nuclear materials identification system for fissile material transfers . Nuclear Instruments and Methods in Physics Research Section B: Beam Interactions with Materials and Atoms , 387-390.

[5] Hanson, K. M. (1984). Tomographic reconstruction of axially symmetric objects from a single radiograph. 16*th Inter. Vong. on High Speed Photography and Photonics*, (pp. 180-187).

CHARACTERISATION, REPACKAGING AND INCINERATION OF NaK AND Na USED FOR HEAT TRANSFER EXPERIENCES ON LMFBR AT THE JRC-ISPRA SITE

M.MAZZUCCATO*, F.D'ALBERTI*, F.D'AMATI
**European Commission, Joint Research Centre*
Nuclear Decommissioning Unit
Via Fermi 210207 Ispra VA – Italy

ABSTRACT

The Joint Research Centre (JRC) is a service of the European Commission and its mission is to provide scientific and technical support to the EU policies. At the Italian JRC Ispra site is currently ongoing a nuclear decommissioning program aimed at dismantling and disposing facilities and materials no longer used for nuclear research purposes, e.g. alkali metals, whose radioactive content has to be checked prior the disposal as radioactive or conventional waste. This paper describes the project phases consisting in characterising, repackaging and disposing of ~607 kg of alkali metals, composed by ~397 kg of NaK liquid alloy and ~210 kg of Na metal. The material was used in the past for scientific experiences on heat transfer for liquid metal fast breeder reactors. The alkali metals are very reactive in presence of water leading to the formation of hydrogen; moreover the NaK had been stored for several years in a bunker inside drums unable to guarantee the needed confinement, with the consequent formation of oxygenated compounds in the outer layer of the alloy crust, as Na_2O_2, NaO_2, K_2O_2 and KO_2, unstable if moved in presence of the liquid substrate. To perform the characterization and repackaging operations in a safe manner, avoiding any possible reaction between the liquid alloy and the solid surface of oxides, the alloy has been solidified reducing bunker temperature down to the alloy melting point (-15°C). The sampling has been carried out by means of glove bag sealed on the top of each drum and filled in with inert gas to reduce the presence of humidity. Having characterization campaign proved that the alkali metals could not be classified as radioactive material, the NaK and Na containers were shipped to UK in a refrigerated truck. In order to allow a safe thermal destruction in a conventional incineration plant, additional repackaging has been performed in a UK plant to reduce the amount of alkali metals contained in each batch. The project required the involvement of the relevant Italian, UK and French authorities for transboundary shipment of waste and it was concluded in June 2009 with the complete incineration of the alkali metals.

1. Introduction

Since the early 1980s, the Framework Programmes of the Commission have progressively reduced their focus on nuclear R&D. This and the natural ageing of facilities have led to the accumulation at JRC-Ispra of many shutdown nuclear installations. The management of nuclear installations, makes the European Commission responsible throughout the life of a facility until it is de-licensed. Therefore, the JRC is required to decommission its shutdown nuclear installations and manage their associated waste. To achieve this objective, the JRC has set up at a multi-site level Decommissioning and Waste Management (D&WM) Programme. In particular, alkali metals used in scientific experiences concerning heat transfer for advanced nuclear reactor, as Liquid Metal Fast Breeder Reactor, have been accumulated over more than two decades since eighties. Part of this material includes~397 kg of NaK alloy and ~210 kg of sodium metal. It is useful to mention the features of sodium-potassium alloy used as a coolant in nuclear reactors. The alloy is useful in these applications since it is able to remain liquid at room temperature and is commercially

available. NaK is highly reactive with air humidity or water; as a consequence it must be handled with special precautions. Amounts as small as one gram can induce fire or explosion risk if exposed to air [1-3]. Despite these disadvantages, NaK is often used because it remains in a liquid state without the need of pipe heating system to keep the coolant liquid, as required with sodium metal. Studies carried out in the past have demonstrated the hazardous aspects related to an inappropriate conservation of the alloy in storage areas. It is clear the NaK capability to form solid crust on the liquid surface generated by oxidative compounds of Na and K, *inter alia* peroxide and superoxide species. The chemical reactions of sodium and potassium leading to the formation of the oxygenated species are hereinafter reported with the corresponding values of $\Delta G°$[4]:

$$4\,Na + O_2 = 2\,Na_2O \qquad \Delta G°_{298} = -758\ kJ\ mol^{-1}$$
$$2\,Na_2O + O_2 = 2\,Na_2O_2 \qquad \Delta G°_{298} = -141\ kJ\ mol^{-1}$$
$$Na_2O_2 + O_2 = 2\,NaO_2 \qquad \Delta G°_{298} = +12\ kJ\ mol^{-1}$$

$$4\,K + O_2 = 2\,K_2O \qquad \Delta G°_{298} = -646\ kJ\ mol^{-1}$$
$$2\,K_2O + O_2 = 2\,K_2O_2 \qquad \Delta G°_{298} = -211\ kJ\ mol^{-1}$$
$$K_2O_2 + O_2 = 2\,KO_2 \qquad \Delta G°_{298} = -53\ kJ\ mol^{-1}$$

In presence of water vapour the Na and K oxides can induce the formation of hydroxides NaOH and KOH that can trigger the creation of other hydrate species, as Na/KOH·nH$_2$O (n = 1, 2, 3…). The same result can be achieved by peroxides species. A schematic view of the alloy crust layers is reported in Figure 1.

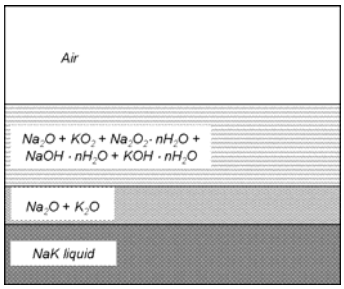

Fig. 1. oxidative layers formed on NaK surface by water interaction.

The accidental interaction of the hydrate layer with the liquid alloy can induce violent reaction capable to cause explosion. Surely an inappropriate conservation of the alloy, (e.g. in unsealed drums stored for a long period in places without controlled ventilation and air humidity conditions), is able to induce the formation of oxidative compounds capable to coordinate water molecules.

2. Project

In 2004 the JRC started a program aimed at moving outside Ispra site the alkali metals no longer used for scientific purposes. The handling, shipment and disposal of this material have required a three steps project with the following phases: characterization; design/licensing and operational phase. The duration of the entire project was initially estimated being 26 months.
The NaK and Na were stored in 100L primary drums inside 250 L drums apart two items stored in containers with uncommon shapes and dimensions without overpacks: a cylinder and a parallelepiped referable to components of the circuits used during the experiences. Table 1 reports in details the amounts of each item and a short description of the containers.

Drum No.	Content	Weight (kg)	Container
NaK1	NaK	20,5	100 L drum in 250 L drum as overpack

NaK2	NaK	42	100 L drum in 250 L drum as overpack
NaK3	NaK	59	100 L drum in 250 L drum as overpack
NaK4	NaK	18	100 L drum in 250 L drum as overpack
NaK5	NaK	50	100 L drum in 250 L drum as overpack
NaK6	NaK	40	100 L drum in 250 L drum as overpack
NaK7	NaK	47	100 L drum in 250 L drum as overpack
NaK8	NaK	40,5	100 L drum in 250 L drum as overpack
NaK23	NaK	80	Stainless steel container (Ø 38 cm, H = 85cm)
Na10	Na	76	100 L drum in 250 L drum as overpack
Na19	Na	48	100 L drum in 250 L drum as overpack
Na24	Na	70	Cylindrical stainless steel container (Ø 30cm, H = 170cm)
Na26	Na	15	100 L drum in 250 L drum as overpack

Tab 1: Content of NaK and Na for each item with container description.

In order to define the appropriate strategy to transfer and dispose the alkali metal, it was necessary to proceed with the material characterisation. Despite the available reports showed that the alkali metals had never been used in primary circuits of nuclear facilities, the characterisation was needed as a measurable confirmation of absence of any residual radioactivity and with the aim to comply with the exportation rules for conventional hazardous waste having no radiological relevance.
The characterisation phase started in January 2008. Due to potential presence of crust on the alloy surface, the material was frozen during sampling and repackaging operations. In fact, the temperature decreasing down to the alloy melting point permits to solidify the NaK, avoiding accidental interaction triggered by the immersion of the hydrate oxides in the liquid during the further handling activity. The temperature needed for working in a safe manner is -15°C, as it guarantees the complete freezing of the eutectic alloy ($Na_{(22)}K_{(78)}$). Eutectic alloy is the worst scenario since it is characterized by the lower melting point (-12.5°C) of NaK mixture [5]. It was decided to refrigerate the entire storage bunker instead of the single drum. The bunker was therefore insulated putting polyurethane panels on the internal walls, and a false ceiling was built to reduce the volume of the bunker from 80 m^3 to around 56 m^3. The insulation was placed with several logistic difficulties due to the small space available in the building and the impossibility to move the NaK drums. A freezing unit inside the bunker, and a polycarbonate structure outside the main entrance (as antechamber to reduce temperature variations during the transit inside the building) were also installed. Thermocouples were placed on the bunker walls and inside a dummy drum with $CH_3(CH_2)_{10}CH_3$, with the aim to validate the temperature in the bunker and in the drums . In particular, Dodecane is suitable to simulate NaK for two reasons: a) its long carbon chain gives it low reactivity if put accidentally in contact with alkali metals b) its melting point is at - 9.6°C, therefore very close to that of the eutectic alloy. In order to supervise in real time the operations at very low temperature inside the building, a CCTV system was put in place. The replacement of the secondary containers with UN Class 1 drums, appropriate for a safe shipment as requested by ADR transport regulation (Figure 2a), was carried out during the characterization phase. Item Na24 did not fit the size of a standard drum so it was necessary to fabricate and validate a brand new container. The sampling was performed item by item removing the inner drum lids (Figure 2b); A glove-bag, hold up with a self stand structure and filled with Ar, assured an inert atmosphere in the sampling environment. At the end of the sampling activity the atmosphere inside the secondary container was purged with inert gas. The sampling and repackaging activity at JRC took around 2 weeks with 72 hours needed to reach the working temperature in the building. The operators wore appropriate overalls clothes to cope with the -15°C during the entire duration of the sampling and repackaging. The samples were collected in containers made on purpose for this project and capable to resist in case of violent exothermic reactions.

a

b

Fig.2 replacement of the overpack (a) and glove-bag used for sampling

The radiological results of the characterization campaign showed levels of radioactivity for H-3, Co-60, Cs-137 and Am-241 below the detectable limits of the instruments: < 0.4 Bq/g. The sample's radiological activities were suitable for the proposed way of disposal, i.e. to transfer the material to UK for the subsequent repackaging and safe incineration in a High Temperature Incinerator, HTI. The caesium and americium results confirmed the paper documents on no exposure to irradiated nuclear fuel. The results concerning K-40 proved levels matching with expected natural levels; however, an accurate analysis on potassium content was carried out to exclude any accidental neutron irradiation origin. Chemical analyses of the sodium/potassium ratio in each sample have been performed. Estimations may also be made from the K-40 level: natural potassium contains 0.012% by weight of K-40, half-life 1.27 x 10^9 years, which is equivalent to a radioactivity of approximately 31 Bq/g. The percentage of potassium calculated from the results is shown in Table 2 alongside the measured values; only K-40 values above level of detection are used. The agreement between the measured values and those calculated from the K-40 measurements is satisfactory.

Drum No.	K-40 Bq/g	K wt% calculated	Na/K calculated	Na/K analytical
NaK1	<6	<19		71.7
NaK2	8	26	2.9	2.1
NaK3	11	35	1.6	1.3
NaK4	<11	<35		1.2
NaK5	<4	<13		1.0
NaK6	13	42	1.2	0.9
NaK7	<9	<29		11.8
NaK8	<2	<6		38.4
NaK23	10	32	8.5	9.1

Tab 2: Additional chemical analysis carried out on the samples to verify the measured levels of K-40 in relation with the natural content.

Taking into consideration the results of the characterisation on the items, it was possible to proceed with the transfer of the material to UK in licensed facilities to perform the repacking and the disposal of the alkali metals as conventional waste. The waste exportation was organised following the EU legislative requirement for transboundary shipment of waste [6]. After the obtainment of the export license and the agreement to the export the alkali metal from Italy to the UK via France, the NaK, now packaged in UN Class 1 containers, was frozen again to -15°C at the Ispra site before being loaded onto a refrigerated trailer in April 2009 (Figure 3). Although there was now additional confidence in the composition of this

material from the results of the analysis, it was frozen prior to and during transport in order to mitigate any risk of chemical reactivity of exposed alkali metal in the event of a road traffic accident.

Fig. 3: item Na24 frozen during the loading on the trailer

The material was transported to waste packaging site located in the UK, which is licensed to treat waste considered as hazardous material in class 4.3. The material was unloaded and the highly risky NaK containers were temporarily stored in freezer units. A special repackaging facility was set up, comprising a bespoke three-cell glove-box, nitrogen purge system, freezer units and storage area. The entire NaK drums could thus be stabilised by freezing prior to opening, and all operations were carried out under inert gas to eliminate the possibility of a NaK reaction. A single container was processed within the glove-box at any time, with the container lid being first removed by grinder/saw to allow visual assessment of the state and quantity of the alkali metal contents. The alkali metal was removed by cutting/ladling (as appropriate to the consistency and density of the metal) and placed in 15kg lots into 34 litre screw-top polyethylene UN Class 1 drums. Upon discharge from the glove-box, these polyethylene drums were marked with an identifying number, then loaded in groups of four into 322 litre UN Class 1 steel drums; the contents of all drums were nitrogen purged. Waste materials were similarly packaged into dual drums.
The re-packaged material was transported to the High Temperature Incineration in June 2009. The material was incinerated by the plant operators over the 3 days and a Destruction Certificate provided to the JRC.

3. Conclusions

The lack of historical data for the alkali metals, and the difficulties in accessing the material for surveying and sampling purposes, meant a lot of difficulties during the operations carry out at the JRC-Ispra. However, the project was positively concluded at the end of June 2009, 10 months before the official time schedule end. This was mainly due to the technical choice to change the overpacks at the same time of the sampling activity, reducing the time of intervention at JRC-Ispra and the cost related to the freezing unit operation inside the NaK store. Alkali metals removal from the JRC-Ispra was another step towards the reduction of European Commission liability regarding hazardous material present on site.

4. Acknowledgements

UKAEA Ltd and NDSL for their technical support and JRC ISM for administrative support.

5. References

[1] Sodium-NaK engineering handbook. Volume I. Sodium Chemistry and Physical Properties. O.J.Foust . 1972.

[2] Liquid alkali metals: Encyclopedia of Physical Science and Technology (Third Edition), C.C. Addison, 2004, pp 661-671
[3] Handling and uses of the alkali metals: The Manufacture of Potassium and NaK, C. B. Jackson, R.C. Werner, Chapter 18, 1957**,** pp 169-173
[4] Reaction of Sodium-Potassium alloy with inert gas impurities – Potential hazard after oxidation. J Desreumaux, M. Calais, R. Adriano, S. Trambaud, C. Kappenstein, M. Nguefack. Eur. J.Inorg. Chem. 2000, pp 2031-2045.
[5] Viscosity of NaK 78 at Low Temperatures. G.Macur, E. L. Grove, A.J. Gaynor, C. K. Hersh *J. Phys. Chem.*, 1965, *69* (11), pp 3782–3785
[6] Regulation (EC) No 1013/2006 of the European Parliament and of the Council of 14 June 2006 on shipment of waste

CONTROL ROD EJECTION ACCIDENT ANALYSIS FOR A PWR WITH THORIUM FUEL LOADING

D.F. DA CRUZ
Nuclear Research and Consultancy Group NRG, Westerduinweg 3, P.O. Box 25,
1755 ZG Petten, The Netherlands

ABSTRACT

This paper presents the results of 3-D transient analysis of a pressurized water reactor (PWR) core loaded with 100% Th-Pu MOX fuel assemblies. The aim of this study is to evaluate the safety impact of applying a full loading of this innovative fuel in PWR's of the current generation. A reactivity insertion accident scenario has been simulated using the reactor core analysis code PANTHER, used in conjunction with the lattice code WIMS. A single control rod assembly, with the highest reactivity worth, has been considered to be ejected from the core within 100 milliseconds, which may occur due to failure of the casing of the control rod driver mechanism. Analysis at both hot full power and hot zero power reactor states have been taken into account. The results were compared with those obtained for a representative PWR fuelled with UO2 fuel assemblies. In general the results obtained for both cores were comparable, with some differences associated mainly to the harder neutron spectrum observed for the Th-Pu MOX core, and to some specific core design features.

The study has been performed as part of the LWR-DEPUTY project of the EURATOM 6th Framework Programme, where several aspects of novel fuels are being investigated for deep burning of plutonium in existing nuclear power plants.

1. Introduction

The Thorium cycle presents some clear advantage compared to the uranium cycle, mainly related to the amount of higher actinides produced. Thorium oxide is a highly stable oxide and has improved thermal characteristics like a higher melting point, whereas the thermal conductivity is comparable to that of UOX (10% higher). The main disadvantage of the Thorium cycle is that Thorium is not fissile, and therefore requires a certain amount of fissile isotope (Pu or U) to trigger the cycle. The fissile isotope bred in this cycle, U-233, has improved neutronic characteristics in comparison with Pu-239 in a thermal neutron spectrum. U-233 has the highest neutron production rate, and a slightly higher delayed neutron fraction than Pu-239. In a thermal spectrum the ratio of radiative capture cross section to fission cross section is much smaller than for Pu239 and half the value for U-235.

Within the Thorium project of the 5th Framework Programme several aspects of the thorium cycle have been considered. One of the activities within this project was benchmarking of codes for simulating core behaviour. These efforts are being extended within the LWR-DEPUTY project of the 6th Framework Programme of EURATOM. The safety aspects of PWR cores fuelled entirely or partly with ThPu fuel are being studied, such as feedback coefficients and shutdown margin. The dynamic core behaviour is also being studied by means of core 3-D transient analysis, where control rod ejection accidents are simulated. This article presents a comparison of the core behaviour between a ThPu MOX core and a core fuelled with conventional UO_2 fuel, during steady-state and transient conditions. As

transient, control rod ejection scenarios at hot zero power and full power have been considered.

2. Reactor models

A model of a Westinghouse 3-loop PWR has been selected for the study, with two different loadings. In one of the loadings 100% ThPu MOX assemblies have been used. The fresh fuel has an enrichment of 8.1 wt% (weight percentage of Pu-239+Pu-241), equivalent to a total Pu content of 12.43 wt%. The Pu vector used is derived from a UO_2 pin cell calculation with a target burn-up of 60 MWd/kgHM, and assuming a 7 years decay period before reprocessing of the discharged fuel. The fuel shuffling selected follows a four-batch scheme optimized for this fuel composition. Table 1 shows the main parameters of this reactor model. A core with conventional UO_2 fuel has also been simulated, and served as a comparison case for the ThPu MOX core. A fuel with 4.0% enrichment has been used, and without using any burnable poisons. For the sake of simplicity the shuffling strategy of the assemblies has been kept the same for both cores. Figure 1 shows the position of the control rods, labelled with the control rod bank name.

Table 1 – Main data for the Westinghouse reactor model

A. FUEL ASSEMBLY	
Pin configuration	17x17
Assembly pitch	21.5 cm
B. GUIDE AND INSTRUMENT TUBES	
Material	Zirconium
OD (above dashpot)	1.25 cm
ID (above dashpot)	1.15 cm
D. FUEL ROD	
Clad material	Zirconium
Clad OD	0.95 cm
Clad thickness	0.06 cm
Pellet diameter	0.82 cm
Active stack	365 cm
Pin pitch	1.26 cm
E. CORE PARAMETERS	
Nr of loops	3
Number of assemblies	157
Nominal power produced by the core (MWth)	2800
Power density (W/gHM)	39
Coolant Boron-10 enrichment	natural
F. COOLANT INFO	
Core inlet (C)	286
Core outlet (C)	323
Core average (C)	305
Mass flow through core (m3/hr)	68.143
Pressure (bars)	155
G. CONTROL ROD DATA	
Control rod material	B_4C
Control finger absorber radius (cm)	0.44
Control finger clad outer radius (cm)	0.49
Control finger clad material	Zircaloy

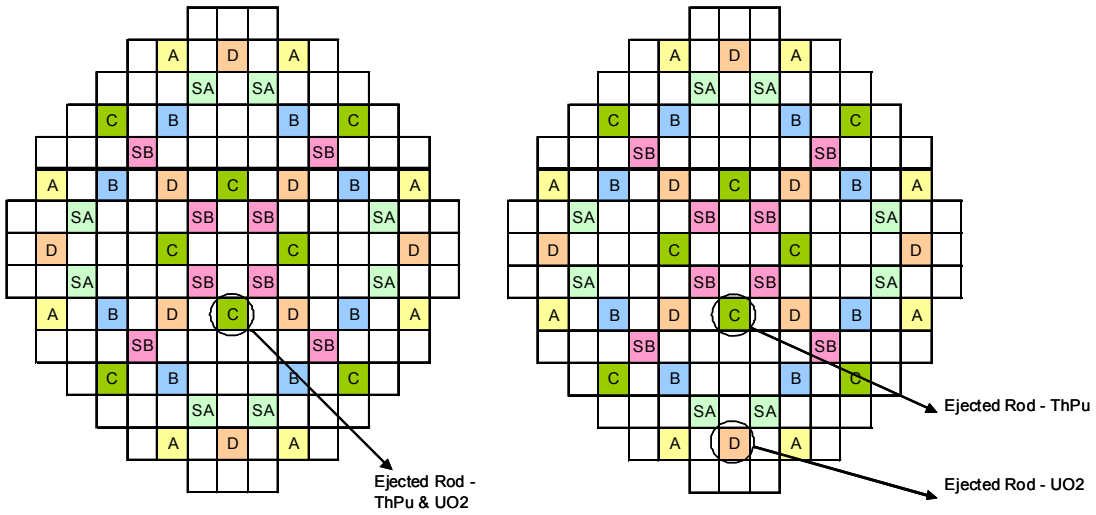

Figure 1 - Position of control rod banks and ejected rods (encircled) for (a) hot zero power case, and (b) full power case

3. Analyses codes

The steady-state and transient analysis have been performed with the PANTHER code [1]. PANTHER is a 3D nodal code for steady-state, fuel management and core transient analyses. In its thermal-hydraulic module no modelling is available of the azimuthal and axial conduction. The user has full control over the material data, namely the conductivity and specific heat capacity, which can be provided as function of temperature, irradiation and rating. Each channel is treated separately and no account is made for flow redistribution between channels. The model cannot predict the propagation of shock waves or choking. Boiling of the coolant is allowed and the code treats it as a vapour/liquid mixture, with the possibility to account for sub-cooled boiling and steam/water slip.

Because of the lack of extensive experimental data on conductivity on ThPu MOX fuel rods, data for UPu MOX has been used instead. The nuclear database used as PANTHER input has been generated with the lattice cell and burnup code WIMS [2], developed for treating all kinds of thermal reactors. The nuclear data used in WIMS8A is based on the JEF2.2 evaluation.

4. Steady-state analysis

The first ThPu MOX core contains fresh assemblies with different enrichments for each of the 4 fuel batches. The equilibrium cycle has been determined by simulating 10 subsequent cycles, where fresh fuel assemblies with 8.1% enrichment are loaded at the beginning of the cycle, and the remaining assemblies are shuffled according to the defined loading scheme.

For the UO_2 core, the equilibrium cycle has been reached after 10 cycles, where fresh UO_2 assemblies are loaded at the beginning of the cycle. Figure 2 shows the boron let-down curves for both equilibrium cores. For the ThPu MOX core design the excess reactivity is quite high at BOC, required to achieve a cycle length of 400 EFPD. This value could be decreased with a design where burnable poisons were integrated in the fuel, or used in separate pins or guide tube positions. Because of the negative temperature coefficients of reactivity, the critical boron concentration at hot zero power (HZP) conditions will be even higher (in the order of 3200 ppm). These high concentrations of natural boron indicate the necessity to switch over to enriched boron in the coolant.

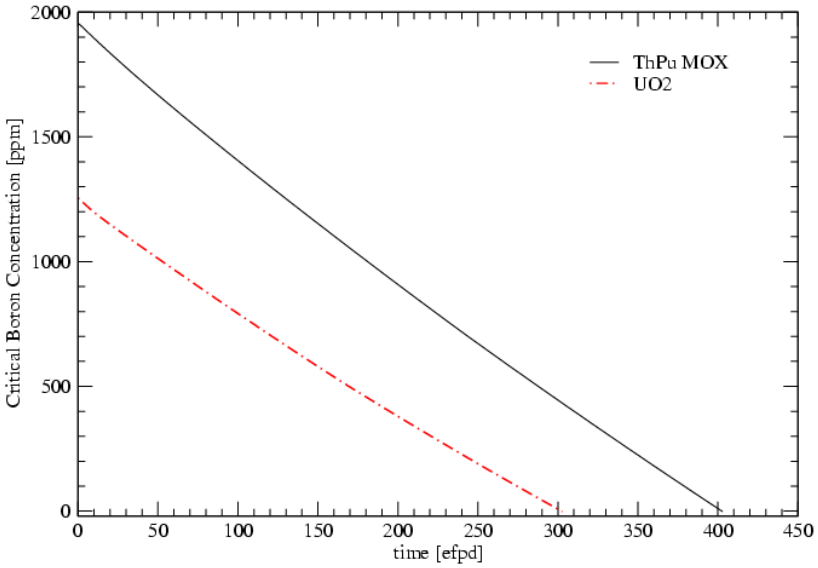

Figure 2- Boron let-down curve for both Westinghouse cores

Table 2 shows some general parameters for both cores at equilibrium at beginning of the equilibrium cycle (BOC) and at full power (FP).

Table 2 - General parameters for both Westinghouse cores at BOC and FP. CBC- critical boron concentration; BU – burn-up; $F_{\Delta H}$ – radial form factor; F_Q – total form factor

	ThPu	***UO_2***
CBC [ppm]	1950	1255
Cycle length [efpd]	405	310
T_{fuel}-max [K]	1060	1115
T_{cool}-max [K]	611	617
$F_{\Delta H}$	1.47	1.68
F_Q	1.95	2.0
ϕ_{heat}-max [W/cm^2]	121	134
BU-max [MWd/kg]	69.4	47.0
β_{eff}[pcm]	329	618

The choice of the same shuffling scheme for both cores has implications for the total cycle length, which is not optimal, and therefore shorter for the UO_2 core. A large difference in power distribution is also observed for both cores. Consequently the two peaking factors (F_Q and $F_{\Delta H}$) are larger, as well as the maximum fuel and coolant temperatures.

Table 3 summarizes the total CR worth, the power defect and the derived shutdown margin (SDM) for both cores, where an allowance (of 10%) for uncertainties in the total CR worth has been included. The SDM differs by 900 pcm between the two cores, and both values are larger than 1%, which is normally required; and also larger than the 3% requirement adopted for PWR's of the new generation.

Table 3 - Total stuck-rod CR bank worth, power defect and shutdown margin (SDM) for both cores

	ThPu	***UO_2***
Total CR worth [pcm]	7078	9233
Power defect [pcm]	3297	4334

SDM	3073	3976

4.1 Reactivity feedback coefficients

Table 4 and Table 5 show the reactivity feedback coefficients determined for both cores, at FP and HZP. Values for both BOC and EOC are mentioned. The power at HZP state is supposed to be 0.1% of the nominal power.

All moderator temperature coefficients are negative, and comparable for the ThPu MOX and UO_2 cores, despite the large difference in critical boron concentration. At HZP the moderator temperature coefficient (MTC) is more negative for the ThPu MOX core. At EOC the MTC values become more negative, as expected because of the decrease in critical boron concentration. The Doppler coefficients are negative in all conditions for both cores, and in the ThPu MOX core it is even more negative than for a UO_2 core. The values are comparable to values in current PWR's. The Boron coefficients for the ThPu core are clearly less negative than for the UO_2 counterpart, caused by the larger CBC. At both HZP and FP the total power coefficients are all negatives and comparable for both cores.

Table 4 - Reactivity feedback coefficients for ThPu and UO_2 Westinghouse cores, operated at FP. MTC- moderator temperature coefficient

	ThPu		***UO_2***	
	BOC	***EOC***	***BOC***	***EOC***
Total MTC [pcm/K]	-34.6	-58.0	-28.98	-67.4
Doppler [pcm/K]	-3.1	-3.3	-2.63	-2.87
Boron [pcm/ppm]	-2.3	-2.7	-7.0	-7.9
Power [pcm/MW]	-0.72	-0.92	-0.66	-1.05
CBC [ppm]	1955	---	1255	---

Table 5 - Reactivity feedback coefficients for ThPu and UO_2 cores, operated at HZP

	ThPu		***UO_2***	
	BOC	***EOC***	***BOC***	***EOC***
Total MTC [pcm/K]	-13.5	-32.3	-2.88	-32.06
Doppler [pcm/K]	-3.98	-3.94	-3.31	-3.45
Boron [pcm/ppm]	-2.5	-2.8	-7.4	-8.1
Power [pcm/MW]	-0.72	-0.95	-0.61	-1.03
CBC [ppm]	3275	1329	1865	665

5. Control rod ejection accident

Transient analysis has been performed for these cores, where the reactivity insertion accidents have been selected. Two control rod ejection scenarios, at HZP and FP, have been investigated. The following sequence of events are assumed, that leads to the control rod ejection:

1. reactor is at HZP state
2. one single CR (with the highest worth) gets stuck in the core
3. reactor is made critical by adjusting the soluble boron concentration
4. due to a failure of the CR shaft, the stuck CR is ejected from the core within 100 ms

The same sequence of events is supposed for the FP case. After ejection it is supposed that the reactor scram fails. The boron concentration in the coolant is kept unchanged during the accident, and equal to the critical value before the onset of the accident, for both scenarios.

5.1 Hot zero power

The results for this scenario are shown in Figure 3 and Figure 4. The reactivity insertion is larger for the ThPu MOX core (0.55 $) than for the UO_2 core (0.18 $). As a result, a higher power is reached: 245 MW in comparison to 180 MW for the UO_2 core. Because of the difference in reactivity insertion the ramp-up in power is much faster for the ThPu MOX core, and the Doppler feedback sets in within a much shorter time span: 25 seconds for the ThPu MOX core and 300 seconds for the UO_2 core. Nevertheless, the maximum fuel temperature reached at equilibrium is comparable for both cores, and amounts to about 660K (starting from a value of about 560K).

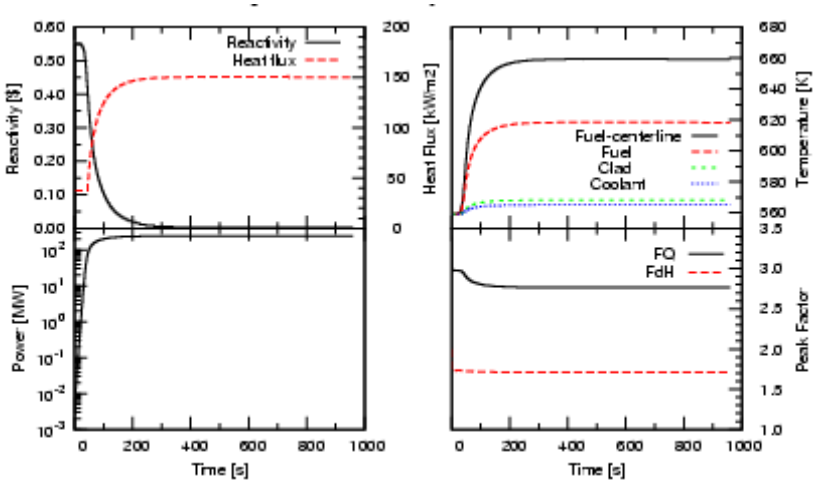

Figure 3 - Control rod ejection transient for HZP case and ThPu core

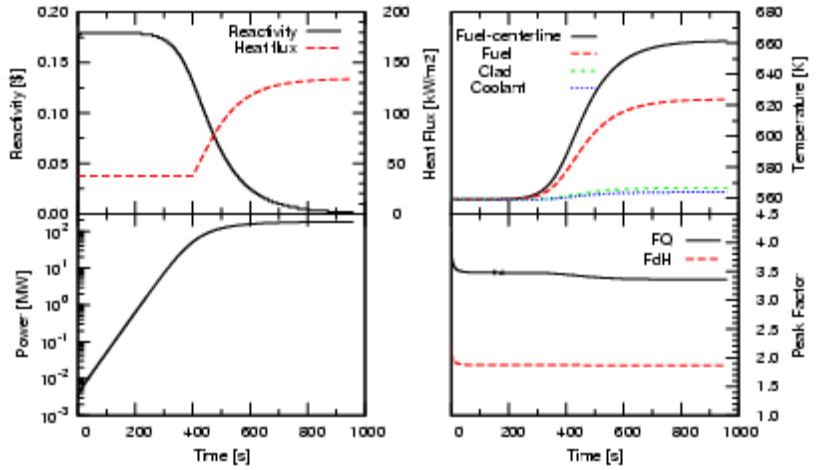

Figure 4 - Control rod ejection transient for HZP case and UO_2 core

5.2 Full power

The results are summarized in Figure 5 and Figure 6. For the ThPu MOX core the reactivity insertion (0.55 $) is larger than for the UO_2 core (0.45 $). As a result the power peak is also larger: 130% and 80% above the nominal power for the ThPu MOX and UO_2 cases, respectively. The power peaks at 100 ms for both cases, when the reactivity insertion reaches its maximum, and instantaneously starts decreasing due to the Doppler feedback. The reactivity (and power) decay constant are comparable for the two cores, because the power feedback coefficients are also comparable (see Table 4).

At the end of the accident the same equilibrium value of power is reached for both cores (around 3000 MW). The UO_2 core reaches however the highest fuel temperature, which is a consequence of two factors: the higher peaking factor and the differences in thermal properties of this fuel type. Nevertheless, the value remains well below the fuel melting temperature (3651 K for ThO_2; and 2663 K for PuO_2; since our fuel is a mixture of these oxides the melting point will be a value between those [3]. The increase in fuel centreline temperature is also larger for the UO_2 core (250 K) than for the ThPu MOX core (100 K).The maximum pin heat flux (1650 kW/m^2) is also reached by the UO_2 core. This value however stays below the maximum values observed in current-generation PWR's.

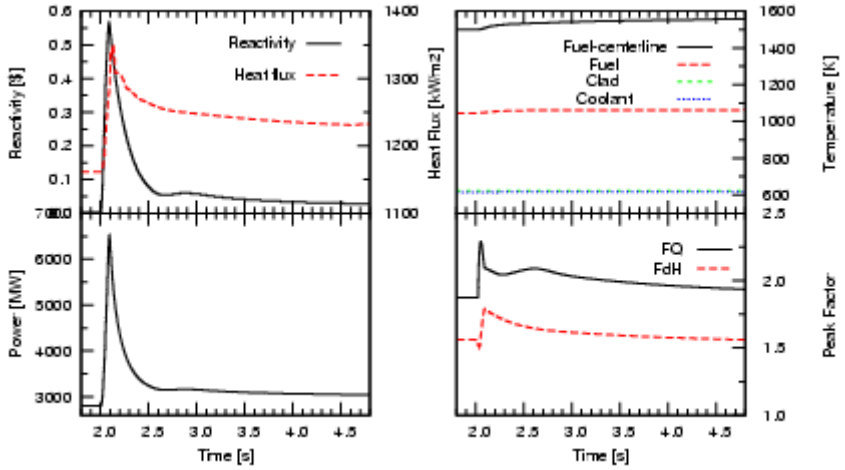

Figure 5 - Control rod ejection transient for FP and ThPu core

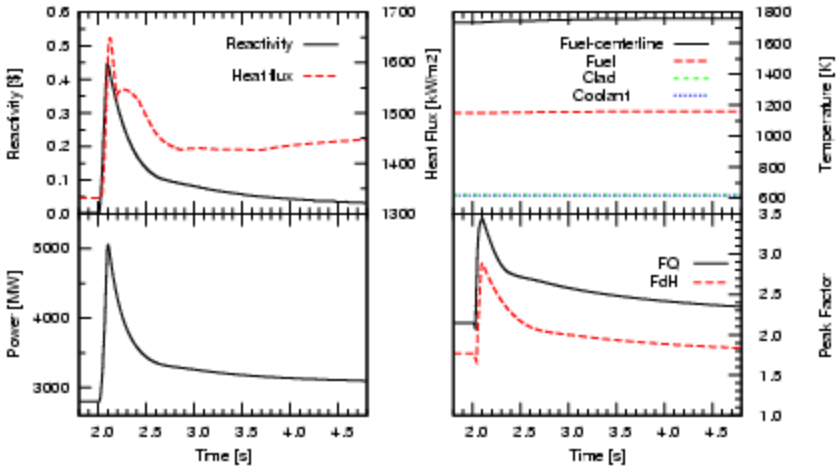

Figure 6 - Control rod ejection transient for FP and UO_2 core

Table 6 and Table 7 show a summary of the results obtained from the simulations of the two cases, and for ThPu MOX core and UO_2 core, respectively. Also included are the parameters for the reactor state prior to the initiation of the event (denoted by steady-state).

Table 6 - Control rod ejection results for a core fuelled with 100% ThPu fuel

	FP		**HZP**	
	steady-state	*transient*	*steady-state*	*transient*
Power max. [MW]	2800	6519	0.0028	245
Reactivity – max [pcm]	---	0.58	---	0.55
Max fuel C/L Temp. [K]	1500	1615	559	659
Max. clad surf. Temp. [K]	620.7	620.9	559	568
Max pin heat flux [W/cm^2]	116	135	3.7	15
$F_{\Delta H}$ – max [-]	1.56	1.79	1.99	1.99
F_Q – max [-]	1.87	2.29	3.39	3.39

Table 7 - Control rod ejection results for a core fuelled with UO_2 fuel

	FP		**HZP**	
	steady-state	*transient*	*steady-state*	*transient*
Power max. [MW]	2800	5053	0.0028	180
Reactivity – max [pcm]	---	0.45	---	0.18
Max fuel C/L Temp. [K]	1733	1982	559	661
Max. clad surf. Temp. [K]	621.4	621.7	559	566.73
Max pin heat flux [W/cm^2]	133	165	3.7	13.3
$F_{\Delta H}$ – max [-]	1.77	2.88	2.28	2.28
F_Q – max [-]	2.15	3.44	4.19	4.19

6. Conclusions

Two core designs for a Westinghouse 3-loop reactor have been developed, fuelled with ThPu MOX and conventional UO_2 fuel. The purpose was to analyse the behaviour of a ThPu MOX core under transient conditions, and compare the results with a similar core fuelled with conventional UO_2 fuel. A four-batch loading scheme has been adopted with a shuffling strategy optimized for the ThPu core. The UO2 core uses the same loading scheme. As consequence some fundamental differences are found between the two cores, regarding the cycle length and the peaking factors. The cycle length for the UO_2 core is 100 days shorter, and the peaking factors larger, which can be partially attributed to the differences in power profile. Shutdown margins and reactivity feedback coefficients have also been determined. The SDM for the UO_2 core shows a higher value than for the ThPu MOX core, ascribed mainly to the lower critical boron concentration. However, for both cores the criterion normally adopted for current generation PWR's is fulfilled. Reactivity coefficients are comparable, except for the total MTC at HZP conditions, where the value for the ThPu core at BOC is more negative.

Control rod ejection scenarios at FP and HZP have been analysed, where the CR with the highest reactivity worth is ejected from the core. The behaviour of the two cores are comparable, and differ mainly due to a combination of factors: differences in reactivity insertion, peaking factors, and fuel thermal properties. The maximum fuel temperature and heat flux are reached for the UO_2 core at FP. Nevertheless, they remain below the limit values adopted for PWR's of the current generation.

In a follow-up study the UO_2 core should be optimized in order to reach comparable values for cycle length and peaking factors. This would allow a more direct comparison between the two cores.

7. Acknowledgment

This work was supported by the European Commission under the LWR-DEPUTY Contract nr. FI6W-036421 of the EURATOM 6th Framework Programme.

8. References

[1] P.K. Hutt et al., "The UK Core Performance Package", Nucl. Energy, 30, No. 5, 291, October 1991.

[2] "WIMS8 User's Guide", ANSWERS Software Service, Winfrith, U.K.

[3] K. Bakker, et al., "Critical evaluation of the thermal properties of ThO_2 and $Th_{1-y}U_yO_2$ and a survey of the literature data on $Th_{1-y}Pu_yO_2$", J. Nucl. Mater. 250 (1997) 1.

LATEST DEVELOPMENTS ON SAFETY ANALYSIS METHODOLOGIES AT THE JUZBADO PLANT

ÓSCAR ZURRÓN-CIFUENTES, DIEGO ORTIZ-TRUJILLO,
LUIS A. BLANCO-FERNÁNDEZ
ENUSA Industrias Avanzadas S. A.
Juzbado Nuclear Fuel Fabrication Plant
Ctra. Salamanca-Ledesma, km. 26
37015 Juzbado, Salamanca - Spain

ABSTRACT

Over the last few years the Juzbado Plant has developed and implemented several analysis methodologies to cope with specific issues regarding safety management. This paper describes the three most outstanding of them, so as to say, the Integrated Safety Analysis (ISA) project, the adaptation of the MARSSIM methodology for characterization surveys of radioactive contamination spots, and the programme for the Systematic Review of the Operational Conditions of the Safety Systems (SROCSS). Several reasons motivated the decision to implement such methodologies, such as Regulator requirements, operational experience and of course, the strong commitment of ENUSA to maintain the highest standards of nuclear industry on all the safety relevant activities. In this context, since 2004 ENUSA is undertaking the ISA project, which consists on a systematic examination of plant's processes, equipment, structures and personnel activities to ensure that all relevant hazards that could result in unacceptable consequences have been adequately evaluated and the appropriate protective measures have been identified. On the other hand and within the framework of a current programme to ensure the absence of radioactive contamination spots on unintended areas, the MARSSIM methodology is being applied as a tool to conduct the radiation surveys and investigation of potentially contaminated areas. Finally, the SROCSS programme was initiated earlier this year 2009 to assess the actual operating conditions of all the systems with safety relevance, aiming to identify either potential non-conformities or areas for improvement in order to ensure their high-performance after years of operation. The following paragraphs describe the key points related to these three methodologies as well as an outline of the results obtained so far.

1. Introduction

Over the last few years the Juzbado Plant has developed and implemented several analysis methodologies to cope with specific issues regarding safety management. This paper describes the three most outstanding of them, so as to say, the Integrated Safety Analysis (ISA) project, the adaptation of the MARSSIM methodology for characterization surveys of radioactive contamination spots, and the programme for the Systematic Review of the Operational Conditions of the Safety Systems (SROCSS). Several reasons motivated the decision to implement such methodologies, such as Regulator requirements, operational experience and of course, the strong commitment of ENUSA to maintain the highest standards of nuclear industry on all the safety relevant activities.

2. The Juzbado Integrated Safety Analysis Project

In 2004, and following a request of the Spanish Regulatory Authority (CSN), ENUSA started at the Juzbado LEU Fuel Fabrication Plant the development and implementation of a risk-informed methodology for accident analysis, which was called the Juzbado Plant Integrated

Safety Analysis (ISA) project. By that time, ENUSA was involved in renewal of the Juzbado Plant Operating License and ISA was one of the items open to discussion with CSN. Several profitable meetings were held to clarify positions in issues such as regulatory basis, scope of the analysis, and time-schedule for the project before CSN issued in May 2004 the Official Request establishing the regulatory basis for the ISA and convening ENUSA to submit a planning for the project. The decision was taken not to issue any specific Spanish regulation on ISA but instead refer to the US 10 CFR Part 70.

As established in the CSN's Official Request, an ISA is a systematic examination of a plant's processes, equipment, structures and personnel activities to ensure that all relevant hazards that could result in unacceptable consequences have been adequately evaluated and the appropriate protective measures have been identified. The relevant hazards considered are all those which can lead to radiological consequences, namely, nuclear criticality, contamination & irradiation, fire & explosion, chemical or environmental, along with natural phenomena (floods, quakes, hurricanes, etc.) and any other external event which could be safety related.

2.1 Risk assessment

The first step was to split the Plant into areas of analysis following process or functional criteria and then, split the areas into nodes, which are the smallest piece to look upon and thus, the basic unit for the study. 20 areas and 117 nodes were identified.

An ISA team for the specific node is then selected and trained. The front-end of the selected ISA approach is shown in Fig. 1. The work begins with the identification of hazards, which is done by means of methods as *What if* or HAZOP (for more complex nodes). This allows the identification of all credible accident scenarios and for each of which, evaluating all possible causes and consequences. At this stage, it is important to highlight that the idea is to identify all the consequences, no matter whether they are radiological or not. Once every individual consequence is identified, the Severity and Unmitigated Likelihood (UML) of the sequence are assessed and combined to derive the Unmitigated Risk (UMR) associated with the considered accident scenario. All the safeguards already implemented (or to implement) to either prevent or mitigate the effects of every single accident scenario are identified by the team members, including those related to low risk events.

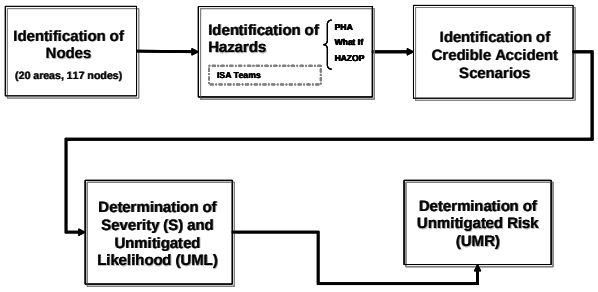

Fig. 1. Front-end of the ISA approach

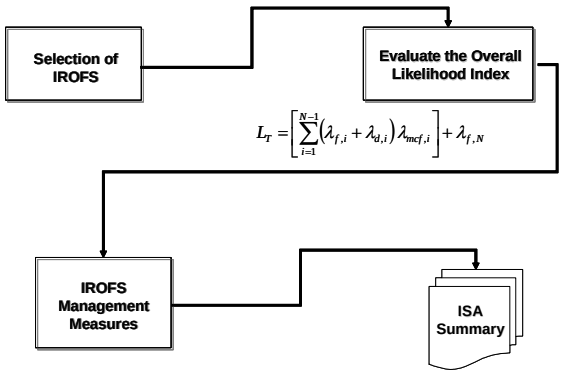

Fig. 2. Back-end of the ISA approach

2.2 IROFS

Then, from this set of safeguards, the Items Relied On For Safety are selected for those intermediate and high risk accident scenarios (see Fig. 2). The IROFS are those safeguards which ensure safety even in the case that the rest of safeguards have been lost. At least two independent IROFS are identified for every intermediate and high level risk accident

scenario. IROFS can be either passive or active engineered controls, or enhanced administrative controls, but not purely administrative controls.

Once the set of IROFS applicable to a specific scenario has been identified, the Overall Likelihood (L_T) index is computed. This takes into account the individual IROFS failure's frequency, the time period (duration) of IROFS failed condition prior to detection, and the existence of (other) independent IROFS. The so computed L_T index is then compared with the acceptance criteria. L_T index must always be smaller than the corresponding clearance criteria. Should L_T index fall out of the limits, the IROFS selection is considered no longer valid and then, a new set of IROFS must be selected and newly subjected to the acceptance process.

3. Inspection Plan for the detection of contamination at the Juzbado Plant

A number of incidents related to the finding of contamination spots outside main operation buildings were detected at different nuclear sites in Spain over 2008. In response to these incidents, the CSN (Spanish Nuclear Regulatory Body) issued requirements demanding all the operators the execution of the site's comprehensive inspection plans in order to ensure that no contamination spots would be found out of control.

The ENUSA's Fuel Fabrication Plant at Juzbado is a nuclear fuel cycle facility whose specific features makes it different to the rest of the Spanish nuclear installations, provided that only Low Enriched Uranium (LEU 5% maximum) is handled as process material. Therefore, the inventory of isotopes consists only of U-isotopes and their daughters. These isotopes can be found in Nature in different amounts, depending, inter alia, on the geologic characteristics of the area. Therefore, the natural background itself can contain spots of the contaminant, and must be taken into account for the preparation of the inspection plan, thus adding complexity to its implementation. The criteria to distinguish background from non background values must be set up (impacted and non impacted areas).

To implement the inspection plan at the Juzbado Plant, the MARSSIM methodology was chosen as a basis. MARSSIM (Multi-Agency Radiation Survey and Site Investigation Manual) is a tool to conduct radiation surveys and investigation of contaminated sites. This method is used by different agencies and it is a reference for the NRC, being described on NUREG 1575. Based upon the MARSSIM approach, the following steps are considered in the Radiation Survey Process once the site under consideration was defined.

3.1 Historical Site Assessment

To prepare the inspection plan, a review of all the activities that took place on site was done. This History Site Assessment (HSA) leads to a map showing the places where contaminated material has been handled at site. As shown in Fig. 3, the outcome of the HSA performed for the Juzbado Plant showed that contaminated material has only been handled in the main building and radioactive liquid treatment facilities. The other main conclusion at this point is that the only radioactive material handled was LEU in the form of oxides.

3.2 Characterization Survey

The first part of the characterization survey is to classify the zones either in land or structures, as the type of survey to be performed is different. Once this is done, a risk based classification is performed. The areas with higher risk of contamination will be classified as Class 1, and the areas with lower risk will be classified either as Class 2 or 3. Conservatively, all the areas on site were considered as impacted areas and thus, they were all subject of the survey. The criterion used to assess the risk was to quote as Class 1 all areas where

contaminated material was handled, whilst the ones surrounding Class 1 areas would be quoted as Class 2, being the rest Class 3.

The land areas identified are shown in Fig. 4 along with their classification in terms of risk. The type of survey necessary to inspect each area was selected using the DQO (Data Quality Objective) process. These areas must be inspected by both a scanning process and a simple measurement. For scanning, gamma measurement is done using portable equipment (INa monitor). For the single measurement a soil sample is taken, and later analyzed by alpha spectroscopy, where ^{234}U and ^{238}U are compared. For material with enriched uranium, the amount of ^{234}U is higher than what is found in Nature. To conclude whether an area is contaminated or not, the ratio ^{238}U:^{234}U (sample) vs. ^{238}U:^{234}U (background) is compared. If the mean ratio in samples from a surveyed area is smaller than the mean background ratio, then LEU contamination is assumed to be present. Otherwise, the uranium present is related to natural background.

For structure areas, a map of the facility was taken, and every building or road was assumed to be an impacted area. Each area was classified in terms of risk as detailed above and split into cells to perform the survey. The size of the cells is smaller for areas with higher risk, thus assuring a larger number of measurements. Again the type of survey to be performed is either a scan or a static measurement, both with portable monitors able to measure alpha radiation. The measure is done without any background subtraction, and later compared to the background of different materials to ascertain whether there is contamination or not.

Fig. 3. Map of the Juzbado Plant showing the areas where contamination may be found (red spots)

Fig. 4. Map of the Juzbado Plant showing the Class 2 (blue) and Class 3 (green) land areas

4. Programme for the Systematic Review of the Operational Conditions of the Safety Systems (SROCSS)

The SROCSS programme was initiated in mid-2009 to assess the actual operating conditions of all safety-relevant systems, aiming to identify either potential non-conformities or areas for improvement in order to ensure their high-performance after years of operation. The program is structured as described in the following paragraphs.

4.1 Identification of parameters

The parameters and limit operating conditions of the safety-relevant systems are established in the License Documents of the Plant. These systems cover a wide range of installations, which vary from utilities such as electric or water supply, to safeguards as the criticality alarm, fire detection or contamination monitoring.

In this first stage all the data, parameters and conditions established for each system in the License Documents are compiled. This information is then subjected to a comprehensive scrutiny aiming to identify the checks and verifications to be performed during the following stages of the program. This is a huge task, provided that every single datum, parameter or condition is peer reviewed and questioned, stating the basis for its later analysis. The job is carried out and documented by the Design Team, specifically designated for each system.

4.2 Verification of data by the Design Team

At this stage, the Design Team performs the pertinent checks of the data, parameters and conditions identified in the previous phase, including experimental verifications, if applicable. As a result of this phase, Technical Reports are issued documenting the checks and verifications done, along with the conclusions drawn during the process. These Technical Reports are produced, reviewed and approved according to the Quality Assurance requirements of ENUSA.

4.3 Verification of data by the Audit Team

The Technical Reports generated in the previous phase are later independently reviewed by the ad-hoc Audit Team designated for the task. This team can request additional information about particular items, require deeper checks or even propose further verifications to Design Team, all according to ENUSA QA requirements

4.4 Update of the Systems' Configuration Control

Conclusions derived from the work performed by Design and Audit teams set out the basis for the update of the configuration control of the system subject of analysis and will be shaped in the revision of drawings, procedures, manuals and License Documents applicable in each case.

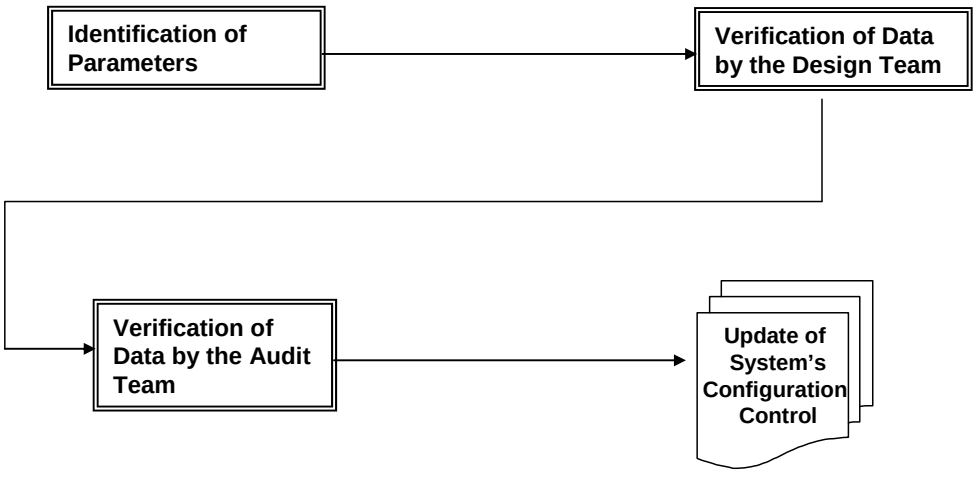

Fig. 5. Flowchart of the SROCSS programme

5. Conclusions

The initial planning submitted to CSN on 2005 for the ISA foresaw a minimum of 5 years for the whole project to be finalised. After more than 4 years of work, 93 nodes have been analyzed with about 2000 accident sequences being identified, out of which 16 where ranked as intermediate risk, none as high risk. Therefore, 16 sets of IROFS have been identified up to the time this paper was written. In most cases, IROFS were selected from the safeguards currently available, but some of them have led to design modifications in the Plant to comply with the ISA requirements for IROFS. Although the project is still ongoing, ENUSA considers that the implementation of the ISA program is increasing qualitatively the degree of knowledge of the potential initiating events and then, leading to an optimization of the safety management of the plant.

The Inspection Plan for the detection of contamination at the Juzbado Plant has already covered up to 65% of the identified areas, showing the absence of contamination spots in all the cases surveyed by the time this paper was written. The Plan is intended to be finished by the end of 2010.

Finally, about the SROCSS, it must be said that the programme is still in an initial phase, provided none of the systems have been already finalized. Nevertheless, ENUSA considers that this programme will lead to a higher degree of knowledge of the safety-relevant systems' performance after many years of operation and will easy the identification of non-conformities and areas for improvement in the management of the safety systems. The SCROCSS programme is scheduled to be completed by mid 2011.

THE FIRST CHEMICAL DECONTAMINATION SYSTEM FOR DECOMMISSIONING IN ITALY "PHADEC TECHNOLOGY" IN CAORSO

F. BENVENUTO, M. LUPU, C. MAZZONI, S. ORLANDI, C. RICCI
Nuclear System Engineering Department, ANSALDO NUCLEARE S.p.A.
Corso Perrone 25, 16161 Genova – Italy

ABSTRACT

The PHADEC Process (Phosphoric Acid Decontamination Process) is designed for surface decontamination of steel scrap using phosphoric acid. It has been successfully installed at Caorso NPP (Piacenza, Italy) at the end of 2008.
The decontamination of steel scrap is done by removing the radioactivity localized in a few micron thickness from the surface with an electro-polishing (Stainless Steel) or acid pickling (Carbon Steel) treatment in basins filled with 40%-Phosphoric Acid that is regenerated and recycled for reuse.

1. Introduction

During the decommissioning activity, which follows the end of the operational life of a Nuclear Power Plant (NPP), a big quantity and variety of radioactive materials are generated. These materials must be adequately managed and treated, with the aim to reduce the volume of equipment and materials requiring disposal in licensed nuclear waste repositories. Moreover, after the treatment the decontaminated material can be eventually released to the market (both nuclear and conventional) for reuse.

Among these materials, thousand tons of radioactive steel scrap are produced. The metallic material not directly exposed to the core radiations mainly presents a surface contamination. Most of the radioactivity is thus generally localized in a few micron thickness from the surface and a surface treatment is a sufficient decontamination method to guarantee the possible free release of the material.

A proven surface decontamination technique is the Phosphoric Acid Decontamination Process (PHADEC). It has been successfully installed at Caorso NPP (Piacenza, Italy) at the end of 2008.
This process combines a Decontamination Unit (DU), in which a 40%wt. phosphoric acid solution performs a chemical decontamination of the steel materials, and a Regeneration Section (RS), in which the dissolved iron is removed and the diluted solution regenerated.

2. The PHADEC Process

As above indicated, the PHADEC Process is composed by a Decontamination Unit and a Regeneration Section.

Decontamination Unit
After the preparation treatment of the dismantled parts, which is the disassembling and cutting of piping and components, the metal scrap is submitted to the following operations.

Leaching and cleansing
- Leaching of the scrap in the lye basin to remove oils/greases, if any.
- Water jet cleaning in a dedicated cleansing cabin after the lye treatment.

Decontamination treatment

- The decontamination [1] is performed by removing the radioactive surfaces of steel scrap by electro-polishing (for stainless steel) or acid pickling (for carbon steel) cleaning procedure in basins filled with 40%-phosphoric acid. This process is based on the following reaction:

$$3Fe + 2\ H_3PO_4 \rightarrow 3Fe^{2+} + 2PO_4^{3-} + 3\ H_2 \qquad [1]$$

- Each basin contains about 4 m^3 of acid solution and is equipped with external heating and water cooling coils (only for electro-polishing basins) for keeping the temperature at about 60°C which is a favourable temperature for pickling.

Acid wash out

- Final water jet cleaning in a dedicated cleansing cabin after the acid treatment.

The Decontamination Unit can be composed by many independents basins: this modularity feature allows a flexibility of operations. When the maximum iron concentration in acid phosphoric is reached, the acid content in a basin is transferred and shall be regenerated, while the other basins continue to operate.

The average decontamination treatment time is 4 hours per batch, which could offer a Decontamination Factor (DF) of about 10^2 up to 10^3. The achieved DF depends on the duration of the treatment and higher values can thus be obtained simply extending the residence time in the acid basins (Decontamination Phase). If any, residual local spots of contamination can be furthermore removed by mechanical methods.

An off-gas system removes permanently the aerosols and gas from the lye and acid basins surface.

In Figure 1 the path of the metal scrap through the DU and the flow of the phosphoric acid solution which is recycled after the treatment on the RS is shown.

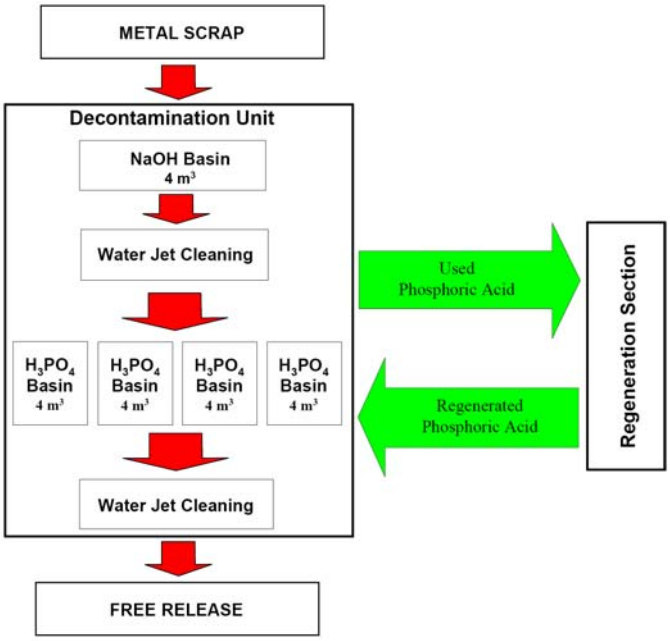

Fig 1. Decontamination Unit

Regeneration Section

At an iron concentration of about 100 g/l in phosphoric acid, the decontamination process is no more efficient and a regeneration of the phosphoric acid is needed. This operation allows to separate dissolved iron in the acid and recover the acid solution for reuse it inside the DU (Figure 2 shows the schematic principle).

The main operations performed during the regeneration of the acid solution are the following.

Precipitation with Oxalic Acid

The exhausted phosphoric acid solution coming from the DU, is mixed with a oxalic acid solution. Most of iron oxalate precipitates within a couple of minutes [2].

$$Fe^{2+} + C_2O_4^{2-} + 2\ H_2O \rightarrow (FeC_2O_4 \times 2\ H_2O) \qquad [2]$$

In order to minimize the secondary waste production, the supernatant (diluted phosphoric acid) is sent to the Evaporator. The remaining sludge is washed using water to recover the interstitial acid. The washing water is reused to prepare the next batch of oxalic acid solution, and the sludge is sent to the Thermolysis.

Concentration of the diluted solution

After sedimentation, the supernatant is filtered and then sent to the evaporator, where it is distilled up to the original 40% wt concentration and stored in the Media and Consumable Supply Unit.

Thermal decomposition of wet iron oxalate

The thermolysis reactor dries the wet iron oxalate [3], and then it transforms it by a thermolysis reaction into iron oxides, carbon monoxide and carbon dioxide [4]. The final conversion of carbon monoxide into carbon dioxide is obtained in the catalyst downstream [5].

$$(FeC_2O_4 \times 2\ H_2O) \rightarrow FeO + CO + CO_2 + 2\ H_2O \qquad [3]$$

$$FeO + ¼\ O_2 \rightarrow ½\ Fe_2O_3 \qquad [4]$$

$$CO + ½\ O_2 \rightarrow CO_2 \qquad [5]$$

The iron oxide produced in this unit represents the most of the secondary waste production of the entire process; the average production of iron oxide is < 2% wt. of the total mass of the treated steel scrap.

The gas released during thermolysis are treated in a dedicated HEPA filtration system then released to the atmosphere through the off-gas system.

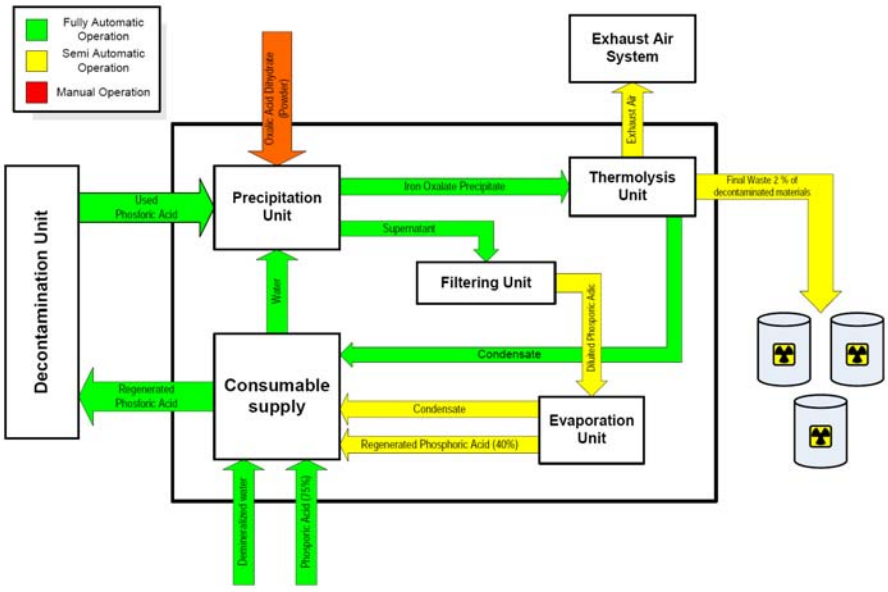

Fig 2. Regeneration Section

Off-gas treatment
The off-gas treatment system collects the gases coming from the decontamination basins (lye and acid) and the gases produced during the thermal decomposition of iron oxalate. The system is composed by wet scrubber and HEPA filtration units in which the gases are treated before to be discharged to the atmosphere. The high filtration efficiency of the system grants very low environmental impact, both for chemical and radioactive contaminants.

3. The PHADEC Facility

A global view of the Decontamination Unit of the PHADEC facility is shown in Figure 3.

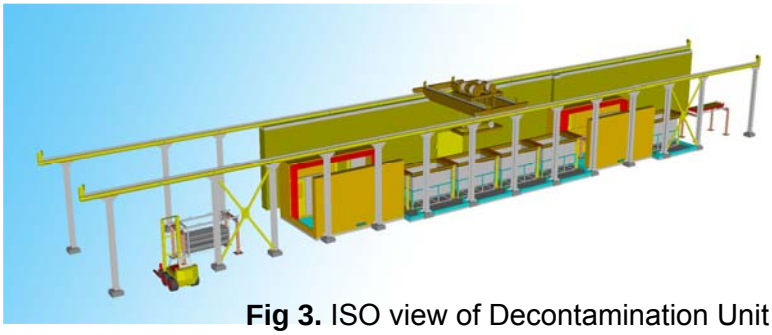

Fig 3. ISO view of Decontamination Unit

The PHADEC system includes the following main equipment:

- Lye basin, rectangular footprint (2500 x 1500 mm ca.) with aspiration duct above the maximum working liquid level (Figure. 4).
- Lye cleansing cabin with top entry for the material from the lye basin and high pressure water lance.
- Four Acid basins, rectangular footprint (2500 x 1500 mm ca.) with aspiration duct above the maximum working liquid level (Figure. 4). The quantity of the basins is depending on the required treatment rate. For the treatment of SS materials the basins can be equipped to combine electro-polishing with pickling.
- Acid cleansing cabin with top entry for the material from the acid basins and high pressure water lance.
- Precipitation unit with buffer tank and two precipitation tanks
- Evaporation unit with fully automated evaporator
- Thermolysis unit with reactor and iron oxide discharge device, dedicated off-gas system including catalyst bed and HEPA filtration
- Off-gas system for the other process equipment with scrubber and HEPA filtration.

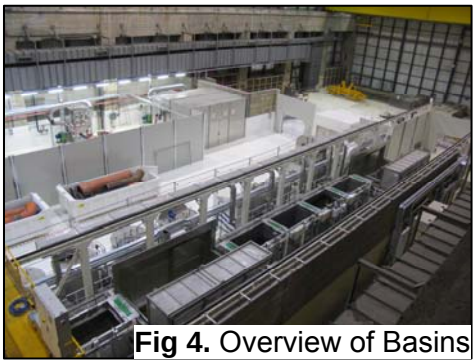

Fig 4. Overview of Basins

The PHADEC Facility installed at Caorso NPP (Piacenza, Italy) is shown in Figure 5.

Fig 5. Overview of Caorso PHADEC

4. The PHADEC Characteristics and Benefits

The main characteristics of PHADEC are schematically reported below:

- The main product of decontamination process is dry iron oxide powder, which can be easily conditioned for final storage;
- The chemical decontamination of steel scrap is done in absence of the operator supervision;
- The regeneration of contaminated acid is done in a semi-automatically closed process (personnel access is mainly not required);
- Radioactive waste is concentrated in a very limited number of components of the plant (shielded when required);
- Plant Modularisation;
- The PHADEC Facility is designed according to the applicable standards and the Accident Prevention Regulations;
- Unrestricted free release of the decontaminated material;
- Minimisation of waste (< 2% of the original material) suitable for final storage;
- Minimising of personal dose / collective dose;
- Easy management of the plant and minimum operational costs.

5. Conclusions

One of the main topics of a decontamination program specifically tailored on the free releasing of the materials is the need of a facility capable of processing important quantities of secondary waste (typically chemical solutions) resulting from the decontamination process. Each of the additional activities, which have to be foreseen in order to transform secondary waste into a properly conditioned product suitable for the final burial, can add to the occupational exposure of removal and could conceivably be greater than the dose received from removal, packing and shipping of the contaminated system without extensive decontamination.
The PHADEC process overcomes these drawbacks considering the following:

- The chemical decontamination using phosphoric acid electrolyte, duly combined with electro-polishing according to the materials to be treated, is proved to be a very efficient process to remove the radioactive contaminants achieving the free releases condition for the steel scrap;
- The process can guarantee a very high volume reduction factor considering that the recovery process for the spent phosphoric acid electrolyte overcomes the disadvantages of other decontamination processes because the secondary waste generated as by-product during the decontamination is < 2% wt. of the original material.

DISTRIBUTION AND TRANSPORT OF DEBRIS PARTICLES ON CONTAINMENT FLOOR DURING BLOWDOWN AND RECIRCULATION

Y.S. BANG, G.S.LEE, S.W.WOO
Reactor Safety Evaluation Department, Korea Institute of Nuclear Safety
19 Gusung-Dong, Yuseong-Gu, 305-335 Daejeon – Korea

J.Y.PARK
Thermal-hydraulic Safety Research Department, Korea Institute of Nuclear Safety
19 Gusung-Dong, Yuseong-Gu, 305-335 Daejeon – Korea

ABSTRACT

Concerning the sump clogging issue, the amount of debris transported to the sump, i.e., transport fraction, is the important contributor in designing the recirculation sump strainer. The present paper is to address how the debris particle is distributed over the containment floor by a loss-of-coolant accident (LOCA) and which effect on the transport fraction may be involved by the debris distribution pattern. For this purpose, a calculation model to solve two-dimensional Shallow Water Equation (SWE) is developed based on Finite Volume Method (FVM) with unstructured triangular grid to predict the transient flow field over the containment. Harten-Lax-van Leer (HLL) scheme is introduced to improve the accuracy of the prediction of dry-to-wet interface. For evaluating the debris transport during both blowdown and recirculation, a particle tracking model is developed, in which Lagrangian equation of motion is solved using the pre-calculated flow field data. The present model is applied to the Optimized Power Reactor 1000 (OPR1000). Number of particles transported to the sump pit during recirculation is calculated for the case that the debris particle is distributed uniformly on the containment floor before recirculation and the case that the distribution pattern was calculated from the beginning of LOCA.

1. Introduction

In the context of the sump clogging issue, the amount of debris transported to the sump is the important contributor to the design of recirculation sump strainer [1]. Following a Loss-of-Coolant Accident (LOCA) of Pressurized Water Reactor (PWR), a large amount of debris particles may be introduced to and re-distributed over the containment floor during blowdown phase. The debris can be transported to the sump screen and the screen may be blocked with the debris by the recirculation operation. Distribution of the debris before the recirculation is the key factor connecting two transport mechanisms. For the recirculation transport analysis, the uniform distribution of the debris over the floor resulting from the blowdown has been assumed based on the research findings and the simplicity of analysis [2]. However, the assumption of the uniform distribution regardless of geometric configuration of the containment floor of interest has been questioned since the distribution pattern may be affected by plant-specific profile and the transport fraction can be affected by the pattern.

The present paper is to discuss how the debris particle is distributed over the containment floor by the LOCA blowdown phase and which effect on transport fraction may be involved when using the uniform debris distribution. For this purpose, transient flow field on containment floor should be calculated. From the previous experiences [3], it is known that a huge amount of computational time and resources are required when applying the computational fluid dynamics (CFD) code calculation to this kind of problem, even short term transient. In the present study, a calculation model to solve the two-dimensional Shallow Water Equation

(SWE) [4] is developed, which is believed practical in computational time when compared to the sophisticated commercial CFD codes. Finite Volume Method (FVM) with unstructured triangular grid is used [5]. To improve the accuracy of the prediction of dry-to-wet interface, Harten-Lax-van Leer (HLL) scheme [6], as an approximate Riemann solver for the hyperbolic SWE, is introduced. For evaluating the debris transport during both blowdown and recirculation, a particle tracking model is developed, in which the Lagrangian equation of motion is solved using the pre-calculated flow field data. In the present model, the hosting cell which contains particles is searched using an efficient algorithm proposed by Martin [7]. The present model is applied to the Optimized Power Reactor 1000 (OPR1000) [8] of Korea. Number of particles transported to the sump pit during recirculation is calculated for the case that the debris particle is distributed uniformly on the containment floor before recirculation and the case that the distribution pattern was calculated from the beginning of LOCA.

2. Model Description

Two-dimensional Shallow Water Equation can be derived by the depth-averaging assumption from the Navier Stokes Equation and has a following form [4] :

$$\frac{\partial \boldsymbol{W}}{\partial t}+\frac{\partial \boldsymbol{F}}{\partial x}+\frac{\partial \boldsymbol{G}}{\partial y}=\frac{\partial \boldsymbol{R}_x}{\partial x}+\frac{\partial \boldsymbol{R}_y}{\partial y}+\boldsymbol{S} \quad \text{..... (1)}$$

$$\boldsymbol{W}=\lfloor h, hu, hv \rfloor^T, \boldsymbol{F}=\lfloor hu, hu^2+1/2gh^2, huv \rfloor, \boldsymbol{G}=\lfloor hv, huv, hv^2+1/2gh^2 \rfloor^T \quad \text{..... (2a)}$$

$$\boldsymbol{R}_x=\left\lfloor 0, \nu\frac{\partial hu}{\partial x}, \nu\frac{\partial hv}{\partial x} \right\rfloor^T,\ \boldsymbol{R}_y=\left\lfloor 0, \nu\frac{\partial hu}{\partial y}, \nu\frac{\partial hv}{\partial y} \right\rfloor^T \quad \text{..... (2b)}$$

$$\boldsymbol{S}=\left\lfloor B(t),\ gh(-\frac{\partial z_b}{\partial x}-\frac{un_m^{\ 2}}{h^{4/3}}\sqrt{u^2+v^2}),\ gh(-\frac{\partial z_b}{\partial y}-\frac{vn_m^{\ 2}}{h^{4/3}}\sqrt{u^2+v^2}) \right\rfloor^T \quad \text{.....(2c)}$$

where h, u, v, z_b, n_m, $B(t)$, and ν denote water level from the bed, velocity components in x and y directions, bed elevation, Manning bed friction coefficient ($m^{-1/3}s$), water source term into flow field and dynamic viscosity, respectively. Source terms due to the bed slope (S_0) and friction with bed (S_f) are included. The equation can be solved by an explicit FVM for the unstructured triangular element. In order to reserve the second order numerical accuracy in time, the predictor-corrector method [4] is applied.

$$\boldsymbol{W}_k^{n+1/2}=W_k^n-\frac{\Delta t}{2A_k}\sum_{j=1}^{3}\{(\boldsymbol{F}_j^n n_{xj}+\boldsymbol{G}_j^n n_{yj})-(\boldsymbol{R}_{x,j}^n n_{xj}+\boldsymbol{R}_{y,j}^n n_{yj})\}L_j+\boldsymbol{S}_k^{\ n}\frac{\Delta t}{2} \quad \text{..... (3a)}$$

$$\boldsymbol{W}_k^{n+1}=W_k^{n+1/2}-\frac{\Delta t}{2A_k}\sum_{j=1}^{3}\{(\boldsymbol{F}_{HLL,j}^{n+1/2} n_{xj}+\boldsymbol{G}_{HLL,j}^{n+1/2} n_{yj})-(\boldsymbol{R}_{x,j}^{n+1/2} n_{xj}+\boldsymbol{R}_{y,j}^{n+1/2} n_{yj})\}L_j+\boldsymbol{S}_k^{\ n+1/2}\frac{\Delta t}{2} \quad \text{..... (3b)}$$

In the predictor step, the intermediate time step properties are calculated using the central difference scheme for convective flux term $\boldsymbol{F}$ and $\boldsymbol{G}$. The corrector step calculates the new time properties, using the values calculated in the predictor step and using an approximate Riemann solver, Harten-Lax-van Leer (HLL) [6] scheme for the convective flux term.

$$\boldsymbol{F}_{HLL}=\begin{Bmatrix} \boldsymbol{F}(\boldsymbol{W}_L) & if \quad s_L>0 \\ \boldsymbol{F}*(\boldsymbol{W}_L,\boldsymbol{W}_R) & if \quad s_L\le 0\le s_R \\ \boldsymbol{F}(\boldsymbol{W}_R) & if \quad s_R>0 \end{Bmatrix} \quad \text{..... (4)}$$

$$\boldsymbol{F}*(\boldsymbol{W}_R,\boldsymbol{W}_L)=\frac{1}{s_R-s_L}\left[(s_R\boldsymbol{F}(\boldsymbol{W}_L)-s_L\boldsymbol{F}(\boldsymbol{W}_R))\cdot\boldsymbol{n}+s_Ls_R(\boldsymbol{W}_R-\boldsymbol{W}_L)\right] \quad \text{..... (5)}$$

where subscripts L and R represent the values at the cell right and at the cell left to the interface. s_R and s_L are wave speed at those cells defined by following equation.

$$s_L = \min(\boldsymbol{V}_L \cdot \boldsymbol{n} - \sqrt{gh_L},\ \boldsymbol{V}^* \cdot \boldsymbol{n} - c^*),\ s_R = \max(\boldsymbol{V}_R \cdot \boldsymbol{n} - \sqrt{gh_R},\ \boldsymbol{V}^* \cdot \boldsymbol{n} + c^*) \quad \text{..... (6)}$$

where velocity vector, $\boldsymbol{V}=u\boldsymbol{i}+v\boldsymbol{j}$, and the averaged terms ($\boldsymbol{V}^*$, c^*) are defined as follows:

$$\boldsymbol{V}^* \cdot \boldsymbol{n} = \frac{1}{2}(\boldsymbol{V}_L + \boldsymbol{V}_R) \cdot \boldsymbol{n} + \sqrt{gh_L} - \sqrt{gh_R}\ ,\quad c^* = \frac{1}{2}(\sqrt{gh_L} + \sqrt{gh_R}) + \frac{1}{4}(\boldsymbol{V}_L - \boldsymbol{V}_R)) \cdot \boldsymbol{n} \text{ ..... (7)}$$

The above hydraulic model was validated by the comparison with the experiment simulating a dam break with L-shaped open channel. The detailed description and validation of the present model can be found in reference [5].

Debris particle following LOCA may be transported with colliding with other particles and settling-down due to its velocity and gravity. The present model did not consider those aspects, which may be unrealistic but conservative in the viewpoint of debris transport.

Position of a particle p at time $n+1$ in two-dimensional Cartesian coordinates can be calculated from the position at n time and movement during time interval as follows:

$$\boldsymbol{x}_p^{n+1} = x_p{}^{n+1}\boldsymbol{i} + y_p{}^{n+1}\boldsymbol{j} = \boldsymbol{x}_p^n + \boldsymbol{w}_p^n \Delta t_P \quad \text{..... (8)}$$

where particle velocity, $\boldsymbol{w}_p = u_p\boldsymbol{i} + v_p\boldsymbol{j}$, can be obtained from the equation of motion with fluid velocity ($V = u\boldsymbol{i} + v\boldsymbol{j}$) which was already determined by the SWE solver,

$$m_p \frac{d\boldsymbol{w}_p}{dt} = -\boldsymbol{D}_p = -A_p C_D \frac{1}{2}\rho_f \left|\boldsymbol{w}_p - \boldsymbol{V}\right|(\boldsymbol{w}_p - \boldsymbol{V}) \text{ ..... (9)}$$

Assume the particle be in spherical shape with diameter d_p and density ρ_p, and express the time derivative term in explicit manner,

$$\boldsymbol{w}_p^n = \boldsymbol{w}_p^{n-1} - \frac{3}{4}\frac{\rho_f \Delta t_p}{\rho_p d_p} C_D^{n-1} \left|\boldsymbol{w}_p^{n-1} - \boldsymbol{V}^{n-1}\right|(\boldsymbol{w}_p^{n-1} - \boldsymbol{V}^{n-1}) \text{ ..... (10)}$$

Drag coefficient, C_D can be expressed by Schiller and Neumann correlation [9]. The hosting cell is searched by the algorithm of Martin [7], i.e., searching a cell in which inner products of vector for particle position and one for center of each side of triangular cell are all negative. The detailed description of the particle tracking model can be found at reference [10].

3. Result and Discussion

The containment floor of OPR1000 was discretized as shown in Fig. 1, which composed of 14016 cells and 7812 nodes. All important structures including primary shield wall, steam generator (SG) pedestal, etc were properly modelled. Hot leg guillotine break LOCA was selected as the most challengeable accident to the debris loading. The break flow from the FSAR was used to define the source term of the SWE. No-slip boundary condition was specified at all the structural walls. For the boundaries to the sumps where the significant vertical flow is present, the boundary condition of flow rate as a function of water level was specified, which was based on the analytic formula on broad crested weir [11].

Fig. 2 shows a distribution of water level and velocity vector of each cell at time of 26 seconds from the accident. One can find that the inside of the secondary shield wall and east half of the annulus region were covered with water.

Fig. 3 shows the calculated distribution of debris particles at 239 second from the transient. Totally, 1000 particles that were injected to the break region of the containment floor were traced. Particles are moved to and located at annulus region and at the inner region of secondary shield wall at that time. The calculated pattern of particle distribution shows a significant difference from the uniform distribution as shown in Fig. 4. Particle tracking was

performed for two cases as explained above. Flow field for recirculation was re-calculated with the sump 1 operation. The total number of particle transported to the sump 1 was compared for the two cases, as shown in Fig. 5.

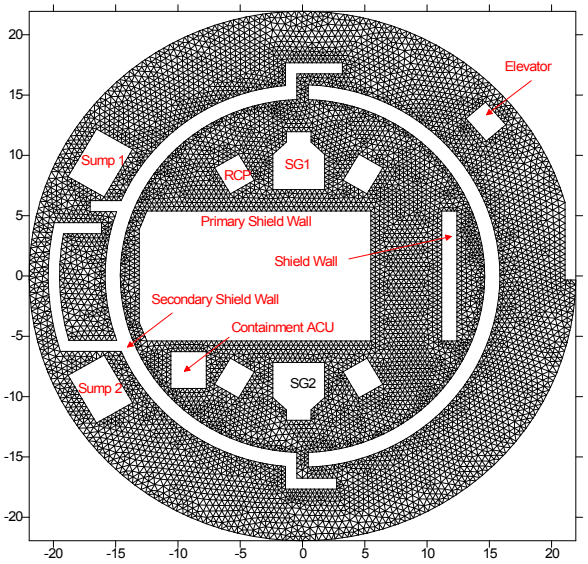

Fig. 1 Computational Mesh

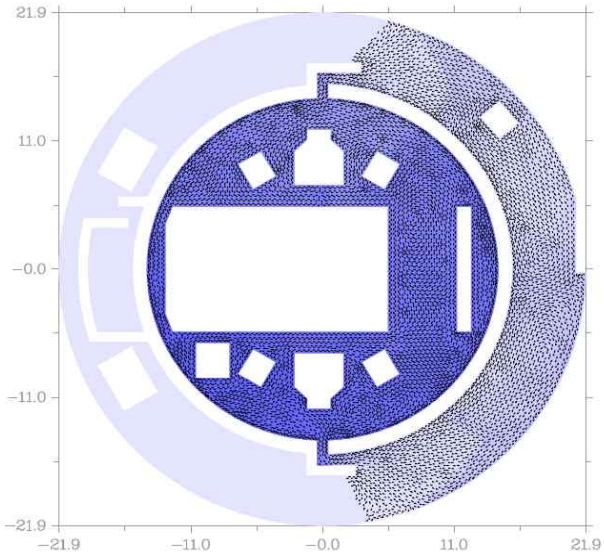

Fig. 2 Calculated Flow Field at 26 sec

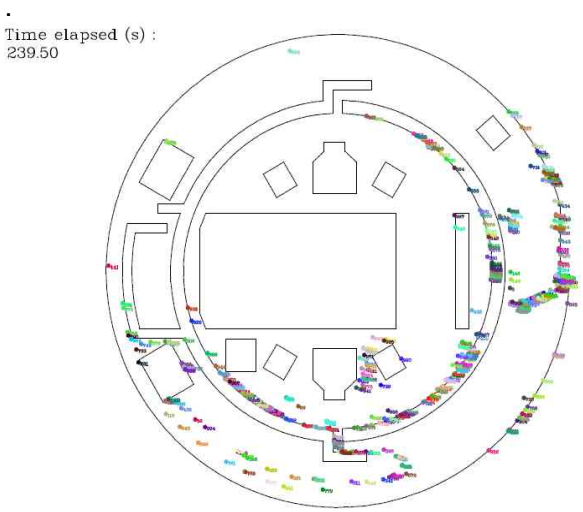

Fig. 3 Particle Distribution at 239 sec

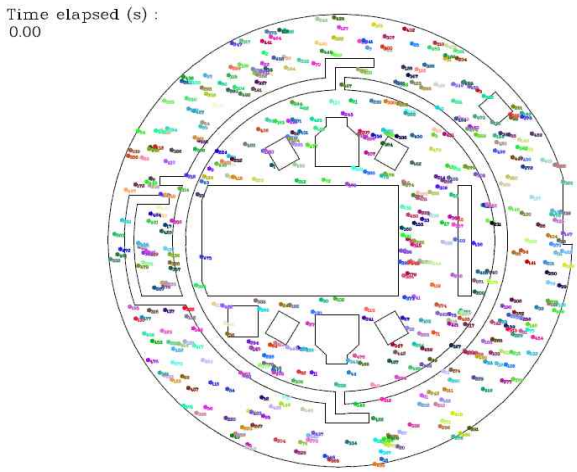

Fig. 4 Uniform Distribution of Particles

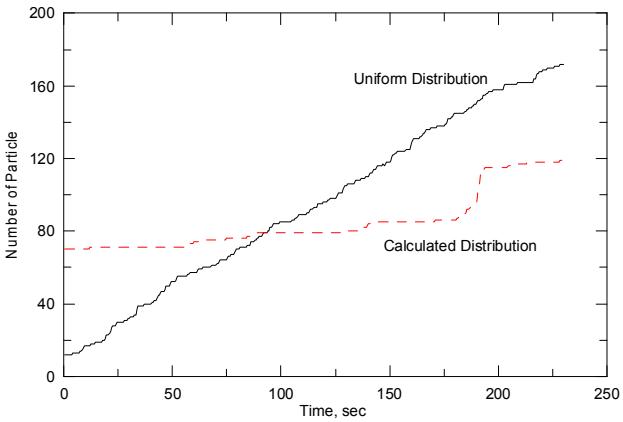

Fig. 5 Comparison of Number of Particles to Sump

As shown in the figure, the transport behaviour was quite different between two cases. For the uniform distribution case, almost linear increase of particles to sump was predicted. The result for the case using the calculated distribution showed that the number of the particle was already transported to sump before recirculation and it slowly increased and suddenly jumped. Since the current result was limited to the 230 sec., the conservatism of the uniform distribution before recirculation cannot be confirmed, however, one can state that plant-specific debris distribution before recirculation should be considered.

4. Concluding Remarks

A calculation model to solve two-dimensional Shallow Water Equation (SWE) with Finite Volume Method (FVM) in unstructured triangular grid and Harten-Lax-van Leer (HLL) scheme was developed to address how the debris particle is distributed over the containment floor by the loss-of-coolant accident (LOCA) and which effect on the transport fraction may be involved by the debris distribution pattern. Particle tracking method by the Lagrangian equation of motion having a drag force term was also developed. Linear increase of the transported particles to sump was found in the uniform distribution case, which was different from the case of calculated distribution. Therefore, the plant-specific distribution of debris particle should be considered unless the conservatism of the uniform distribution is confirmed.

This research was supported by “Development of Safety Standards and Safety Assessment Technology for Supporting the Export of Nuclear Power Plant” research program funded by the national research foundation of Korea.

5. References

[1] V. Rao, et al., GSI-191 Technical Assessment: Parametric Evaluation for Pressurized Water Reactor Recirculation Sump Performance, NUREG/CR-6762, LANL, New Mexico, USA (2002).

[2] USNRC, Safety Evaluation by the Office of NRR Related to NRC Generic Letter 2004-02, NEI Guidance Report “PWR Sump Performance Evaluation Methodology,” USNRC, Washington DC, USA (2004).

[3] J. I. Lee, et al., “Debris Transport Analysis Related with GSI-191 in Advanced Pressurized Water Reactor Equipped with IRWST,” Proc. XCFD4NRS, OECD/NEA, Grenoble, France, (2008).

[4] G. Gottardi and M. Venutelli, “Central Scheme for Two-Dimensional Dam-break Flow Simulation,” Advances in Water Resources, 27, 259~268 (2004).

[5] Y. S. Bang, et al., “Prediction of Free Surface Flow on Containment Floor Using Shallow Water Equation Solver,” NET, 41, 8 1045~1052 (2009).

[6] A. Harten, P.D. Lax, and B. van Leer, “On Upstream Differencing and Godunov-type Schemes for Hyperbolic Conservation Laws,” SIAM Review, 25, 1 (1983).

[7] G. D. Martin, et al., “Particle Host Cell Determination in Unstructured Grids,” Computers and Fluids, 38, 101 (2009).

[8] KHNP, Final Safety Analysis Report of Shinkori Units 1 and 2, (2008).

[9] E. Krepper, et al., “Numerical and Experimental Investigations for Insulation Particle Transport Phenomena in Water Flow,” Annals of Nuclear Energy, 35, 1564 (2008).

[10] Y. S. Bang, et al, “Calculation of Debris Particle Transport on Containment Floor Using Shallow Water Equation,” Paper 10135, Proc. ICAPP ’10, San Diego, USA, (2010).

[11] ANS, Design Criteria for Protection against the Effects of Compartment Flooding in Light Water Reactor Plants, ANSI/ANS-56.11, La Grange Park, USA, (1988).

CORROSION LAYERS ANALYSIS IN VVER 440 STEAM GENERATOR USING MOSSBAUER SPECTROMETRY

J. DEKAN, V. SLUGEŇ, J. LIPKA, I. TÓTH
Department of Nuclear Physics and Technology, Slovak University of Technology Bratislava
Ilkovicova 3, 812 19 Bratislava - Slovakia
julius.dekan@stuba.sk

ABSTRACT

Samples of various corrosion layers from different parts of NPP Bohunice unit were collected in order to specify composition of iron oxides found in these samples. All Mössbauer measurements were performed at room temperature in transmission geometry using a 57Co(Rh) source. Hyperfine parameters of each spectrum including spectral area (Arel), isomer shift (IS), quadrupole splitting (QS), as well as hyperfine magnetic field (Bhf), are analyzed in details. Using Mössbauer parameters we were able to distinguish different types of iron oxides (qualitative analysis), as well as relative ratio of these oxides in each sample (quantitative analysis). Based on estimated magnetite/hematite ratio, conclusion about chemical and operational environment was stated.

1. Introduction

The safe and reliable operation of steam generators is the essential pre-condition for the safe operation of the whole NPP, but also for all economical parameters at the unit. The steam generator has to be able to transfer the heat from the reactor in all operating or accidental regimes.
It is well-known that VVER-440 units have the horizontal steam generators with much higher capacity of cooling water in tank than vertical steam generators, which are normally used in western NPPs. Undoubtedly, these horizontal steam generators are more safe, but due to horizontal design as well as in total 6 loops with additional welds and pumps cover a huge area, which is a limiting factor for containment construction of the unit. The exchange of steam generators is extremely difficult (in some reactor types almost impossible), therefore their optimal operation and clever upgrade is one of essential duty of NPP staff.
Based on operational experiences, mitigation of damages and leak tightness defects in pipelines or collectors cause much more time and money, than prevention measures. It is necessary to keep in mind the actual development in nuclear industry towards NPP lifetime prolongation and power increase. Beside several leakages in primary pipelines (ø16 mm), which can be (in case of horizontal VVER-440 steam generators) relatively easy solved (blended), the corrosion of feed water pipeline system occurred at many VVER-440 units since 1994 [1]. These damages were caused mostly due to corrosion-erosion processes attacking materials familiarly called “black steels” with insufficient resistance against corrosion. Based on experiences from Finland also other countries including Slovakia changed the old feed water pipeline system. In 1998, all steam generators at four VVER-440 units in Bohunice were gradually changed. The basic design from 1977 was improved after 1995 by new feed water pipeline system. There was also change in the type of steel of these pipelines. Instead conventional carbon steel, the austenite steel was used in distribution boxes as well as feed water pipelines.
The variability of the properties and the composition of the corrosion products of the stainless CrNi and mild steels, in dependence on the conditions (temperature, acidity, etc.), is of such range that, in practice, it is impossible to determine the properties of the corrosion products for an actual case from the theoretical data only. Since the decontamination processes for the materials of the water-cooled reactor (VVER-440) secondary circuits are in the progress

of development, it is necessary to draw the needed information by the measurement and analysis of the real specimens [2]. These specimens consist of corrosion products taken from small coolant circuit of pumps, deposits scraped from filters after feed water filtration of steam generator, corrosion products taken from steam generator SG-42 pipelines, mixture of corrosion products from filter of condenser TG 42, deposits from filters after refiltering feed water of steam generators S3-09 and S4-09 during pasivation. Identification of various phase fractions of corrosion deposites is not a simple task. One of the best method for phase analyses of iron-bearing components is Mössbauer spectroscopy.

2. Mössbauer spectroscopy

Mössbauer spectroscopy (MS) is a powerful analytical technique because of its specificity for one single element and because of its extremely high sensitivity to changes in the atomic configuration in the near vicinity of the probe isotopes. MS measures hyperfine interactions and these provide valuable and often unique information about the magnetic and electronic state of the iron species, their chemical bonding to co-ordinating ligands, the local crystal symmetry at the iron sites, structural defects, lattice-dynamical properties, elastic stresses, etc. [2, 3]. Hyperfine interactions include the electric monopole interaction, i.e., the isomer shift, the electric quadrupole interaction, i.e., the quadrupole splitting, and the magnetic dipole or nuclear Zeeman interaction, i.e., hyperfine magnetic splitting. These interactions, so-called Mössbauer parameters, often enable detailed insight into the structural and magnetic environment of the Mössbauer isotope (in this case ^{57}Fe). Mössbauer parameters are different and unique for each iron-bearing compound, thus one can distinguish various corrosion products from provided samples.

3. Experimental details

Six samples for Mössbauer effect experiments were prepared by crushing to powder pieces. These samples consist of corrosion products taken from small coolant circuit of pumps (sample no. 1), deposits scraped from filters after filtration of SG - feed water during operation (sample no. 2), corrosion products taken from SG42 pipelines - low level (sample no. 3), mixture of corrosion products, ionex, and sand taken from filter of condenser to TG 42 (sample no. 4), deposit from filters after refiltering of feed water of SG S3-09 during pasivation (sample no. 5) and finally deposit from filters after refiltering of feed water of SG S4-09 during pasivation (sample no. 6). All samples were measured at room temperature in transmission geometry using a ^{57}Co(Rh) source. Calibration was performed with α-Fe. Hyperfine parameters of the spectra including spectral area (A_{rel}), isomer shift (*IS*), quadrupole splitting (*QS*), as well as hyperfine magnetic field (B_{hf}), were refined using the CONFIT fitting software [4], the accuracy in their determination are of $\pm$0.5 % for relative area Arel, $\pm$0.04 mm/s for Isomer Shift and Quadrupole splitting and $\pm$0.5 T for hyperfine field correspondingly. Hyperfine parameters for identified components (haematite, magnetite, goethite, lepidocrocite, feroxyhyte) are taken from [5].

4. Results

All measured spectra contains iron in magnetic and many times also in paramagnetic phases. Magnetic phases contains iron in nonstoichiometric magnetite $Fe_{3-x}MxO_4$ where Mx are impurities and vacancies which substitute iron in octahedral (B) sites. Another magnetic fraction is haematite α-Fe_2O_3. In one sample also the magnetic hydroxide (goethite α-FeOOH) was identified. Paramagnetic fractions are presented in the spectra by quadrupole doublets (QS). Their parameters are close to those of hydroxides e.g. lepidocrocite γ – FeOOH or to small so called superparamagnetic particles of iron oxides or hydroxides with the mean diameter of about 10 nm.

Mössbauer spectrum (Fig. 1) of sample no. 1. (corrosion products taken from small coolant circuit of pumps) consists of thee magnetically split components, where the component with

hyperfine field B_{hf} = 35.8 T was identified as goethite (α-FeOOH). Hyperfine parameters of remaining two magnetically split components are assigned to A – sites and B – sites of magnetite (Fe_3O_4). One paramagnetic spectral component has appeared. According to water environment and pH [6], this component should be assigned to hydrooxide (feroxyhyte δ-FeOOH).

Sample no. 2. (deposits scraped from filters after filtration of SG - feed water during operation) also consists of three magnetically split components, where two of them were assigned to magnetite (Fe_3O_4) as in previous spectra, and the remaining magnetically split component was identified as haematite (α-Fe_2O_3). Paramagnetic part of the spectra was formed by one dublet, which was hyperfine parameters were assigned to hydroxide (lepidocrocite γ-FeOOH). Spectrum is shown in Fig. 2.

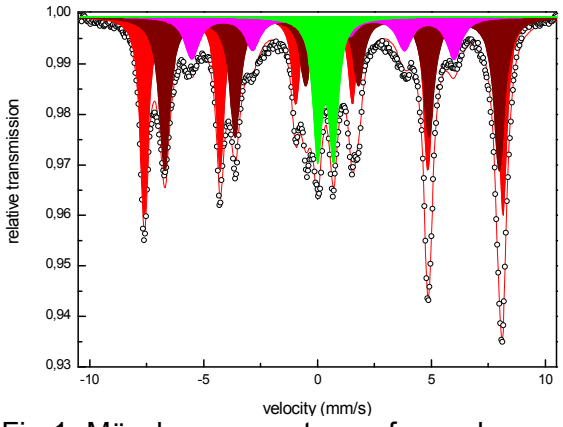

Fig 1. Mössbauer spectrum of sample no. 1. A-site (red), B-site (dark red) magnetite, goethite (pink) and hydroxide (green) was identified.

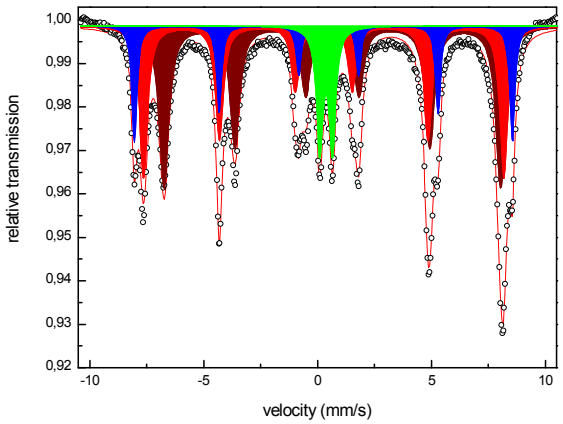

Fig 2. Mössbauer spectrum of sample no. 2. A-site (red), B-site (dark red) magnetite, haematite (blue) and hydroxide (green) was identified.

The spectrum (Fig. 3) of sample no. 3. (corrosion products taken from SG42 pipelines - low level) consists only of two magnetically split components with hyperfine parameters assigned to A – sites and B – sites of nearly stoichiometric magnetite (Fe_3O_4) with relative area ratio β = 1.85.

Sample no. 4. (mixture of corrosion products, ionex, sand taken from filter of condenser to TG 42) also consist of magnetically split component which correspond to haematite (α-Fe_2O_3) and two magnetically split components were assigned to magnetite (Fe_3O_4) as in previous spectra, and the remaining paramagnetic component was identified as hydroxide. Spectrum of sample no. 4 is shown in Fig. 4.

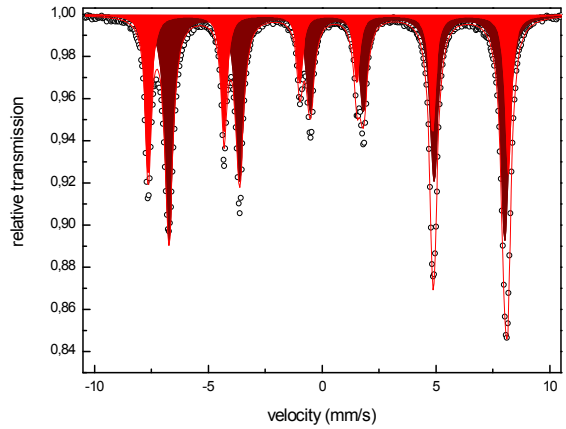

Fig 3. Mössbauer spectrum of sample no. 3. A-site (red) , B-site (dark red) magnetite was identified.

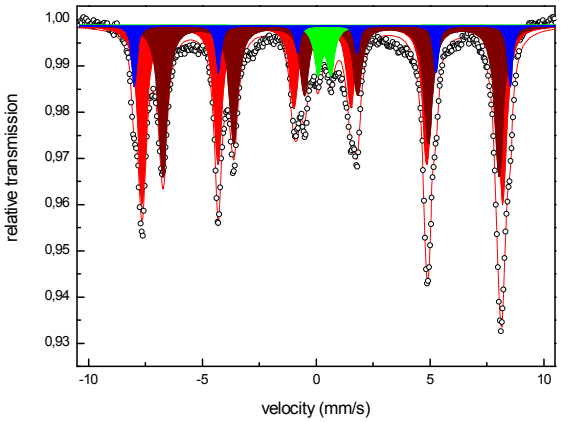

Fig 4. Mössbauer spectrum of sample no. 4. Haematite (blue), A-site (red) , B-site (dark red) magnetite and hydroxide (green) was identified.

Both sample no. 5. (deposit from filters after 340 l of feed water of SG S3-09 during pasivation 27. and 28. 5. 08) and sample no. 6. (deposit from filters after 367 l of feed water of SG S4-09 during pasivation 27. and 28. 5. 08) consists of three magnetically split components, identified as haematite (α-Fe_2O_3) and magnetite (Fe_3O_4) and the remaining paramagnetic component in both spectra was assigned as hydrooxide (lepidocrocite γ-FeOOH). Spectra of sample no. 5. and 6. are shown in Figs. 5. and 6.
As it was mentioned above all hydroxides could be also small superparamagnetic particles.

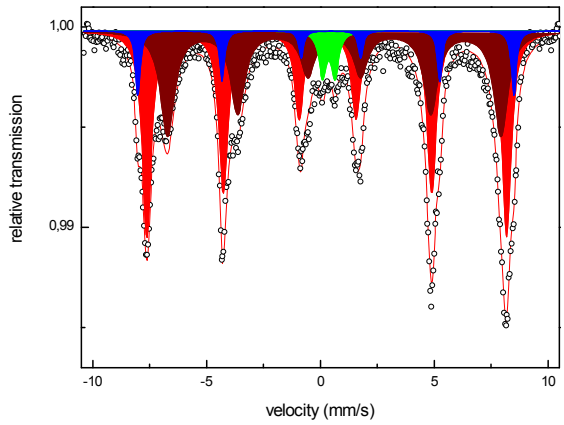

Fig 5. Mössbauer spectrum of sample no.5. Haematite (blue), A-site (red) , B-site (dark red) magnetite and hydroxide (green) was identified.

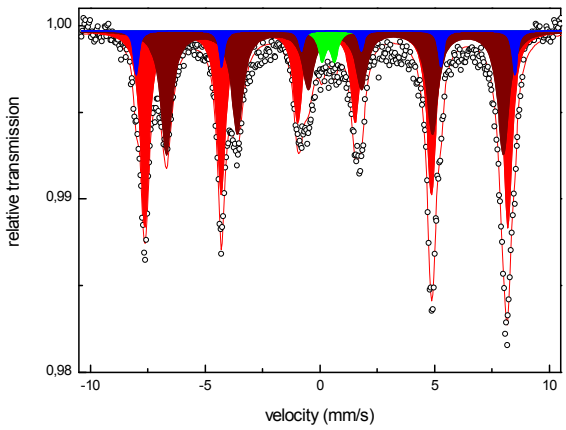

Fig 6. Mössbauer spectrum of sample no. 6. Haematite (blue), A-site (red) , B-site (dark red) magnetite and hydroxide (green) was identified.

The refined spectral parameters of individual components including spectral area (A_{rel}), isomer shift (*IS*), quadrupole splitting (*QS*), as well as hyperfine magnetic field (B_{hf}) are listed in Table 1. for room (300 K) temperature Mössbauer effect experiments.

5. Conclusion

Our results confirm good operational experiences and suitable chemical regimes (reduction environment) which results mostly to creation of magnetite (on the level 70% or higher) and small portions of hematite, ghoetite or hydrooxides. Based on these results, it is possible to conclude that the replacement of STN 12022 steel (in Russian NPP marked as GOST 20K) used in the steam generator feed water systems is necessary and very important from the operational as well as nuclear safety point of view. Steel STN 17 247 proved 5 years in operation at SG35 seems to be optimal solution of this problem. Basically, the corrosion of new feed water pipelines system (from austenitic steel) in combination to operation regimes (as it was at SG35 since 1998) goes to magnetite. Comparison of results obtained from samples 5. and 6. confirms the fact that the longer passivation improves amount of magnetite fraction in the corrosion products composition.
In connection to planned NPP Mochovce 3, 4 commissioning (announced officially at 3.10.2008) it is recommended that all feed water pipelines and water distribution systems in steam generators should be replaced immediately before putting in operation by new ones constructed from austenitic steels. The Bohunice design with feed water distribution boxes is highly recommended and it seems to be accepted from the utility side.

sample	Component	Area [%]	Isomer shift [mm/s]	Quadrupole shift/splitting [mm/s]	Hyperfine field [T]
Sample no. 1. Small coolant circuit of pumps	magnetite A-site	36.3	0.28	0.00	48.90
	magnetite B-site	37.2	0.64	0.00	45.60
	goethite	14.4	0.36	-0.25	35.80
	hydrooxide	12.1	0.36	0.70	-
Sample no. 2. Deposites scraped from filters after filtration of SG - feed water during operation	haematite	15.8	0.38	-0.23	51.56
	magnetite A-site	32.6	0.28	0.00	49.14
	magnetite B-site	41.8	0.65	0.00	45.91
	hydrooxide	9.7	0.38	0.56	-
Sample no. 3. SG42 pipelines - low level	magnetite A-site	34.6	0.28	0.00	49.14
	magnetite B-site	65.4	0.65	0.00	45.83
Sample no. 4. Mixture of corrosion products, ionex, sand taken from filter of condenser TG 42	haematite	9.2	0.38	-0.22	51.29
	magnetite A-site	45.4	0.28	0.00	49.20
	magnetite B-site	40.7	0.66	0.00	45.87
	hydrooxide	4.7	0.37	0.56	-
Sample no. 5. Deposit from filters after 340 l of feed water of SG S3-09 during pasivation 27. and 28. 5. 08	haematite	8.3	0.36	-0.22	51.33
	magnetite A-site	49.3	0.30	0.00	49.11
	magnetite B-site	38.5	0.61	0.00	45.51
	hydrooxide	3.9	0.37	0.55	-
Sample no. 6. Deposit from filters after 367 l of feed water of SG S4-09 during pasivation 27. and 28. 5. 08	haematite	6.4	0.38	-0.25	51.26
	magnetite A-site	50.3	0.29	0.00	49.14
	magnetite B-site	40.7	0.66	0.00	45.61
	hydrooxide	2.6	0.37	0.54	-

Tab 1. Spectral parameters of individual components including spectral area (A_{rel}), isomer shift (IS), quadrupole splitting (QS), as well as hyperfine magnetic field (B_{hf}) for each

6. References

[1] Savolainen, S., Elsing, B., Exchange of feed water pipeline at NPP Loviisa, Proceedings from the 3rd seminar about horizontal steam generators, Lappeenranta, Finland, (18.-20.10.1994)

[2] Cohen, L., Application of Mössbauer spectroscopy, Volume II. ed. Academic Press, USA, New York, (1980).

[3] G. Brauer, W. Matz and Cs. Fetzer, Hyperfine Interaction 56 (1990) 1563.

[4] Kučera J., Veselý V., Žák T.: Mössbauer Spectra Convolution Fit for Windows 98/XP, (2007),

[5] Cornell R. M., Schwertmann U., In: The Iron Oxides, (1996), ISBN 3-527-28576-8

[6] Kritsky, V. G., Water Chemistry and Corrosion of Nuclear Power Plant Structural Materials, 1999, ISBN 0-89448-565-2

CONTAMINATION REDUCTION IN A HOT CELL BY USE OF A REMOTE-OPERATED LASER SYSTEM: A PROOF OF CONCEPT

F. CHAMPONNOIS, C. LASCOUTOUNA, H. LONG, P.-Y. THRO, P. MAUCHIEN
DEN/DANS/DPC/SCP
CEA/Saclay
Bât. 467, 91191 Gif-sur-Yvette Cedex, France
pierre-yves.thro@cea.fr

G.-M. DECROIX, J. VIARD
DEN/DANS/DMN/SEMI
CEA/Saclay
Bât. 467, 91191 Gif-sur-Yvette Cedex, France

ABSTRACT

Complete or partial decontamination of hot cells for decommissioning or refurbishment is a source of potentially high human exposure. After having emptied the hot cell, highly contaminated spots can remain on the walls or the floor and could be difficult to remove. Commonly used techniques have limited decontamination factor (brushes…) or produce large amount of secondary waste (gels, particles or gas projection…). And most of the time the final step has to be done by workers who are then exposed to high radiation doses.
In this contribution we describe the use of a remotely operated laser system which is able to remove contamination through laser ablation. The advantage of this system is that it could be able to reach high decontamination efficiency with a low production of waste. The system is based on a low power (20 W), pulsed laser whose beam can be scanned over a plane surface (30x30 cm²). Ablated matter containing the contaminants is then collected and sent to filters.
For the first demonstration, the system was introduced in a hot cell which was used to conduct research and analyses on used nuclear fuel. Activities were stopped in 1995 and the installation is now awaiting a plan for decommissioning.
The laser system was introduced in two parts from a 60 cm wide hole in the roof and was then assembled in the cell using two telemanipulators. They were also used to maintain the system in place during the process. Decontamination tests were conducted on the wall and on the floor. In order to attest the decontamination efficiency, radiation measurements were made before and after processing on the surface and in the waste containers. First results show that the decontamination factor is as high as 20 and in the same order as for gels for example.

1. Introduction

Laser is a highly attractive tool for decontaminating nuclear installations: It could be very efficient, reliable, automated, limiting both worker exposure and waste volume. We developed a new decontaminating system based on pulsed fibre lasers. It is described elsewhere in these proceedings [1]. It has the advantage of being compact and scalable and can collect all particles and gases emitted during the laser process. This last point is important to avoid moving the contamination from one place to the other in a more intractable form (very small particles spread all over the cell).

In this contribution we describe the use of a laser system in a hot cell. When a hot cell has to be dismantled or refurbished the first operation is to remove all the items from the cell. Most of the time, before workers can enter the room, a first decontamination has to be undertaken to lower the activity to a reasonable level. It is of course desirable that the chosen technique is efficient, produces as little secondary waste as possible and is carried out remotely.

The goal of the experiment described here is to verify the feasibility and the efficiency of our decontamination laser system called ASPILASER to decontaminate or, at least, to reduce the activity down to sufficiently low level to allow man access inside the shielded cell. The system has to be of course completely remote-handled by the existing telemanipulators. The system was tested in real nuclear environment (in a nuclear facility in the CEA centre of Saclay, France) and showed its potentiality in comparison with other techniques.

2. The hot cell Célimène

The hot cell used for these experiments, called Célimène, is a shielded cell which was used for post-irradiation examination of spent fuel. It was shutdown 15 years ago and replaced by newer installations. It had high level of radioactivity spread widely over all the internal surfaces and the equipments. Almost all the items were removed from the cell and a first decontamination was conducted by CO_2 jetting to reduce the activity and keep it in a safe state pending final dismantling.

The cell is 6m long by 3m deep and 6 m high. It has two portholes and four operating telemanipulators. It has a 60 cm wide hole on the roof to introduce equipments. The cell walls are covered with paint metallic sheets. Figure 1 shows a schematic view of the cell.

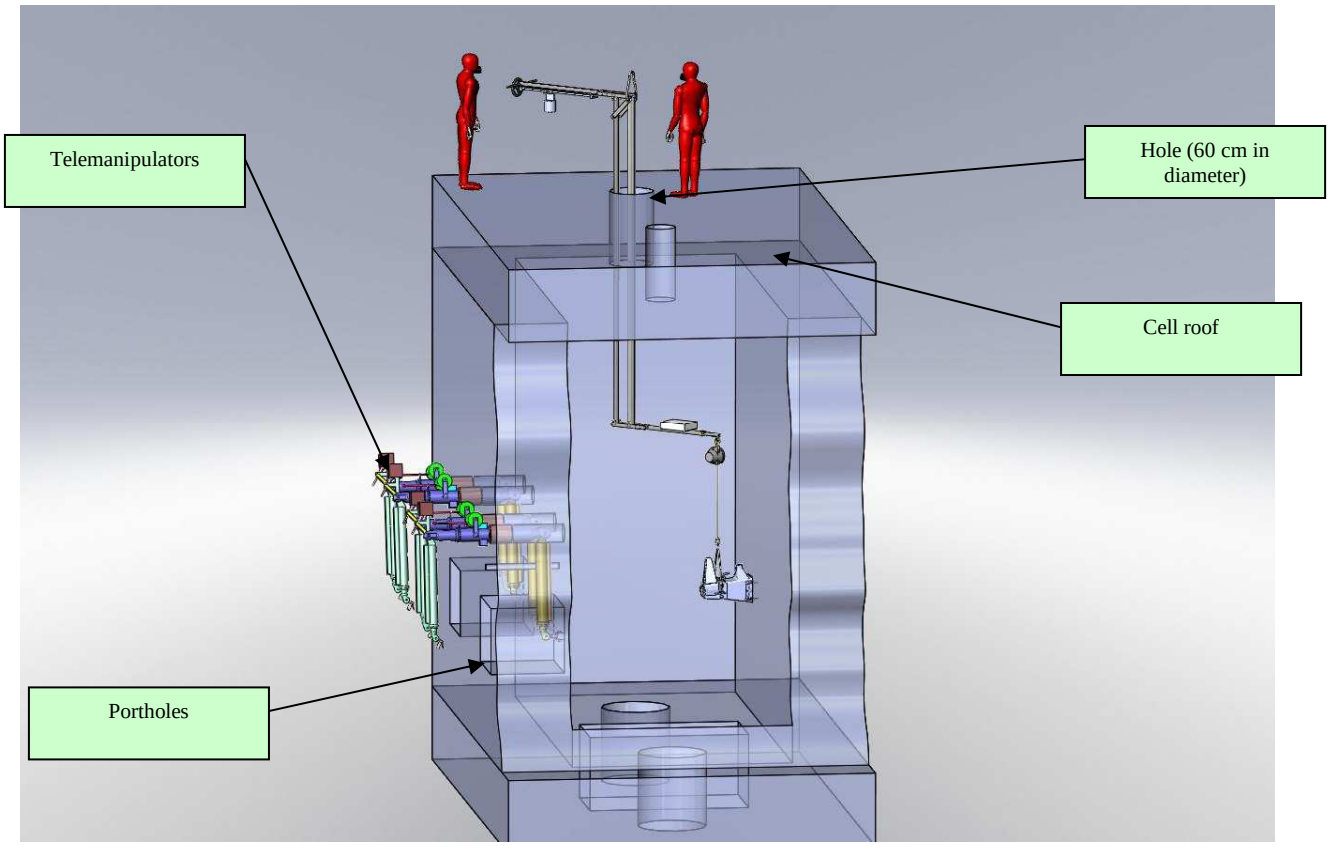

Fig.1: Schematic view of the Célimène hot cell

3. Modification of the laser system

The system is based on compact, industrial and reliable pulsed fibre lasers. These lasers have a moderate average power (20 to 50 W) and produce 1 mJ pulses at high repetition rates (20 to 50 kHz) and short pulse length (140 ns). To work in the ablation regime (where the matter is heated up to the vaporisation temperature) the laser beam is focused onto the surface by a lens. A scan head is associated to the laser to perform the beam scanning over a unit area of 30x30 cm². A vacuum cleaner collects all the gases and particles emitted by

the process and send them to nuclear grade filters. To guarantee that all the particles are collected an aspiration cone is put in front of the ASPILASER between the surface to be decontaminated and the focusing lens (see figure 2).

The system is modular and can accept up to four lasers to increase the efficiency or decrease the process time. For the present test we only used one 20-watt laser. The total power of the system can be increased by a factor of 10 by using four 50-watt lasers.

As the overall system is larger than 60 cm, the aspiration cone and the laser head have to be introduced separately and assembled in the cell. The aspiration pipe brings the collected particles to the filters which are located outside the cell, on the roof in our case.

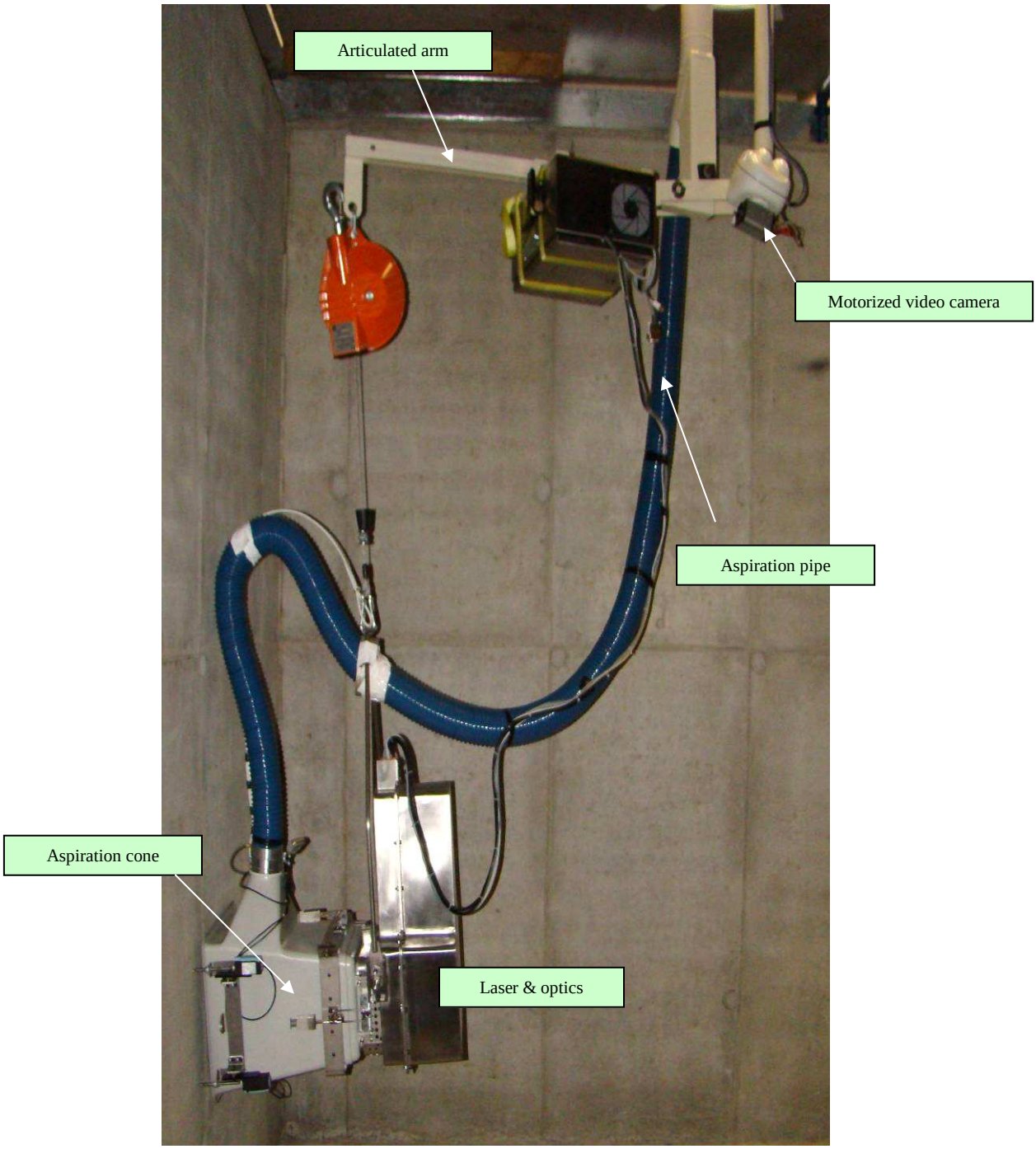

Fig. 2: Photograph of the decontamination system in the test cell

To bear the weight of the system (30 kg) an articulated arm was conceived by the company SALVAREM. This arm is used to hold the system and the telemanipulator moves it to desired place and keep in place during the process (figures 1 and 2).

The complete system was qualified in a test cell before introduction in Célimène. Figure 2 shows a photograph of the apparatus. A motorized video camera is fixed on the arm to guide the ASPILASER movements. It is useful because the view through the porthole is very limited and distorted.

4. Results

Three smear tests were carried out in order to evaluate the initial contamination: two on the wall, one on the floor. The results are given in table 1.

Table 1: Results of the smear tests before decontamination on the wall and the floor

	Value (shot/s)
Smear test n°1 (wall)	400
Smear test n°2 (wall)	200
Smear test n°3 (floor)	800

The whole system was then introduced in the shielded cell from the roof and assembled with two telemanipulators. The decontamination was then undertaken where the smear tests were performed. The laser beam was scanned 3 times over the surface and then a second set of smear tests was done to evaluate the decontamination factor.

Fig.3: ASPILASER in the shielded cell

We obtain a decontamination factor (DF) of 20 in case 1 and 3. For case 2, the material was soiled when removed from the cell and couldn't be analysed. This DF could be easily improved by increasing the number of passes.

5. Conclusion

We tested a newly developed decontamination system based on a compact laser source in a hot cell. We showed that the system can be remote handled and can efficiently remove contamination on walls and floor. The decontamination factor obtained in this first experiment was approximately 20 which is in the same order of magnitude than for example gels. The system was assembled with the telemanipulators and run without raising any problem.

This system could be very useful to decontaminate hot cells before dismantling or refurbishment. It produced little secondary waste and can be remotely handled thus limiting dose to the operators.

Some improvements are underway especially in order to avoid any assembly in the cell and to bring the main part of the electronics outside.

The Aspilaser system is industrialised the ASTRIANE (Manosque, France).

6. References

[1] Champonnois F. & al., *Optimized laser system for decontamination of painted surfaces*, Proceedings ENC 2010, 2010

RISK QUANTIFICATION IN DETERMINISTIC PROCEDURES: OUTAGE KEY SAFETY FUNCTIONS EVALUATION USING PROBABILISTIC RISK ASSESSMENT

M.M. CID, J.DIES, C.TAPIA, O.VIÑALS
Nuclear Engineering Research Group (NERG), Department of Physics and Nuclear Engineering (DFEN), Technical University of Catalonia (UPC)
Av.Diagonal 647, 08028 Barcelona – Spain

ABSTRACT

In 2007 a collaboration agreement between the Nuclear Industry and the Nuclear Engineering Research Group of the Technical University of Catalonia (NERG-UPC) began on the Risk-Informed Operation Decision Management field.
A Manual has been created; it provides a guidance of the systematic of using Probabilistic Risk Assessment for the evaluation of guides or procedures which ensure the compliment of Outage Key Safety Functions (OKSF) in nuclear power plants.
The evaluation base is probabilistic; the core damage frequencies (CDF) values determine the acceptance of the analyzed guides and encourage suggestions for improvements in the contained procedures. Acceptance criteria from Plants Supervision System (Ref.1) are used throw out quantifications. The developed methodology pretends to evaluate the risk associated to the availability system configurations during the outage. The documents used in the development have been: PRA, OKSF procedure and Performance Technical Specifications (PTS) from a 3 loops Westinghouse PWR. As a pilot experience, the methodology has been applied to the 3th and 13th Operational Plant State (OPS), always within the operational mode 4.
Some conclusions of the analysis:
The analyzed procedure requires the operability of just one charge pump as boric acid supply source. PRA gives a CDF increase (ΔCDF) of $1{,}19 \cdot 10^{-6}$ $year^{-1}$ for the pump in standby, consequently, an exposure time T= 53,6 hours. Given an average time for the OPS of 40 hours, it is concluded the correct treatment of the procedure. However, it could be improved with the inclusion of an additional inventory replacement function. This would limit the charge pump unavailability. On the other hand, the availability of the external electrical sources is ratified. The procedure requires the operability of both supplies during the OPS. The unavailability of one of them (transformer fail) involves a ΔCDF equal to $1{,}64 \cdot 10^{-5}$ $year^{-1}$ and a T= 3,89 hours. Then, it is considered appropriate the treatment of the procedure from the PRA point of view.

1. Introduction

The developed methodology seeks the risk assessment associated to the systems availability configurations during the outage. Alternative modes PRA determines the acceptance of the assumed risks. For this, an approximation is made based on the analysis of the PTS and the guide which develops the maintenance of the OKSF in any OPS. It is achieved through the following tasks:

Obtaining a PRA model. Setting out from the database (full power or alternative mode depending of the object of the Guide) and from the PRA information of the plant, it is necessary to create a new database restricted to the Operation Mode (M Mode) studied. The

process consists in the elimination of the maintenances, calibration and testing events, filter the scenarios of the M mode and finally prorate the frequencies of the initiating events (IE).

Safety functions analysis. First, it is necessary to analyze the OKSF contained in the PTS, the Manual and the PRA. From these documents will be extracted the Key Safety Functions (KSF) contemplated or required for each one of them. KSF are compared to allow their separation depending if these are common to the three documents or not. Each group of functions is called zone. PRA functions are obtained from the M mode scenarios headers.

Configuration analysis. For each of the configurations, focusing on the performance of the functions, it is determined their allowance (or in which level) for later quantification.

Risk quantification. Once the different zones have been separated and the restricted database is completed, the quantification begins. Using the indicated software, Core Damage Frequency (CDF), Core Damage Frequency Variation (ΔCDF) and maximum exposure Time (T. exp.) are evaluated for a Core Damage Probability (CDP) equal to 10^{-6}.
First of all, it will be analyzed the PRA exclusive KSF. Then, common functions will be examined. Finally, the obtained results will be used to reach conclusions and set out recommendations and changes.

2. Acquiring of the M mode exclusive database

To realize the quantification calculus is needed previously the conversion of the PRA database in a restricted one for a concrete mode (M mode). It is necessary to remove the events unavailable for maintenance. The result of this procedure is a base core damage frequency CDFM0. It this section, it will be explained the procedure to obtain this value.

2.1 Unavailability events for maintenance to zero

The first step is to exclude from the study basic events related with the components unavailability associated with programmed tasks such as maintenance, tests or calibration unavailability. These events are already considered in the guide configurations. It has been assigned a FALSE condition to them in the database. This will give to events a null unavailability value which entail these do not exist.
Once discards are done, the value of the CDF may decrease. This database is defined such as Intermediate 1 database (DBI1).

2.2 Scenarios selection

Next step consist in eliminate all the scenarios with no relation with the M operation mode. The frequency value for the scenarios not belonging to the M mode must be set to zero. Some of these scenarios can be shared with N mode. It is obtained DBI2.

2.3 Prorate of the M mode scenarios frequencies

If the PRA considers an annual frequency per year for the initiators, it must be obtained an specific initiator frequency for the mode M.
The M mode operation time supposes a TM% percentage of all operation time of the plant. This percentage is divided among the operational plant states (OPS) the M mode contains.
It must be taken into account that M mode shared with N mode scenarios may be only a few. For this reason, it won't be considered the N mode percentage time (TN%) but the own time of every Plant Operation State time ($TPOS_i$ %). Not M mode exclusive scenarios may be subject to slight correction of its frequency.

Given the frequency for M and N modes $f_{M+N,}$ the new frequency restricted to M mode f_M can be found following:

$$f_M = \frac{TM\%}{\sum_{i=1} TOPS_i\% + TM\%} \cdot f_{M+N} = X \cdot f_{M+N}$$

Where the X factor will be multiplied by shared events. With the new values can be finally calculated the CDF in the M mode: CDFM0.

3. Sources analysis

The object of the methodology is to analyze limitations of the key safety functions unavailability based on risk. For this reason, it is necessary to lay down the limitations to study, given by KSF and PTS. On the other side, it is required an assessment of the functions considered in the PRA. This assessment can establish the PRA abilities such as finding risk significance functions not contemplated previously.

Obtaining of the functions from the diverse sources is detailed bellow:

3.1 Key Safety Functions in the PRA

Starting from the headers considered in the sequence analysis, can be determined the safety functions in the PRA.

3.2 PTS and OKSF assessment

Both in the safety functions procedure and in the performance technical specifications, following tasks must be carried on:

Locate the specifications for the OPS related to the first level PRA. Limiting conditions will be present.
Group the specifications in safety subfunctions, following the required functions by the PRA.
Classify all the functions previously obtained.

The next step is to assess the contribution to the CDF because of the absence of the functions.

4. Quantification parameters:

In the quantification of the risk significance of the different functions, are used the following parameters:

4.1 Core Damage Frequency (CDF)

The first risk measurement is the punctual core damage frequency. This parameter determines the frequency of core damage considering the analyzed functions or component as unavailable.
This value is obtained from the quantification of the PRA restricted model (described in 2). Setting to TRUE the basic event or gate that represents the functions. This measure allows to know the relative impact of the tested configuration.

4.2 Maximum exposure time for a Core Damage Probability Variation (ΔCDP) of 10^{-6}

In the risk analysis is accepted a core damage probability variation equal to 10^{-6} (Ref.1). Using this value and the core damage frequencies of the evaluated configurations, it can be obtained a recommended maximum exposure time.
Time T determines the recommended maximum duration to keep safety a configuration. The ΔCDP can be found according to the following expression:

$$\Delta CDP = \frac{\Delta CDF\,(year^{-1}) \cdot T(h)}{8760\,\frac{h}{year} \cdot TM\%}$$

Where ΔCDF is obtained from the CDF calculated previously for the configuration and the CDF with null maintenance by the following expression:

$$\Delta CDF = CDF\text{-}CDF_{M0}$$

Isolating the exposure time T and imposing $\Delta CDP = 10^{-6}$:

$$T(h) = 10^{-6} \cdot \frac{8760\,\frac{h}{year} \cdot TM\%}{\Delta CDF\,(year^{-1})}$$

TM% is the annual percentage of the total M mode operation time of the plant.

5. Results:

The documents used in the development have been: PRA, OKSF procedure and Performance Technical Specifications (PTS) from a 3 loops Westinghouse PWR. As a pilot experience, the methodology has been applied to the 3th and 13th Operational Plant State (OPS), always within the operational mode 4.
The analyzed safety functions in this mode are: reactivity control, residual heat removal, availability of electrical power, containment integrity and coolant inventory control.
Highlights of the study:

- The analyzed procedure requires the operability of both emergency Diesel Generators (DG) during the PTS. The DG with a higher risk implication supposes a CDF increase (ΔCDF) of $8{,}03 \cdot 10^{-7}$ $year^{-1}$. Therefore, a maximum exposure time of 79 hours. Given an average time for the OPS of 40 hours, it is concluded an unwarranted restriction according to the PRA. That is, it may consider permitted the maintenance in this OPS provided that its duration does not exceed the calculated 79 hours.

- On the other hand, the availability of the external electrical sources is ratified. The procedure requires the operability of both supplies during the OPS. The unavailability of one of them (transformer fail) involves a ΔCDF equal to $1{,}64 \cdot 10^{-5}$ $year^{-1}$ and a T= 3,89 hours. Then, it is considered appropriated the treatment of the procedure from the PRA point of view.

- The analyzed procedure requires the operability of just one charge pump as boric acid supply source. In case of Lost of Coolant Accident (LOCA), it is not considered the function reposition of inventory. PRA gives a CDF increase (ΔCDF) of $1{,}19 \cdot 10^{-6}$ $year^{-1}$ for the pump in standby, consequently, an exposure time T= 53,6 hours. Given an average time for the OPS of 40 hours, it is concluded the correct treatment of the procedure. However, it could be improved with the inclusion of an additional inventory replacement function. This would limit the charge pump unavailability.

6. Conclusions:

It has been created a methodology for the evaluation (using the PRA) of the configurations permitted in the OKSF procedures. The methodology could be used for a generic evaluation of this kind of procedures. Thus, could be ratified the limitations, recommend new limitations or relax the existing.
Following this methodology, a pilot experience has been developed. The study has been applied in particular OPS. Results, in most of the cases, ratify the correct treatment of the functions in PTS and OKSF. In other cases, the procedure is too conservative, allowing more relaxed risk criteria for the procedure.
Finally, note that for this type of analysis it is required a probabilistic risk assessment without a high level of uncertainties or excessive conservatism. On the contrary, recommendations would not be in accordance with the risk reality.

7. References

1. **CSN**. PG.IV.07 Integrated Plant Supervision System (SISC). Spanish Nuclear Safety Council. 2007.
2. **CSN**. Integrated Program Implementation and Use of Probabilistic Safety Assessment (PSA) in Spain. Other Documents Collection, 7.1998. 2nd Edition. Spanish Nuclear Safety Council. 1998.
3. **USNRC**. SR P Cap. 19, Rev. 1. Use of Probabilistic Risk Assessment in Plant-specific Risk-Informed Decision-making: General Guidance. November, 2002.
4. **CSN**. GS-1.15 Updating and maintenance of Probabilistic Safety Analysis. Spanish Nuclear Safety Council. 2004.
5. **EPRI.** EPRI-TR 05396, PSA Applications Guide. Final Report. 1995.
6. **USNRC**. Risk-Informed Regulations Implementation Plan. Secy-00-0213, October 16, 2000; Updated December 5, 2001 As Secy-01-0218.
7. **USNRC**. “An Approach For Plant-Specific, Risk-Informed Decision-Making” In-Service Testing, Regulatory Guide 1.175, August 1998.
8. RISKSPECTRUM PSA PROFESIONAL MANUAL .
9. **NUMARC 91-06.** Guidelines for Industry Actions to Assess Shutdown Managment. December 1991.
10. **CSN**. PT.IV.301 Determination Process significance for Power Operations (SISC). Spanish Nuclear Safety Council. 2006.

CONDENSATION WITHIN SMALL COMPARTMENTS DURING DESIGN BASIS ACCIDENTS

D. GRGIĆ, N. ČAVLINA
Faculty of Electrical Engineering and Computing, University of Zagreb
Unska 3, 10000 Zagreb, Croatia

A. ANTOLOVIČ
NPP Krško, Engineering Department
Vrbina 12, 8270 Krško, Slovenia

ABSTRACT

During design basis events (LOCA, MSLB) in containment exists possibility for additional condensation within compartments and enclosures with different electrical equipment that can result in submergence of its parts and possible malfunction. The condensation within limit switch compartments (valve actuators) and attached electrical conduits during limiting LOCA and MSLB accidents in containment was analyzed using Gothic computer code with the assumptions corresponding to the ones used to generate containment EQ profiles for thermal-hydraulic EQ parameters. The outcome of the analysis is volume of the liquid within the compartment and corresponding liquid level before and after additions of bottom openings (T-drains) required to drain condensed liquid. Different compartment sizes were analyzed during different LOCA and MSLB scenarios. After addition of bottom openings maximum possible condensed liquid level can not cause actuator malfunction.

1. Introduction

During design basis events (Loss OF Coolant Accident - LOCA, Main Steam Line Break - MSLB) in containment exists possibility for additional condensation within compartments and enclosures with different electrical equipment that can result in submergence of its parts and possible malfunction. The problem is usually covered within Environmental Qualification (EQ) activities or it is direct extension of EQ calculation. The condensation within Limitorque limit switch compartments (actuators SMB000, SMB00 and SB00) and attached electrical conduits during limiting LOCA and MSLB accidents in containment was analyzed for the input design basis events used in the development of NPP Krsko (NEK) EQ zone parameters as described in report “Development of NEK Environmental Qualification Zone Maps and Conditions”, ref. [11].

The outcome of the present analysis is volume of the liquid within the compartment and corresponding liquid level before and after additions of bottom openings (T-drains) required to drain condensed liquid. The calculation is performed using GOTHIC computer code, ref. [33], with the same assumptions used in development of containment thermal-hydraulic EQ parameters, ref. [42]. Actual plant valve actuators configurations were considered in calculation. Model SMB000 actuator limit switch compartment has the smallest volume and as such represents the conservative case in the sense of possible flooding. Limit switch compartment dimensions are taken from plant’s drawings. Two galvanized rigid metal conduits (Trade Size: 1,5“, ID: 1,624“, OD: 1,900“) enter limit switch compartment from the top. Conservative 50 m length of each conduit was considered in calculation based on performed plant walk downs. Connection between limit switch compartment and conduit is not steam tight. Based on performed calculations, two 1/8“ T-drains are installed at the bottom of limit switch compartment. The liquid level for the new configuration and all possible

accidents was checked. The liquid level was calculated based on minimum bottom area (possible different orientations can be taken into account using calculated liquid volume).

2. Mathematical model used in calculation

2.1 Description of the GOTHIC model

The computer code GOTHIC, ref. [43], was used for calculation of containment thermal hydraulic behavior and condensation in conduits and limit switch compartments. The code solves conservation of: mass, momentum, and energy equations for multiphase (vapor phase, continuous liquid phase, droplet phase) multicomponent (water, air, H2, noble gases) compressible flow. Constitutive relations predict interaction between phases for nonhomogenous nonequlibrium flow. Heat structures are modeled as 1D heated or unheated structures. Hydraulic volumes can use 1D, 2D, 3D or lumped approach. It is possible to simulate operation of engineered safety equipment: pumps, fans, valves and doors, vacuum breakers, spray nozzles, heat exchangers, heaters and coolers, controlled by trip logic based on: time, pressure, vapor temperature, liquid level, conductor temperature. The code is tested and qualified to perform calculations similar to this analysis.

The model of the containment and mass and energy releases needed to drive condensation were based on calculations performed, ref. [32], during preparation of environmental conditions in NEK containment in frame of EQ project, ref. [11]. In order to predict maximum possible condensation within conduits and terminal boxes all LOCA and MSLB inputs are screened, as well as one High Energy Line Break (HELB) in letdown line of Chemical and Volume Control System (CVCS). Due to different number of flow boundary conditions used in mass and energy release description for LOCA and MSLB, NEK containment models used for LOCA and MSLB calculations are slightly different. Containment model used for MSLB calculation is shown in Fig. 1. The same containment model is used for letdown break calculation and for MSLB. Two conduits and one Limitorque limit switch compartment were added to EQ model in order to calculate amount of condensate in conduits and valve compartment. Three different types of Limitorque control valve compartments were analyzed (SMB000, SMB00, SB00), Fig. 2. The smallest compartment (Limitorque SMB000) is supposed to be most limiting from point of view of condensate amount and was initially used to estimate possible consequences.

The total free volume of the containment was modeled as one compartment, compartment number 1 on Fig. 1. The containment annulus was modeled as another separate volume, compartment number 2. The values are taken from NPP Krsko Updated Safey Analysis Report (USAR), ref. [4]. Initial conditions inside containment were chosen to maximize containment pressure (48.9 ^{o}C, 101.325 kPa, 30% RH). The temperature of the outside air was 34 ^{o}C. 14 containment heat structures were used based on USAR containment evaluation model. The heat structures 1 and 2 are used for representing steel liner and structures 3 and 4 are used for concrete containment wall. All other heat structures are internal containment heat structures. HVAC cooper heat structure is additional passive heat structure (model of fan cooler doesn't include thermal inertia). Material thermal properties were taken from USAR too. The heat transfer coefficient was based on Uchida condensation correlation and natural convection heat transfer coefficient, for all heat structures exposed to the containment atmosphere. In addition, in case of LOCA, Tagami heat transfer correlation was used for internal metal heat structures during blowdown. For internal heat structures one side of the structure is insulated. For structures 3 and 4 right side is exposed to the environment with fixed temperature (34 ^{o}C) and fixed heat transfer coefficient of 11.36 W/m^{2}K.

Three flow boundary conditions were present in the initial model, Fig. 1. Boundary conditions 1 and 2 are used to model each side of the break. Two flow boundary conditions per break side could be used to split fluid flow in liquid (the water is discharged in form of droplets) and gas phases explicitly. Only one boundary condition was used to describe mass and energy

release after split break in letdown line. Flow paths 1, 2 are associated with break flow boundary conditions. Boundary condition 3F and flow path 3 were used for modeling of spray flow from RWST (Refueling Water Storage Tank). GOTHIC spray nozzle component was used at the end of flow path to convert all water flow to droplets. The mean drop size used in calculation was 700 μm. Constant spray mass flow rate was used (75.8 kg/s). One spray line was modeled in case with one train available (MINSI) and two spray lines in case with both spray lines available. In both cases only one flow boundary condition was used and one spray component, but with two times larger mass flow. In case of LOCA calculation additional components describe behavior of the system during recirculation phase of the accident. Four Reactor Containment Fan Cooler (RCFC) units are present in the containment (two of them are active for MINSI sequence). Each reactor containment fan cooler was modeled separately as volumetric fan (1Q) + finned tube air-to-water heat exchanger (fan cooler) (1H). The dimension of the tubes and fins, total heat transfer area and other RCFC operational data were realistically taken into account based on RCFC Instruction manual. Flow paths 4, 5, 6 and 7 are used to model flow of steam and air mixture over RCFC units 1 to 4 cooling surfaces. The influence of RCFC units was not taken into account during normal operation (before break) due to lack of the model for heat losses from the primary side. Actuation of both sprays and RCFC units depends on accident scenarios.

The model of limit switch compartment and related conduits is added to existing EQ model. Actual plant configuration, is considered in calculation. Model SMB000 actuator limit switch compartment has the smallest volume and as such represents the conservative case in the sense of possible flooding. Limit switch compartment dimensions (SMB-000, SMB00, SB00) are defined on Fig. 2. Limit switch compartment is GOTHIC volume number 3. Two galvanized rigid metal conduits (Trade Size: 1,5“, ID: 1,624“, OD: 1,900“), GOTHIC volumes 4 and 5, enter limit switch compartment from the top (flow paths 8 and 9). Other side of the conduits is open to the containment atmosphere (flow paths 10 and 11). The connection is based on the full internal cross section area of empty conduit. Conservative 50 m length (to maximize steam volume) of each conduit is considered in calculation. The volume of the conduits is taken as 80% of the inside volume of the empty conduit (the larger volume of the steam present in the conduit, the larger condensation is expected on the conduit wall). Connection between limit switch compartment and conduit is not steam tight. Leakage through the connections is taken into account with one additional flow path (12) at the top of the limit switch compartment. The cross section area is taken as one full cross section area of the conduit. Installation of two 1/8“ T-drains is assumed at the bottom of limit switch compartment (flow path 13). The valve (1V) is located on the flow path in order to make possible both calculations, with and without drain. Metal wall of the conduits is modeled with heat structures 15 and 16 (connect inside of the conduit with surrounding containment atmosphere). The side walls of the limit switch compartment are represented with heat structure 17 and top of the box with structure 18. Uchida condensation heat transfer coefficient is assumed on both sides of the structures.

2.2 Mass and energy release scenarios

Mass and energy releases and accident scenarios driving condensation in limit switch compartments are taken from corresponding EQ scenarios, ref. [2]. It is assumed that added volumes and heat structures can bring only small perturbation in original calculation case. Eight LOCA calculations were performed taking into account different break sizes, positions and discharge coefficients:

- Double Ended Hot Leg break (DEHL)
- Double Ended Cold Leg break (DECL)
- Double Ended Pump Suction with minimum SI (DEPS min SI)
- Double Ended Pump Suction with maximum SI (DEPS max SI)
- 0.6 Double Ended Pump Suction with minimum SI (0.6 DEPS min SI)
- 0.6 Double Ended Pump Suction with maximum SI (0.6 DEPS max SI)
- 3 ft^2 Pump Suction Split with minimum SI (PSS min SI)

- 3 ft^2 Pump Suction Split with maximum SI (PSS max SI)

Fifteen MSLB calculations were performed assuming different initial power levels (amounts of water available and initial pressure), sizes and liquid entrainments:

- Large Double Ended Ruptures (LDER) at 0, 30, 70 and 102% of nominal power
- Small Double Ended Ruptures (SDER) (without entrainment - dry) at 30, 70 and 102% of nominal power
- Small Double Ended Ruptures (with entrainment - wet) at 0, 30, 70 and 102% of nominal power
- Split ruptures at 0, 30, 70 and 102% of nominal power

One additional case was calculated assuming letdown line break inside containment in order to check influence of smaller release rates (plant experienced similar event when leakage in RTD bypass line appeared and when condensate was found in some limit switch compartments). The flow was assumed terminated after 1800s, and the calculation was carried out till 7200 s. The RCFC units and containment spray were assumed to be inactive during this calculation.

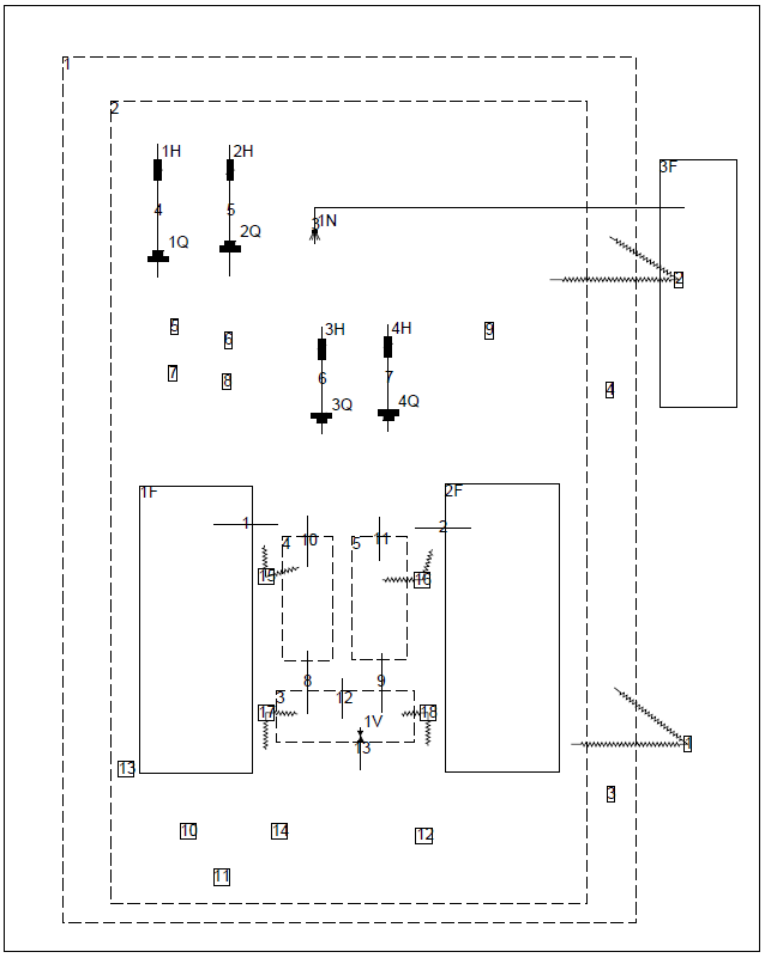

Fig. 1 GOTHIC model of the containment and valve compartments

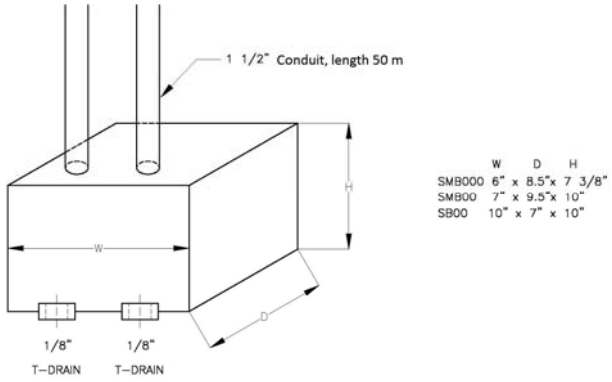

Fig. 2. Limit switch compartment layout and dimensions

3. Analysis of the condensation in the compartments

The calculations were performed first for the compartment with the smallest volume (SMB000). That should be the limiting case for submergence of limit switches due to smallest free volume inside the compartment for given amount of condensate. The liquid is condensed directly on inside surface of the compartment, condensed inside conduits and drained to the box, or brought to the compartment as liquid droplets in the stream of the steam and air mixture (in GOTHIC, part of the fluid can be discharged through the break in form of liquid droplets). Taking into account thermal-hydraulic conditions within containment during LOCA, DEPSG MINSI case was used to check potential for condensate accumulation. The results expressed as liquid volume fraction and liquid elevation, for all three compartments, are shown in Fig. 3. and Fig. 4. All compartments are filled between 10 and 20% up to 1000 s after break opening and then steep increase is present ending with completely filled SMB000 box and SMB00 and SB00 almost full of water (between 80 and 90% full). The graphs with liquid levels are little bit different due to different heights of the compartments, but it is clear that compartment SMB000 is full of water. Taking into account obtained results all three compartments are equipped with two 1/8“ T-drains and calculations were repeated. All possible cases were analyzed for the smallest compartment (SMB000), Fig. 5. and Fig. 6. For most limiting LOCA case (DEPSG MINSI) liquid fraction for compartment with drain stays below 10%, Fig. 5. Highest liquid volume fraction experienced during MSLB scenarios was around 3%, for case LDER from 0% power. For letdown break liquid fraction, after drain addition, stays below 2%. In order to check two other compartment configurations limiting LOCA case (DEPSG MINSI), two MSLB cases (LDER 0% and 70% (early peak)) and letdown break case were selected, Fig. 7. For all three configurations DEPSG MINSI was limiting case (producing largest amount of condensate within box). For SMB000 up to 9% of volume can be filled with condensate when drain is present and for SMB00 and SB00 that number is around 6%. When that results are expressed in terms of liquid levels (based on empty volume and nominal box cross section) that is around 1.7 cm for SMB000 and around 1.5 cm for SMB00 and SB00, and problems with submergence of limit switches are not expected.

4. Conclusion

The conservative calculation of condensation within small compartments in containment during design basis accidents was performed using assumptions usually found in similar EQ calculations. The results of the analyses indicate that it is possible that significant amount of liquid condensate collects within limit switch compartments and other small metal enclosures if they are not steam tight. The problem is especially important if more than one opening exist (e.g. not just connection through related conduit) as was the case with leakage at connection between conduit and enclosure box. After addition of small T-drains the problem will disappear (condensate will drain) resulting in only small amount of remaining liquid within the box.

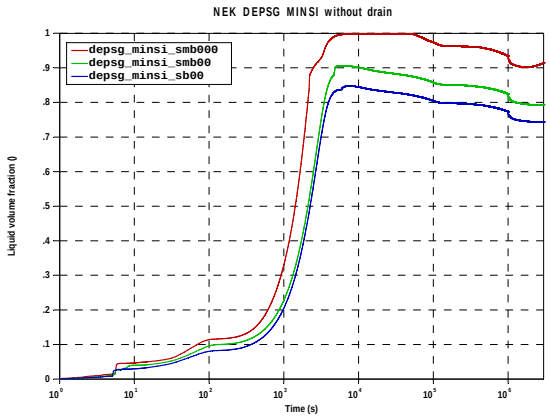

Fig 3. LOCA Liquid volume fraction

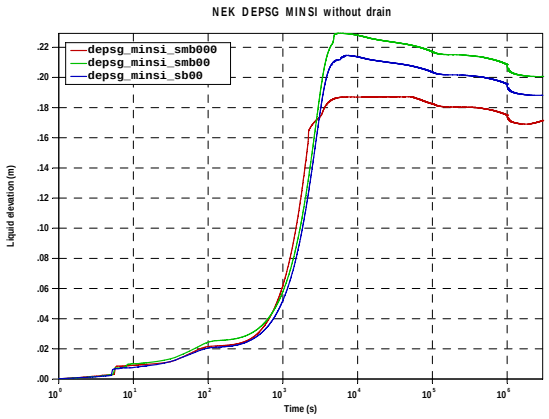

Fig 4. LOCA Liquid level in compartment

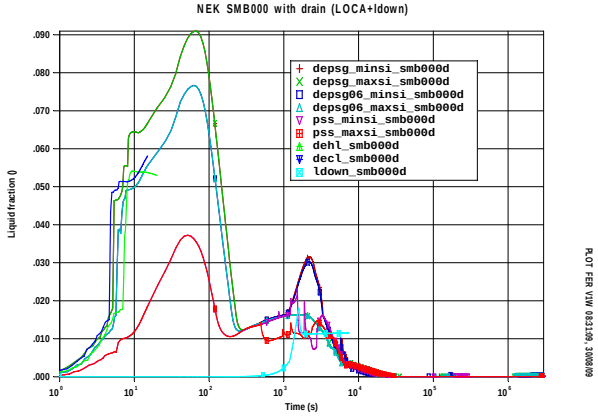

Fig 5. SMB000 compartment with drain liquid fraction, LOCA

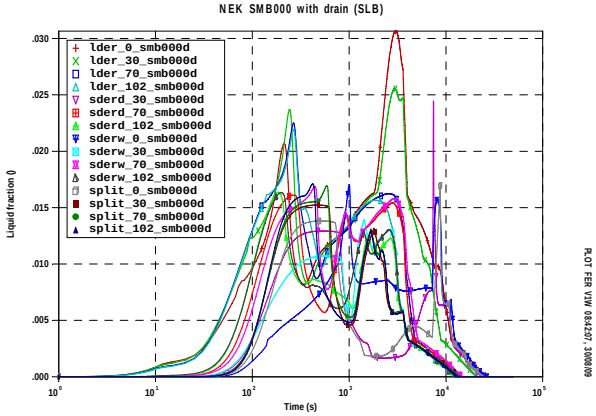

Fig 6. SMB000 compartment with drain liquid fraction, MSLB

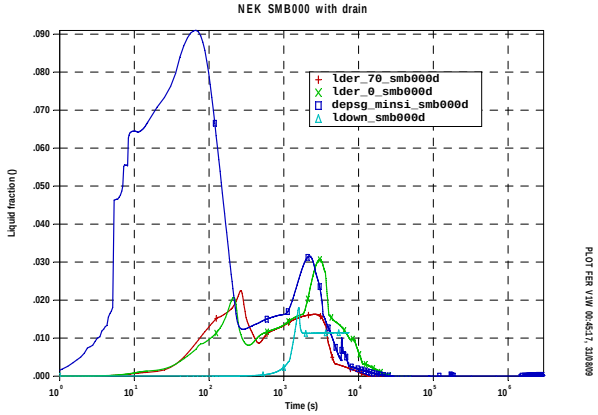

Fig 7. SMB000 compartment with drain liquid fractions

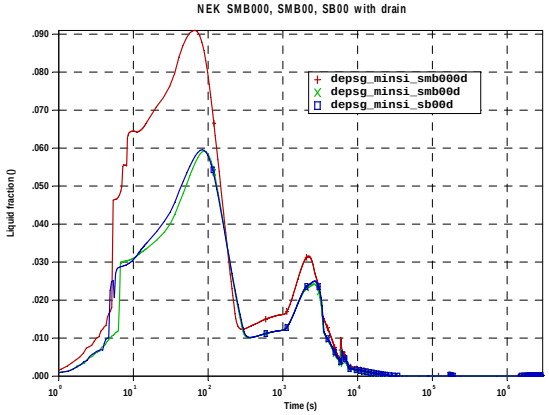

Fig 8. Limiting liquid fractions for compartments with drain

5. References

[1] D. Grgić et al, Development of NEK Environmental Qualification Zone Maps and Conditions, FER-ZVNE/SA/EQ-TR06/07-2, FER Zagreb 2009.

[2] D. Grgić et al, Support Calculation for Development of NEK EQ Zone Maps and Conditions, FER-ZVNE/SA/EQ-CN01/07-3, FER Zagreb 2009.

[3] Thomas George et al, GOTHIC Containment Analysis Package, Version 7.2b (QA), NAI 8907-02, Rev 18, Numerical Applications, Inc., Richland, Washington, USA, March 2009.

[4] Nuclear Power Plant Krsko, Updated Safety Analysis Report, Revision 16, NEK 2009

MOBILE HOT CELL TRANSITION DESIGN PHASE STUDY FOR RADIACTIVE WASTE TREATEMENT ON THE HANFORD RESERVATION SITE

Y. PONS
AREVA TA
BP 17 Gif-sur-Yvette – France

At the US Department of Energy's Hanford Reservation site, 4 caissons in under ground storage contain approximately 23 cubic meters of Transuranic (TRU) waste, in over 5,000 small packages. The retrieval of these wastes presents a number of very difficult issues, including the configuration of the vaults, approximately 50,000 curies of activity, high dose rates, and damaged/degraded waste packages. The waste will require remote retrieval and processing sufficient to produce certifiable RH-TRU waste packages. This RH-TRU will be packaged for staging on site until certification by CCP is completed to authorize shipment to the Waste Isolation Pilot Plant (WIPP).

The project has introduced AREVA' s innovative Hot Mobile Cell (HMC) technology to perform size reduction, sorting, characterization, and packaging of the RH waste stream at the point of generation, the retrieval site in the field. This approach minimizes dose and hazard exposure to workers that is usually associated with this operation.

The HMC can also be used to provide employee protection, weather protection, and capacity improvements similar to those realized in general burial ground.

AREVA TA and his partner AFS will provide this technology based on the existing HMCs developed and operated in France:

- ERFB (Bituminised Waste Drum Retrieval Facility): ERFB was built specifically for retrieving the bituminised waste drums (approximately 6,000 stored in trenches in the North zone on the Marcoule site (in operation since 2001).
- ERCF (Waste Drum Recovery & Packaging Facility) : The ERCF was built specifically to retrieve bituminized waste drums stored in 35 pits located in the south area.on Marcoule site (in operation)
- FOSSEA (Legacy Waste Removal and Trench Cleanup) : The FOSSEA project consists of the retrieval of waste stored on the Basic Nuclear Facility. Waste from the 56 trenches will be inspected, characterised, and if necessary processed or repackaged, and shipped to BNF number 164, named CEDRA on Cadarache site (in operation in 2009).

AREVA TA (ATA) is pleased to provide AREVA Federal Services (AFS) a phased plan to provide an Adaptation Design Technical Report and Organization. This approach will facilitate the assessment of the Final design Phase (After September 2010) and funding to support the engineering, procurement, and construction planning leading to the fabrication of a Mobile Hot Cell (MHC).

EUROPEAN NUCLEAR SOCIETY

Rue Belliard 65, 1040 Brussels, Belgium
Telephone +32 2 505 30 54, Fax + 32 2 502 39 02
enc2010@euronuclear.org - www.euronuclear.org